

## Mn-micronodules from the sediments of the Clarion-Clipperton zone (Pacific Ocean): Origin, elemental source, and Fe-Cu-Zn-isotope composition

Dekov Vesselin M. <sup>1,2,\*</sup>, Rouxel Olivier <sup>2</sup>, Gueguen Bleuenn <sup>3,4</sup>, Wegorzewski Anna V. <sup>5</sup>, Khripounoff Alexis <sup>6</sup>, Menot Lenaick <sup>6</sup>

<sup>1</sup> Tokyo University of Marine Science and Technology, 4-5-7 Konan, Minato-ku, Tokyo 108-8477, Japan

<sup>2</sup> Unité de Géosciences Marines, IFREMER, Z.I. Pointe du diable, BP 70 - 29280 Plouzané, France

<sup>3</sup> CNRS, Univ Brest, UMR 6538 Laboratoire Géosciences Océan, F-29280 Plouzané, France

<sup>4</sup> CNRS, Univ Brest, UMS 3113, F-29280 Plouzané, France

<sup>5</sup> Federal Institute for Geoscience and Natural Resources (BGR), Stilleweg 2, D-30655 Hannover, Germany

<sup>6</sup> REM-EEP-LEP, IFREMER, 29280 Plouzané, France

\* Corresponding author : Vesselin M. Dekov, email address : [vdekov0@kaiyodai.ac.jp](mailto:vdekov0@kaiyodai.ac.jp)

### Abstract :

Mn- micronodules and nodules of the Clarion-Clipperton zone (Pacific Ocean) are composed of 10 Å and 7 Å phylломanganates, and δ-MnO<sub>2</sub>. The Mn-micronodules are built of fine concentric growth layers of three types (1, 2a, and 2b) according to their Mn/Fe ratio and Ni, Cu, and Co content. Applying previously developed geochemical discrimination approaches we found that the Mn-micronodules were diagenetic precipitates that were a result of suboxic diagenesis, whereas the paired Mn-nodules were diagenetic-hydrogenetic formations. The most common growth layers (type 2) within the Mn-micronodules are suboxic-diagenetic, whereas the rare growth layers (type 1) are mixed diagenetic-hydrogenetic and hydrogenetic precipitates. The suboxic diagenetic formation of the Mn-micronodules seems to be a result of the fluctuation of the oxic-suboxic front in the sediment since the Last Glacial Period (LGP). The migration of the oxic-suboxic front close to the seawater/sediment boundary during the LGP has likely resulted in suboxic reduction of Mn<sup>4+</sup> and other elements in the sediment and their upward diffusion. Post-LGP deepening of the oxic-suboxic front has seemingly led to re-oxidation of Mn<sup>2+</sup> in the pore waters and Mn-micronodule precipitation. The suboxic quantitative re-mobilization of seawater-derived Ce solid phase in the sediment (positive Ce anomaly) and its subsequent sequestration by Mn-micronodules resulted in positive Ce anomaly of the Mn-micronodules and Ce-deficient pore water. This Ce deficiency was recorded in the diagenetic Mn-nodules (negative or no Ce anomaly). The sediment pore waters were source of most elements in the Mn-micronodules and to the bottom seawater.

The diagenetic processes were the major control on the Fe-Cu-Zn isotope composition of the Mn-micronodules and nodules. Measured Fe-isotope composition of the Mn-micronodules can equally be explained by hydrogenetic and diagenetic precipitation. Considering our mineralogical and geochemical data we would suggest a rather diagenetic than hydrogenetic control on the Fe-isotope composition of the Mn-micronodules: suboxic diagenetic reduction of the sedimentary Fe in the sediment, fractionation of Fe-isotopes that produces an isotopically light dissolved Fe pool, which leads to light Fe isotope

---

composition of both the Mn- micronodules and nodules ( $-0.63$  to  $-0.27\text{‰}$ ). The preferential scavenging of  $^{63}\text{Cu}$  from seawater on the hydrogenetic Mn-Fe-oxyhydroxides accounts for the Cu-isotope composition of the hydrogenetic-diagenetic Mn-nodules ( $+0.21$  –  $+0.35\text{‰}$ ), which is lighter than that of seawater. The identical Cu-isotope composition of the diagenetic Mn-micronodules is a result of oxidative dissolution of the sedimentary Cu-containing minerals, release of isotopically heavy  $\text{Cu}^{2+}$  in the pore waters and record of this diagenetic Cu-isotope pool in the Mn-micronodules. The hydrogenetic-diagenetic Mn-nodules have Zn-isotope composition ( $+0.75$  –  $+0.87\text{‰}$ ) heavier than that of the seawater which is interpreted to be a result of equilibrium isotope partitioning between dissolved and adsorbed Zn: preferential sorption of  $^{66}\text{Zn}$  on Fe-Mn-oxyhydroxides surfaces. Preferential adsorption of  $^{66}\text{Zn}$  from the light Zn isotope pool of the pore waters on the Mn-Fe-oxyhydroxides has resulted in heavy Zn-isotope composition of the Mn-micronodules and diagenetic layers of the Mn-nodules.

The lack of robust assessment of the Mn-micronodule abundance in sediment volume unit and the insufficient geochemical data for the Mn-micronodules prevents a meaningful estimation of their resource potential.

### Highlights

► Mn-micronodules from the Clarion-Clipperton zone are a result of suboxic diagenesis. ► Sediment pore waters are source of most elements in the Mn-micronodules. ► Diagenetic processes are major control on Fe-Cu-Zn isotope composition of the micronodules.

**Keywords** : Fe-Cu-Zn-isotopes, geochemistry, Mn-micronodules, Mn-nodules, pore waters, suboxic diagenesis

## 1. Introduction

Chester and Hughes (1967) estimated that about 85% of the manganese (Mn) in pelagic sediments occurs in Mn-micronodules. Mn-micronodules are morphologically, structurally and mineralogically similar to their big counterparts, Mn-nodules. Despite these similarities, there is a striking discontinuity in the sizes of Mn-micronodules and Mn-nodules: the former hardly ever exceed ~1 mm in diameter, whereas the later are almost always >10 mm. It was interpreted that the Mn-micronodules are not proto-Mn-nodules (Heath, 1981).

Although the Mn-micronodules appear to be an important component in the global cycle of one of the major elements on Earth, manganese, they have received far less scientific interest than Mn-nodules. This has seemed to be logical in view of their economic potential estimated to be lower than that of the Mn-nodules. However, with the globally increasing demand in strategic elements like the rare earth elements (REE), In, Ge, W, etc. and revitalized interest in oceanic metalliferous sediments (Kato et al., 2011) the economic potential of Mn-micronodules needs to be revised. Although the Mn-micronodules are scattered within the upper part of the seafloor sedimentary blanket, they form at much wider areas of the seafloor than the metalliferous sediments and therefore, they may have greater economic value.

The main focus of the investigations of Mn-micronodules has been on their chemistry and mineralogy (Kidd and Ármannsson, 1979; Hishida and Uchio, 1981; Lallier-Verges and Clinard, 1983; Poppe et al., 1984; Stoffers et al., 1984; Mukhopadhyay et al., 1988; Sval'nov et al., 1991a,b; Dekov et al., 2003; Ito et al., 2005; Menendez et al., 2017; Liao et al., 2019; Yasukawa et al., 2019; Dubinin et al., 2020; Li et al., 2020; Xu et al., 2020; Yasukawa et al., 2020, 2021). The data received was used in the interpretations of the origin of Mn-micronodules. The proposed genetic models were refined with studies on the chemistry of coexisting Mn-micronodules and Mn-nodules, and host sediments (Addy, 1978; 1979; Stoffers et al., 1981; Kunzendorf et al., 1989; 1993; Pattan, 1993; Pattan et al., 1994; Dubinin and Sval'nov, 1995; 1996; Winter et al., 1997; Dubinin and Sval'nov, 2000a,b; Dubinin and Sval'nov, 2003; Dubinin et al., 2008; 2013). Although the early works hypothesized that, the Mn-micronodules have diagenetic origin (Immel, 1974; Immel and Osmond, 1976) later studies attempted to relate their chemistry and

growth to the depositional environment (Ohashi, 1985; Sugisaki et al., 1987; Chauhan and Rao, 1999), biogenic activity (Banerjee and Iyer, 1991) and seafloor hydrothermal discharge (Sugitani, 1987; Dekov et al., 2003).

A review of all previous works on the seafloor Mn-micronodules reveals that our current knowledge on them is incomplete and has some gaps:

(1) Previous geochemical investigations of the Mn-micronodules report mainly on their major (Mn, Fe), some trace (Cu, Co, Ni) and rare earth elements concentrations and only few works (Dekov et al., 2003; Dubinin et al., 2013; Yasukawa et al., 2020) provide data on wide range of trace elements. Thus, a modern evaluation of the economic potential of the Mn-micronodules needs information for the concentrations of a wide spectrum of elements in them.

(2) The studies on Mn-micronodules/Mn-nodules pairs were at random sample sites and did not consider the differences in Mn-nodule facies. A correct assessment of the processes of trace element concentration in the Mn-micronodules/Mn-nodules requires consideration of the nodule facies.

(3) The hypotheses for diagenetic origin of the Mn-micronodules were rather inferred logically (Mn-micronodules form in the sediment pore space filled with pore waters that are diagenetic fluids) than based on combined studies of Mn-micronodules and corresponding pore waters. This has resulted in speculative conceptions for the sources of elements to the Mn-micronodules.

(4) The conventional geochemical approaches (like elemental concentrations and ratios) cannot further extend our knowledge on the origin and evolution of the Mn-micronodules as important components of the global Mn cycle. The stable isotope ratios of transition elements (e.g., Fe, Cu, Zn) can provide new possibilities for getting insight into the processes of Mn-micronodule (-nodule) formation (e.g., precipitation, adsorption, redox reactions) and trace metal concentration (e.g., source of metals). We are not aware of any published Fe-Cu-Zn-isotope data for Mn-micronodules and the available data for Fe-Cu-Zn-isotope composition of Mn-nodules are scarce: 20 sub-samples from 5 Mn-nodules analyzed for Fe isotopes (Beard and Johnson, 1999; Levasseur et al., 2004; Marcus et al., 2015), surface layers of 31 Mn-nodules analyzed for Cu isotopes (Albarède, 2004), and surface layers of 40 Mn-nodules analyzed for Zn isotopes (Maréchal et al., 2000).

These limitations of our knowledge on the Mn-micronodules motivated us to undertake a study of the mineralogical, chemical (major, trace, and rare earth elements) and Fe-Cu-Zn-isotope composition of pairs Mn-micronodules/Mn-nodules from different facies at the Clarion-Clipperton Mn-nodule field along with the chemistry of pore waters from the sediment that hosts the micronodules and nodules. Here we report the results of this study.

## 2. Geologic setting and Mn-nodule facies

Samples for this study were collected from the French exploration contracts managed by the International Seabed Authority in the Clarion-Clipperton zone (CCZ) (Fig. 1) during the BIONOD cruise (April-May, 2012) onboard the R/V *L'Atalante*. The area of investigations is a part of the province of abyssal hills (Morel and Le Suavé, 1986; Le Suavé, 1989). Although a hilly area (Fig. 1) it was described as a sedimentary plateau in a general sense (Morel and Le Suavé, 1986; Le Suavé, 1989). Red pelagic clays with minor biogenic component (tests of foraminifera and radiolarians) are the principle sediment type in the area. Their vertical profile shows signs of gravity mass movements interpreted to be a result of submarine erosion and tectonic readjustments (Morel and Le Suavé, 1986; Le Suavé, 1989). Details on the variations of the seafloor morphology, sediment thickness, sediment erosion, and their tectonic and hydrologic controls can be found elsewhere (Morel and Le Suavé, 1986). Primary productivity in the surface waters above the studied seafloor is estimated to be moderate (Veillette et al., 2007). Bottom-water temperature is  $\sim 1^{\circ}\text{C}$  and near-bottom currents have velocity of 3.5-4 cm/s (Veillette et al., 2007).

Previous studies in the area (Veillette et al., 2007) defined four Mn-nodule facies (0, A, B and C) that differ in shape, size, surface morphology and the degree to which Mn-nodules are exposed above the sediment-water interface (Fig. 1). Facies 0 does not contain any Mn-nodules at the sediment surface. Facies A contains small (10-20 mm) rounded Mn-nodules with granular surface and has a high density of Mn-nodules coverage. Facies B contains Mn-nodules of medium size (20-80 mm) and pieces of broken Mn-nodules, which often show patterns of secondary growth healing the broken surfaces. The density of Mn-nodule coverage of facies B is high. The nodules' upper surfaces are smooth whereas their lower surfaces are granular and an equatorial belt is often present. Facies C contains big nodules,  $>80$  mm in diameter. Their upper

surface is smooth whereas their lower surface is botryoidal and granular. The equatorial belt is well pronounced. As it marks the limit between the buried part of the Mn-nodule in the sediment and the part in contact with seawater, it seems that a large part of these Mn-nodules is buried in the sediment (more than a half of the Mn-nodule). The nodule density coverage is high.

### 3. Samples and methods of investigation

#### 3.1. Sampling and sample preparation

Mn-nodules and underlying sediment were sampled with USNEL box-corer (50 x 50 cm) at 15 sites located within the areas of distribution of the nodule facies 0 (6 box-cores), B (6 box-cores) and C (3 box-cores) (Fig. 1; Table 1). Two deployments of the box-corer in the facies A, located in a small area surrounded by pillow lava flows (Fig. 1), failed.

Mn-nodules were collected by hand, washed with distilled water, transferred into plastic bags and stored in a fridge at ~4°C. Mn-micronodule extraction from the sediment began immediately after recovery of the box-core. The uppermost two sediment layers, 0-5 cm and 5-10 cm, were wet-sieved in order to collect the >250 µm fraction that was inferred to contain the major part of the Mn-micronodules (Israel and Osmond, 1976). After drying in an oven with laminar air flow at 30°C for 24 hours the Mn-micronodule concentrates were further purified by hand-picking of the detrital grains and biogenic remnants by steel needle under stereo-microscope (WILD M8).

Dried Mn-micronodules and paired Mn-nodules from the sediment surface were ground manually in an agate mortar up to fine powders, which were used in all further analyses.

Aiming at figuring out the sources of elements to the Mn-micronodules and Mn-nodules we sampled and analysed the pore waters from the sediment hosting the Mn-micronodules and underlying the Mn-nodules. Plexiglas push cores (10 cm diameter, 50 cm length) with holes (2 mm diameter) every centimeter along the core were inserted into the sediment in the box-corer immediately after recovery. Pore waters were extracted from the sediment taken in the Plexiglas push core using Rhizons® flex with nylon wire (Rhizosphere Research products) in cold (4°C) laboratory environment following the method described by Seeberg-Elverfeldt et al. (2005). The Rhizons® were inserted into the sediment through the holes of the Plexiglas push core every

centimeter in the upper 20 centimeters of the core, and then every 2 centimeters for the remaining core. We waited for two hours until the syringes collected enough pore water (5 - 10 mL) and then transferred the pore waters in 15 mL Nalgene vials pre-cleaned with 10% HCl. Collected pore waters were stored in refrigerator ( $\sim 4^{\circ}\text{C}$ ) before further analyses.

### 3.2. Mineralogical, morphological, and internal structure studies

The bulk mineralogical composition of 28 finely powdered sub-samples including Mn-micronodules and Mn-nodules was determined by X-ray diffraction (XRD) analysis (Panalytical X'Pert Pro X-ray diffractometer with monochromatic  $\text{Co } K_{\alpha}$  radiation) of random mounts in Si low-background sample holder: X-ray scans from  $1$  to  $85^{\circ} 2\theta$  with  $0.03^{\circ} 2\theta$  step, 15 s/step measuring time, automatic divergence slit, and  $\text{Ni-}K_{\beta}$  filter at the BGR and IFREMER.

Due to the possible occurrence of two different  $10 \text{ \AA}$  manganese phases, such as  $10 \text{ \AA}$  vernadite (phyllomanganate) and todorokite (tectomanganate), a drying procedure was necessary before the XRD analysis. Both the  $10 \text{ \AA}$  vernadite and todorokite have a layer-to-layer distance of  $\sim 10 \text{ \AA}$ , which is due to hydrated cations (e.g., Mg) within the interlayers (Bodeř et al., 2007). In addition to the octahedra layers, the todorokite has also vertical octahedra walls (3 to 10 octahedra), which stabilize the sheet structure against collapsing and form a so called “tunnel structure” (Bodeř et al., 2007). After heating the samples at  $105^{\circ}\text{C}$  for 24h, the  $10 \text{ \AA}$  peak of the phyllomanganates will decrease and therefore, the  $7 \text{ \AA}$  peak will increase ( $7 \text{ \AA}$  vernadite), or the  $10 \text{ \AA}$  peak will collapse completely. In contrast, the  $10 \text{ \AA}$  peak of todorokite will remain unchanged upon heating at  $105^{\circ}\text{C}$  (e.g., Manceau et al., 2014; Wegorzewski et al., 2020). Therefore, we performed XRD analyses of six Mn-micronodule samples twice: after sample drying at  $30^{\circ}\text{C}$ , and after sample heating at  $105^{\circ}\text{C}$  for 24h (e.g., Uspenskaya et al., 1987; Wegorzewski et al., 2015).

For a better mineralogical characterization, we analysed ten Mn-micronodule samples from different Mn-nodule facies and two Mn-nodule standards (Nod-P-1 and Nod-A-1) by Fourier-Transformed Infrared Spectroscopy (FTIR). The mid- (MIR) and far- (FIR) infrared spectra were collected on pressed pellets made of 1 mg sample mixed with 200 mg KBr. The analyses were carried out on a ThermoNicolet Nexus FTIR spectrometer (MIR beam splitter KBr, detector

DTGS TEC; FIR beam splitter solid substrate, detector DTGS PE) at the BGR. The resolution was adjusted to  $2\text{ cm}^{-1}$ .

Morphology of the Mn-micronodules was studied using FEI Quanta 200 scanning electron microscope (SEM) ( $V=10\text{ kV}$ ,  $I=100\text{ }\mu\text{A}$ , electron beam diameter of  $2\text{ }\mu\text{m}$ ) at IFREMER. Secondary electron images (SEI) and energy dispersive X-ray spectra (EDS) were obtained on selected Mn-micronodules, mounted on aluminum stubs using carbon tape and coated with Au.

The internal structure of the Mn-micronodules was investigated on carbon-coated polished section of Mn-micronodules (impregnated with araldite in a block; sample NODKGS63 0-5 cm) by FEI Quanta 600 FEG SEM at BGR. Back-scattered electron images (BEI) were obtained through scanning of the specimen with a focused electron beam (diameter  $1\text{-}5\text{ }\mu\text{m}$ , maximum magnification 250000 times) produced by a field emission gun (W-crystal) using a  $20\text{ kV}$  acceleration under high vacuum conditions ( $9\text{-}10\text{ mbar}$ ).

### *3.3. Dissolved oxygen concentration profiles in the sediment*

Dissolved oxygen concentrations were measured across the collected sediment (box-corer) using a Clark-type oxygen microprobe provided with an included reference and an internal cathode. The micro-sensor had a diameter of  $\leq 100\text{ }\mu\text{m}$  at its extremity. The elapsed time prior to the response was 90% in less than 10 seconds. Signal collected by the probe (oxygen tension) was recorded after signal amplification.

In each box-core we performed oxygen concentration profiles at both (1) sediment surface free of Mn-nodules, and (2) sediment surface under a Mn-nodule.

### *3.4. Elemental concentrations measurements of Mn-micronodules and Mn-nodules*

Concentrations of Mn, Fe, Si, Al, Ca, Mg, Na, K, Ti, P, S, Li, Be, B, Sc, V, Cr, Co, Ni, Cu, Zn, Se, As, Rb, Sr, Y, Zr, Nb, Mo, Cd, Sn, Sb, Te, Ba, Hf, Ta, W, Tl, Pb, Bi, Th, U, Au, Pt and REE in the Mn-micronodules and Mn-nodules (bulk samples) were measured by Inductively Coupled Plasma-Mass Spectrometry (ICP-MS) (ThermoElectron Element XR) at the Pôle de Spectrométrie Océan (PSO, IFREMER, Brest, France) after digestion of bulk powdered samples according to the following procedure. About  $5\text{ mg}$  of each sample (finely powdered) were



dissolved with 0.8 mL double-distilled concentrated HNO<sub>3</sub>, 0.8 mL 6 M HCl and 0.2 mL concentrated HF in 2 mL Teflon vials. After evaporation of the solutions to dryness on hot (90°C) plate, the residues were re-dissolved with 0.2 mL double-distilled concentrated HNO<sub>3</sub> and stored in 2 mL Teflon vials after adding of 1.8 mL 18.2 MΩ H<sub>2</sub>O. The ICP-MS instrument was calibrated using a set of Mn-nodule standards matching the Fe-Mn-oxyhydroxide matrices: Nod-P-1 [United States Geological Survey (USGS) standard for Pacific Mn-nodule], and Nod-A-1 (USGS standard for Atlantic Mn-nodule). The analytical error (2σ) calculated on replicate analyses of the standards was below 5% for most elements.

Chemical composition of the individual layer growth structures within the Mn-micronodules was investigated on a carbon-coated polished block section (sample NODKGS63 0-5 cm) by Electron Probe Micro-Analyzer (EPMA) (JEOL JXA-8530F) at BGR. The diameter of the EPMA electron beam was adjusted between 5 and 20 μm, depending on the dimension of the growth structures and type of the material. The accelerating voltage was set at 15 kV and a beam current of 40 nA was used. The counting times for the analyzed elements were: 10 s for Mn, Fe, Ni, Cu, Na, Mg, Al, Si, K, Ca, Ti, P and S, 40 s for V, 50 s for Co, 100 s for Ba, and Mo. Rhodochrosite (Mn), haematite (Fe), cobaltite (Co), synthetic Ni<sub>2</sub>Si (Ni), cuprite (Cu), albite (Na), kaersutite (Mg, Al, Si), biotite (K), apatite (Ca, P), rutile (Ti), barite (S, Ba), molybdenite (Mo), and vanadium metal (V) were used as standards (BGR standards). According to the high water content of the different Mn (oxy)hydroxides (up to 25 % for phylломanganates; Jones and Milne (1956), Chukhrov et al. (1979)) and the high porosity of the samples, total analytical sums of >60% were accepted (e.g. Niegorszewski and Kuhn, 2014).

### 3.5. Elemental concentrations measurements of pore waters

Concentrations of Na, K, Ca, Mg, S, Si, B, Sr, Fe, Mn, Al, P, Li, Rb, Ba, Mo, V, Zn, Cu, Ni, Co, Cr, Cd, U, Ti, Ge, La, Ce, and Nd in the pore waters of core NODKGS65 were measured by ICP-MS (ThermoElectron Element XR) at the Pôle de Spectrométrie Océan (PSO, Ifremer, Brest, France) in 2 mL aliquots of 100-fold diluted (with 18.2 MΩ H<sub>2</sub>O) pore water samples. The ICP-MS instrument was calibrated using a set of in-house (SW-XR-2) and internationally-certified (NASS-5 and IAPSO) seawater standards matching the pore waters matrices. The analytical error (2σ) calculated on replicate analyses of the standards was below 3% for most

elements. The procedural blanks were below the detection limits of the instrument for all measured elements.

### 3.6. Fe-Cu-Zn-isotope analysis of Mn-micronodules and Mn-nodules

For Fe-Cu-Zn-isotope analyses of the Mn-micronodules and Mn-nodules, we put 1 mL from each of the stored after total digestion sample solutions in 2 mL Teflon vials and evaporated them to dryness on a hot plate (90°C). The residues were re-dissolved with 1 mL 10 M HCl. Sample solutions were ready for column load after addition of 10  $\mu$ L H<sub>2</sub>O<sub>2</sub> in each sample.

Fe, Cu and Zn were separated from the matrix components (element purification) by anion-exchange chromatography using AG MP-1 resin (2.0 mL wet volume in Teflon columns). Blanks and standards (Nod-P-1) were included in the sample sets and subjected to the same anion-exchange chromatography procedure. Our protocol contained six major steps: (1) columns with AG MP-1 resin were washed with 10 mL 3 M HNO<sub>3</sub>, 10 mL 18.2 M $\Omega$  H<sub>2</sub>O, 5 mL 1.2 M HCl and 2 mL 10 M HCl; (2) samples (in 1 mL 10 M HCl with 10  $\mu$ L H<sub>2</sub>O<sub>2</sub>) were loaded on the columns and the matrix fraction was eluted with 6.5 mL 10 M HCl; (3) Cu fraction was recovered in 23 mL Teflon vials with 16 mL 5 M HCl; (4) Fe fraction was recovered in 15 mL Teflon vials with 14 mL 1.2 M HCl; (5) Zn fraction was recovered in 15 mL Teflon vials with 14 mL 0.0012 M HCl; (6) columns were washed with 10 mL 18.2 M $\Omega$  H<sub>2</sub>O. All elutions were evaporated to dryness at 90°C, re-dissolved in 2 mL ~0.28 M HNO<sub>3</sub> and transferred into 2 mL vials.

Isotope ratios (<sup>56</sup>Fe/<sup>54</sup>Fe, <sup>57</sup>Fe/<sup>54</sup>Fe, <sup>57</sup>Fe/<sup>56</sup>Fe, <sup>65</sup>Cu/<sup>63</sup>Cu, <sup>66</sup>Zn/<sup>64</sup>Zn and <sup>68</sup>Zn/<sup>66</sup>Zn) were measured with a *Nephele* multi-collector inductively coupled plasma mass spectrometer (MC-ICP-MS) at the Pôle de Spectrométrie Océan (PSO, Ifremer, Brest, France). Isotope ratios were estimated relative to the same ratios measured for an isotope standard (IRMM-14 for Fe, NIST-SRM 976 for Cu, and NIST-SRM 3168a for Zn) and reported in delta notation:

$$\delta^i E_{sample} = (R^{i/j}_{sample}/R^{i/j}_{standard} - 1) \times 1000,$$

where *i* and *j* are the specific isotopes used in ratio *R* of element *E* in the sample of interest and standard reference material. Following the conventional practice, we use isotope *i* in the  $\delta$  values discussed in the paper and note the specific ratios  $R^{i/j}$  we have used. All  $\delta^{66/64}\text{Zn}_{sample}$  values reported relative to our internal isotope standard NIST 3168a were recalculated relative to JMC-Lyon isotope standard because this reference standard is commonly used in the literature for

reporting Zn isotope composition of natural samples (Archer et al., 2017). We determined  $\delta^{66/64}\text{Zn}$  value of NIST 3168a against the Zn-ETH isotope standard (Archer et al., 2017) and obtained  $\delta^{66/64}\text{Zn}$  value of  $-1.207 \pm 0.028\text{‰}$ , which corresponds to  $-0.94\text{‰}$  relative to JMC-Lyon isotope standard (using the consensus value of  $\delta^{66/64}\text{Zn}$  of Zn-ETH against JMC-Lyon of  $0.27\text{‰}$ ). Hence,  $\delta^{66/64}\text{Zn}$  of SRM 3168a is  $0.94\text{‰}$  lower than JMC-Lyon.

Instrumental fractionation of Cu and Zn in the mass spectrometer during analysis was corrected with internal isotopic standards Zn NIST SRM 3168a and Cu NIST SRM 976, respectively, doped in Cu sample solution and Zn sample solution according to a Cu/Zn ratio of 1:2 coupled to a standard-sample-bracketing procedure (Marechal et al., 1999). Samples were introduced in the plasma through a double quartz cyclonic spray chamber coupled to a  $50\ \mu\text{L}/\text{min}$  PFA nebulizer and isotopic ratios were measured in low resolution mode. Iron isotope ratios were corrected using a Ni isotopic standard NIST SRM 986 doped in samples solution at a concentration ratio Fe/Ni of 1:1, and a standard-sample-bracketing procedure was also employed (Rouxel et al., 2005). Samples were introduced in the plasma through an Apex Q (Elemental Scientific) desolvation introduction system coupled to a  $50\ \mu\text{L}/\text{min}$  PFA nebulizer. Iron isotopic ratios were measured in medium resolution mode to resolve argide interferences.

The performance of the mass spectrometer for Fe, Cu and Zn isotope ratios measurements was assessed through replicate measurements of isotopic standards (Fe IRMM-14, Cu NIST-SRM 976, and Zn JMC and NIST-SRM 3168a). Precision on the samples is reported as a two-standard deviation (2sd) calculated on replicate measurements of the isotopic standards. Replicate analyses of digest replicates ( $n=5$ ) of USGS geological reference material Nod-P-1 yielded average values of  $-0.58 \pm 0.04\text{‰}$  (2sd) for  $\delta^{56/54}\text{Fe}_{\text{IRMM-14}}$ ;  $0.33 \pm 0.03\text{‰}$  (2sd) for  $\delta^{65/63}\text{Cu}_{\text{SRM976}}$ ; and  $1.72 \pm 0.06\text{‰}$  (2sd) for  $\delta^{66/64}\text{Zn}_{\text{SRM3168a}}$ . These isotopic values are consistent with the data reported in the literature: for Fe (Dideriksen et al., 2006; Williams et al., 2014), and for Cu and Zn (Chapman et al., 2006; Bigalke et al., 2010a; Little et al., 2017).

## 4. Results

### 4.1. Mn-nodule distribution, and Mn-micronodule morphology and internal structure

The deepest Mn-nodule facies, 0 (Table 1), does not contain Mn-nodules at the surface (Fig. 2A). Small (<10 mm), rounded Mn-nodules (Fig. 2A) with finely granular surfaces were scattered within the sediment. As stated above (see 3.1) we could not sample Mn-nodules of facies A with box-corer, but we collected some with an epi-benthic sledge. Facies A is densely covered (Fig. 2B) of small (10-20 mm), rounded, black nodules with granular surfaces (Fig. 2B). The shallowest Mn-nodule facies, B (Fig. 2C), contains the highest abundance of nodules on a surface unit: 17.4 kg/m<sup>2</sup> (Table 1). Mn-nodules of this facies are of medium size (20-80 mm), flat, ellipsoidal (Fig. 2C) with smooth upper surface and botryoidal lower surface. Mn-nodule facies C (Fig. 2D) is located at middle depths and contains 15.5 kg/m<sup>2</sup> nodules in average (Table 1). These nodules are big (>80 mm), ellipsoidal, flat (Fig. 2D), with smooth upper surface and botryoidal lower surface.

Mn-micronodules are either elongated (Fig. 3A) or isometric (Fig. 3B). They are black, with botryoidal surfaces (Fig. 3A,B). We could not find any relation of their morphology with the depth of occurrence in the sediment.

Mn-micronodules appear to have concentrically zoned internal structure composed of concentric fine dense layers (Fig. 3C-F) that form botryoidal and columnar growth structures (Fig. 3C,D).

## 4.2. Mineralogy of Mn-micronodules and Mn-nodules

### 4.2.1. X-ray diffraction analysis

The XRD patterns of all analysed samples showed two diffraction humps (broad and of low intensity) at ~9.5 Å (001) and at ~7 Å (001) with *hk* bands around ~2.45 Å (10) and ~1.42 Å (01; Fig. 4; Appendixes 1-3). The first hump can be assigned to two different Mn-minerals: 10 Å distorted phyllomanganate (vernadite) and 10 Å tectomanganate (todorokite) (Bodeř et al., 2007; Wegorzewski et al., 2015). After heating the samples at 105°C for 24h, the hump at ~9.5 Å disappeared completely and the 7 Å peak increased and became more distinct. This is common for the phyllomanganates. Furthermore, no splitting of the peak at ~2.45 Å (to 2.45 and 2.39 Å), which is typical for todorokite (Manceau et al., 2014; Wegorzewski et al., 2020) was observed (Fig. 4). This suggests that the studied Mn- micronodules and nodules are composed of 10 Å phyllomanganates, but not of tectomanganates like todorokite or even of “defected” todorokite

(Bodeř et al., 2007; Wegorzewski et al., 2015; 2020). Furthermore, a turbostratic 7 Å vernadite phase can be recognized, already before the heating. The occurrence of a third phyllomanganate such as vernadite ( $\delta$ -MnO<sub>2</sub>) cannot be excluded. The  $\delta$ -MnO<sub>2</sub> (vernadite) shows only two *hk* bands at the XRD pattern (~2.45 and 1.42 Å) and they are similar to those of the 10 and 7 Å phyllomanganates (Fig. 4). Vernadite seems to be intergrown with an X-ray amorphous Fe-phase and therefore without a stacking order in *c*\* direction, resulting in the absence of the 00*l* reflections (Burns and Burns, 1977). The layer symmetry of the phyllomanganates that compose the studied Mn- micronodules and nodules is hexagonal because the calculated ratio of the d-spacings of the two *hk* bands is ~1.73 (close to  $\sqrt{3}$ ) and the band at ~1.42 Å is almost symmetrical (e.g., Drits et al., 1997; Bodeř et al., 2007; Drits et al., 2007). Presence of significant amounts of asbolane is unlikely, because the 002 reflection of the phyllomanganates is of lower intensity than the 001 reflection (Fig. 4).

In addition to the major Mn-(Fe)-minerals, minor amounts of detrital quartz and feldspars were detected in the studied Mn- micronodules and nodules (Fig. 4; Table 2).

#### 4.2.2. Infrared spectroscopy

The FTIR spectra of the Mn-micronodules and Mn-nodule standards (Fig. 5; Appendix 4) show two to three bands, which are characteristic for Mn-phases (Wegorzewski et al., 2020). The bands in the region between 800 and 400 cm<sup>-1</sup> arise from Mn-O lattice vibrations (Kang et al., 2007). The hydrogenetic Mn-nodule standard (Nod-A-1) shows a hump around 433 cm<sup>-1</sup> and a distinct band at 464 cm<sup>-1</sup>. The mixed hydrogenetic-diagenetic nodule standard (Nod-P-1) displays bands at 433 (weak), 464 (strong) and 502 cm<sup>-1</sup> (medium), respectively. The FTIR spectra of the Mn-micronodules are similar to the FTIR spectrum of Nod-P-1: bands at 426-434 cm<sup>-1</sup>, 462-468 cm<sup>-1</sup>, and 501-512 cm<sup>-1</sup> (Fig. 5; Appendix 4). These three bands correspond to the IR characteristics of layered Mn-oxides (Potter and Rossman, 1979; Golden et al., 1986; Kang et al., 2007; Wegorzewski et al., 2020). No IR bands typical for a tectomanganate like todorokite could be distinguished. According to the previous IR studies (Julien et al., 2004; Atkins et al., 2014; Wegorzewski et al., 2020) a band at ~748-760 cm<sup>-1</sup> occurs in the IR spectra if todorokite is the main Mn-mineral in the studied samples. The lack of this band in the FTIR spectra of the studied Mn-micronodules testifies that todorokite is not present.

### 4.3. Geochemistry of Mn-micronodules and Mn-nodules

At the site NODKGS49 we recovered sediment with Mn-micronodules only, but did not find any Mn-nodules on the sediment surface (facies 0). Site NODKGS44 (facies 0) is close to site NODKGS49 (Fig. 1) and we found rare Mn-nodules on the sediment surface. Therefore, we may consider as a pair representative for facies 0 the Mn-nodule and Mn-micronodules collected at sites NODKGS44 and NODKGS49, respectively.

The Mn-micronodules are richer in Mn, Cu, Ni, Zn, and Sn (two to five times), Cr, Sb, K, Mg, and Rb than the Mn-nodules (Table 3). Mn/Fe ratios of the Mn-micronodules are two to three times higher than that of the Mn-nodules. The Mn-micronodules of facies 0 are the richest in Si, whereas the micronodules of facies C are the poorest in Si. Mn-micronodules of facies 0 contain more Ca than the paired Mn-nodules. This trend is opposite for the Mn-micronodule/Mn-nodule pairs of facies B, whereas the Mn-micronodules and Mn-nodules of facies C have similar Ca concentrations. Titanium, Sr, and Pb are more abundant in the Mn-micronodules than in the Mn-nodules of facies 0, but less in the micronodules than in the nodules of facies B and C. Molybdenum concentrations are higher in the micronodules than those in the nodules of both facies 0 and C, and are similar in both micronodules and nodules of facies B. Tungsten and Bi are more abundant in the micronodules than in the nodules of facies 0 and C, and more abundant in the nodules than in micronodules of facies B. Manganese, Cu, Co, Ni, Cd, Sb, As, Tl, U, Na, and REE concentrations in the micronodules generally increase upward the sediment cores towards the sediment/seawater interface. Potassium increases upward the sediment in the Mn-micronodules from facies 0 and B, but decreases upward in the Mn-micronodules of facies C (Table 3).

The studied Mn-nodules are richer in Al, Sc, Nb, Ta, Li, Be, B, V, Co, As, Cd, Ba, and U than the Mn-micronodules (Table 3). The concentrations of Fe, S, Na, Pt, Zr, and REE in them are about two times (P, Te, Tl, Hf, and Th up to two-three times; Y two to five times) higher than those in the Mn-micronodules (Tables 3, 4). Content of Se is the highest in the Mn-nodules of facies B and the lowest in the nodules of facies 0 (Table 3).

Mn-micronodules from the facies 0 have positive Ce anomaly whereas the Mn-nodules from the same facies have weak negative Ce anomaly (Table 4; Fig. 6A, B). In facies B and C both the micronodules and nodules have positive Ce anomaly, but it is higher in the micronodules

than in the nodules (Table 4; Fig. 6C-F). The positive Ce anomaly of the Mn-micronodules from all the facies decreases upwards the sediment (Table 4).

Mn- micronodules and nodules from all facies have weak positive Eu anomaly (Table 4; Fig. 6A-F). It is larger in the micronodules than in the nodules (Table 4). In the micronodules from facies 0 and B the Eu anomaly slightly decreases upwards, whereas in the micronodules from facies C it slightly increases (Table 4).

Mn- micronodules and nodules from all facies show a slight depletion in the light REE relative to the heavy REE ( $La_{NASC}/Lu_{NASC} < 1.00$ ; Table 4). The Mn-nodules are more depleted in light REE than the micronodules (Table 4).

North American Shale Composite (NASC)-normalized REE distribution patterns of the investigated Mn-nodules (Fig. 6A, C, E) are similar to that of the Pacific Mn-nodule standard (Nod-P-1, Fig. 6G). The NASC-normalized REE distribution patterns of the Mn-micronodules (Fig. 6B, D, F) also show some similarity to that of the Pacific Mn-nodule standard (Fig. 6G), but exhibit more pronounced positive both Ce and Yb anomalies. Their positive Ce anomaly is similar to that of the Atlantic Mn-nodule standard (Nod-A-1, Fig. 6H).

#### *4.4. Geochemistry of individual growth structures of Mn-micronodules*

EPMA analyses of the individual growth structures of the Mn-micronodules show high Mn/Fe ratios (2.6 - 699) and Ni+Cu content (1.11 - 5.45 wt.%), while Co contents range from below the detection limits to 0.5 wt.% (Table 5). Nickel and Cu are highly enriched in the growth structures with high Mn/Fe ratio (>6) whereas Co is enriched in the growth structures with lower Mn/Fe ratio (<6). Conspicuous are the very high Mo concentrations of up to 1196 mg/kg in growth structures with low Mn/Fe ratios and up to 1877 mg/kg in growth structures with high Mn/Fe ratios (Table 5).

In general, three different layer growth structures can be distinguished according to their reflectivity and chemistry. Layer type 1 has low reflectivity and low analysis totals (66 – 73 wt.%), probably a result of the porosity of these growth structures. It has low Mn/Fe ratios (2.6 – 6), low Ni+Cu content (1.11 – 1.88 wt.%) and Co contents varying from 0.14 to 0.5 wt.%. These growth structures occur rarely, mostly as coatings around the Mn-micronodules (Fig. 3E,F).

The studied Mn-micronodules consist mostly of layer growth structures with high Mn/Fe ( $\gg 6$ ), high Ni+Cu content, and low Co concentrations (Layer type 2; Table 5). These layer growth structures can be divided into two sub-types according to their reflectivity.

Layer type 2a is dense and has high reflectivity (Fig. 3C-F). Layer growth structures of this type have Mn/Fe ratios varying from 34 to 699, Ni+Cu content between 1.44 and 5.45 wt.%, low Co content ( $< 0.07$  wt.%) and Mo concentrations up to 1704 mg/kg (Table 5).

Layer type 2b has high porosity and low reflectivity (Fig. 3C-E). These layer growth structures have Mn/Fe ratios varying from 8 to 95 and Ni+Cu content slightly lower than that of the layer type 2a (1.93 - 4.17 wt.%). Cobalt content of this layer type is up to 0.5 wt.% whereas Mo content is up to 1877 mg/kg (Table 5).

#### 4.5. Geochemistry of pore waters

Vertical distributions of the elemental concentrations in the pore waters along the sediment core NODKGS65 (Table 6) show three distinct trends (Fig. 7).

(1) Manganese and Fe show relatively stable vertical distribution with similar concentrations along the core with an exception of Mn content increase in the uppermost sediment layer (0-1 cm) (Fig. 7). Phosphorus and Zn also show a similar vertical trend, but have a slight increase in the uppermost (0-5 cm) sediment layer (Fig. 7).

(2) Upward decrease in the content of Si, S, Mg, Ca, and Cr (Fig. 7). Two different patterns of vertical decrease are observed for the different elements: (a) a steady upward decrease along the entire upper 40 cm of the sediment (Si), and (b) an increase in the content from ~40 cm to 20-10 cm sediment depth and decrease toward the seafloor (seawater/sediment interface) (S, Mg, Ca, and Cr; Fig. 7).

(3) Upward increase in the content of Na, K, Rb, Li, Mo, Cd, B, Ni, V, Cu, Ba, Co, U, and Sr (Fig. 7). Although the patterns of increase of the concentrations of these elements differ in details the general trend of their vertical distribution is upward increase.

We do not have data for the vertical distribution of dissolved  $O_2$  concentration along the sediment core NODKGS65. Therefore, in our interpretations of the vertical distribution of elements dissolved in the pore waters of core NODKGS65 we will use the dissolved  $O_2$  profiles along the sediment core NODKGS63, which is close to NODKGS65 (Fig. 1). Dissolved  $O_2$



distribution along the sediment core NODKGS63 and close to a Mn-nodule shows abrupt downward decrease from 177  $\mu\text{mol/L}$  in the bottom seawater to  $\sim 60$   $\mu\text{mol/L}$  at 1 cm depth and then gradual decrease to  $\sim 31.5$   $\mu\text{mol/L}$  at 8 cm depth in the sediment (Fig. 7). Dissolved  $\text{O}_2$  profile beneath the same Mn-nodule (from the same core) shows similar distribution pattern: sharp decrease from  $\sim 120$   $\mu\text{mol/L}$  just below the Mn-nodule to  $\sim 52$   $\mu\text{mol/L}$  at 0.5 cm depth followed by a smooth downward decrease to  $\sim 30$   $\mu\text{mol/L}$  at 9 cm depth (Fig. 7). Similar vertical distribution of dissolved  $\text{O}_2$  in the pore waters of sediments is observed east from the studied area, but still within the CCZ (Mewes et al., 2014, 2016; Kuhn et al., 2017a; Volz et al., 2018):  $[\text{O}_2]$   $\sim 150$ - $160$   $\mu\text{mol/L}$  in the bottom seawater, its abrupt decrease to  $\sim 50$   $\mu\text{mol/L}$  within the upper 5-6 cm of the sediment and a smooth decrease to suboxic values ( $[\text{O}_2] < 5$   $\mu\text{mol/L}$ ; Hein and Koschinsky, 2014). The oxic-suboxic front (oxygen penetration depth) was found at 1.8-3.0 m (Mewes et al., 2014).

#### 4.6. Fe-Cu-Zn-isotope composition of Mn-micronodules and Mn-nodules

Mn-micronodules have Fe-isotope composition ( $\delta^{56}\text{Fe} = -0.43 - -0.27\text{‰}$ ) slightly heavier than that of the paired Mn-nodules ( $\delta^{56}\text{Fe} = -0.63 - -0.39\text{‰}$ ) (Table 7; Fig. 8A). Fe-isotope composition of the studied Mn-micronodules and nodules falls within the  $\delta^{56}\text{Fe}$  range of the Mn-nodules [from  $-1.27$  to  $-0.07\text{‰}$ ; Beard and Johnson (1999), Levasseur et al. (2004), Marcus et al. (2015)] and Fe-Mn-crusts [from  $-1.12$  to  $+1.54\text{‰}$ ; Zhu et al. (2000), Chu et al. (2003), Levasseur et al. (2004), Horner et al. (2015)] measured so far, and is lighter than that of the terrestrial igneous rocks [ $0.09\text{‰}$ ; Beard and Johnson (2004)] (Fig. 9A).  $\delta^{56}\text{Fe}$  of the Mn-micronodules from facies 0 gets lower upward the sediment cores (towards the seawater-sediment interface), whereas that of the micronodules from facies B and C does not change (within the error) across the sediment (Table 7).

Mn-micronodules ( $\delta^{65}\text{Cu} = +0.20 - +0.35\text{‰}$ ) and paired Mn-nodules ( $\delta^{65}\text{Cu} = +0.21 - +0.35\text{‰}$ ) have similar (within the error) Cu-isotope composition (Table 7; Fig. 8B), which falls within those of the Mn-nodules [from  $+0.05$  to  $+0.60\text{‰}$ ; Albarède (2004)] and Fe-Mn-crusts [from  $+0.12$  to  $+0.58\text{‰}$ ; Little et al. (2014b)] investigated previously, and is heavier than that of the terrestrial igneous rocks [ $0\text{‰}$  (Albarède, 2004);  $0.06$ - $0.07\text{‰}$  for bulk silicate Earth (Moynier

et al., 2017)] (Fig. 9B). A slight decrease in  $\delta^{65}\text{Cu}$  of Mn-micronodules is observed upward the sediment cores (Table 7).

The range of Zn-isotope composition of the Mn-micronodules ( $\delta^{66}\text{Zn}_{\text{JMC}} = +0.61 - +0.90\text{‰}$ ) is slightly wider than that of the Mn-nodules ( $\delta^{66}\text{Zn}_{\text{JMC}} = +0.75 - +0.87\text{‰}$ ) although the Zn-isotope composition of the paired micronodules-nodules is quite similar (Table 7; Fig. 8C). They both are within the range of the Zn-isotope composition of the Mn-nodules [from +0.53 to +1.16‰; Maréchal et al. (2000)] and at the lighter end of the Zn-isotope composition of the Fe-Mn-crusts [from +0.80 to +1.23‰; Little et al. (2014b)] studied so far, and are heavier than that of the terrestrial igneous rocks [0.2 – 0.3‰ (Albarède, 2004; Chen et al., 2013); 0.15‰ for bulk silicate Earth (Moynier et al., 2017)] (Fig. 9C).  $\delta^{66}\text{Zn}$  of the Mn-micronodules does not show a visible change (within the error) upward the sediment cores (Table 7).

## 5. Discussion

### 5.1. Mineralogy of Mn-micronodules

Previous works on the mineralogy of the Mn-micronodules (Kidd and Ármannsson, 1979; Lallier-Verges and Clinard, 1983; Poppe et al., 1984; Stoffers et al., 1984; Dekov et al., 2003; Ito et al., 2005; Liao et al., 2019; Little et al., 2020) reported that the main minerals that compose the Mn-micronodules are todorokite and  $\delta\text{-MnO}_2$ . Birnessite and busserite were reported rarely. Mineralogical determinations in most of these works were based on conventional powder XRD only, which casts some doubt on the precision of these determinations. Therefore, we put a little effort on the precise mineralogy of the studied Mn-micronodules.

Our XRD and IR spectroscopy analyses showed clearly that the studied Mn-micronodules and Mn-nodules are dominantly composed of phyllomanganates (10 Å and 7 Å vernadites) and vernadite ( $\delta\text{-MnO}_2$ ). The vernadite and an X-ray amorphous FeOOH were inferred on the basis of the EPMA analyses of the layer growth structures. Vernadite intergrown epitaxially with X-ray amorphous FeOOH is typical for the layer growth structures with low Mn/Fe ratios (Wegorzewski and Kuhn, 2014; Wegorzewski et al., 2015). The low intensity and broadness of the 10 Å and 7 Å peaks at the XRD patterns indicated high distortion of the Mn-octahedral layers as well as very low stacking order of the phyllomanganates (Bodei et al., 2007).

Presence of todorokite in the studied Mn- micronodules and nodules is not supported by our XRD and IR studies. The chemical composition of the Mn-micronodules supports the XRD-IR based conclusion that there is no todorokite. In general, the todorokite-rich Mn-nodules incorporate much lower amounts of Ni and higher amounts of Cu than the phyllomanganate-rich Mn-nodules (Atkins et al., 2014; Heller et al., 2018; Wegorzewski et al., 2020). This suggests that the studied Mn- micronodules and nodules (Tables 3, 5) are composed of phyllomanganates. Furthermore, the Mg concentrations of the Mn- micronodules and nodules (Tables 3, 5) are too low for being todorokite-rich. In principle, the Mn-nodules may contain minor amounts of “defected” todorokite (Bodeř et al., 2007) rather than todorokite (Wegorzewski et al., 2015; 2020). According to the recent studies (Wegorzewski et al., 2020) todorokite appears to be a typical transformation product of 10 Å phyllomanganates after being buried in the sediment column (down to 5 – 10 m) at prevailing suboxic-conditions for a long period of time.

## 5.2. Origin of Mn-micronodules

### 5.2.1. Trace elements constraints

The Mn/Fe ratio and trace element content of the seafloor Fe-Mn-oxyhydroxide deposits have been employed to relate the deposits to their mode of formation (Bonatti et al., 1972; Halbach et al., 1988; Wegorzewski and Kuhn, 2014; Josso et al., 2017). The triangular discrimination diagram of Bonatti et al. (1972) that considers the contents of Fe, Mn and the essential trace elements Cu, Ni and Co in the Fe-Mn-deposits has been widely used. This simple and easily understandable geochemical approach motivated many scientists to improve and make it more precise. Thus, Halbach et al. (1988) proposed a similar diagram recently improved by Wegorzewski and Kuhn (2014), whereas Josso et al. (2017) involved additionally in this conception both the high field strength (HFSE) and rare earth elements.

Employing the diagrams of Wegorzewski and Kuhn (2014) and Josso et al. (2017) (Fig. 10A, B) we can see that the studied Mn-micronodules are diagenetic precipitates (Fig. 10A) that are a result of suboxic diagenesis (Fig. 10B). This conclusion seems to be in contradiction with the current redox state of the pore waters in the sediments from where the Mn-micronodules were collected (0-5, and 5-10 cm) (Fig. 7). Although the dissolved O<sub>2</sub> vertical distribution across the studied sediment shows that below 1 cm depth [O<sub>2</sub>] (~60-30 µmol/L) is 3-6 times lower than that

of the bottom seawater ( $177 \mu\text{mol/L}$ ) (Fig. 7) the dissolved  $\text{O}_2$  concentrations are still well above the suboxic value ( $[\text{O}_2] < 5 \mu\text{mol/L}$ ; Hein and Koschinsky, 2014) [see Tostevin and Poulton (2019) for suboxic sediment characteristics]. Dissolved  $\text{Mn}^{2+}$  concentrations in the studied pore waters ( $0.55 \mu\text{g/kg} = 0.01 \mu\text{mol/L}$ ; Table 6) are similar to those in the upper oxic zone in the sediments east of the area of our studies ( $< 0.1 \mu\text{mol/L}$ ; Mewes et al., 2014) and much lower than those in the suboxic zone in the same sediments ( $0.1 - 50 \mu\text{mol/L}$ ; Mewes et al., 2014). This means that the pore waters in the sediments from which the studied Mn-micronodules were collected are currently oxic although depleted in  $\text{O}_2$  in respect to the bottom seawater (Fig. 7). The suboxic diagenetic origin of the Mn-micronodules may be explained with temporal fluctuation of the oxic-suboxic front in the sediment. Volz et al. (2020) found that the deoxygenation in the NE Pacific during the LGP resulted in compression of the oxic zone in the sediments and precipitation of upward diffusing pore water  $\text{Mn}^{2+}$  in the upper 5 cm of the sediment. The increasing  $[\text{O}_2]$  in the bottom seawater after the LGP has led to a deepening of the oxic-suboxic front in the sediment (Volz et al., 2020). We may speculate that in the past (presumably, during the LGP) the oxic-suboxic front in the studied sediments was close to the seawater/sediment boundary. This might have resulted in suboxic reduction of both solid-phase  $\text{Mn}^{4+}$  (and release of the trace elements adsorbed on it) and solid phases of the trace elements (e.g., Ni, Cu, Mo, etc.) from the sediment, and the upward diffusion of the reduced species (e.g.,  $\text{Mn}^{2+}$ ). Recent deepening of the oxic-suboxic front might have led to re-oxidation of  $\text{Mn}^{2+}$  back to  $\text{Mn}^{4+}$  in the pore waters of the upper sediment layer (0-10 cm) and Mn-micronodule precipitation.

The studied Mn-nodules are diagenetic-hydrogenetic formations according to the diagram of Wegorzewski and Kuhn (2014) (Fig. 10A) whereas the diagram of Josso et al. (2017) classifies them as diagenetic (Fig. 10B). The Mn-nodule standard Nod-A-1 (Atlantic Mn-nodule) is hydrogenetic according to both the Wegorzewski and Kuhn (2014) (Fig. 10A) and Bonatti et al. (1972) (not presented here) diagrams, but hydrogenetic-diagenetic according to the diagram of Josso et al. (2017) (Fig. 10B). The later little deviation makes us assuming that the hydrogenetic and diagenetic fields in the diagram of Josso et al. (2017) (Fig. 10B) need slight refinement. We replaced the original name of the Diagenetic (oxic diagenesis) field (Josso et al., 2017) with Diagenetic only (Fig. 10B) considering that the term oxic diagenesis is not correct (Wegorzewski and Kuhn, 2014; Kuhn et al., 2017b). We have also replaced the metal-rich-hydrothermal trend

(Josso et al., 2017) with the more precise transition metal-rich hydrothermal (Fig. 10B). Thus, we consider that the studied Mn-nodules are rather diagenetic-hydrogenetic than pure diagenetic formations. Mn-nodule standard Nod-P-1 (Pacific Mn-nodule) plots close to our Mn-nodule samples (Fig. 10A, B), which seems reasonable in view of the fact that Nod-P-1 Mn-nodules were collected from the same Clarion-Clipperton zone (Flanagan and Gottfried, 1980) and close to the area of collection of the studied Mn-nodules (Fig. 1). Therefore, we would classify the Nod-P-1 as diagenetic-hydrogenetic Mn-nodules standard.

Both genetic parts of the Mn-nodules, hydrogenetic (upper) and diagenetic (lower), are exposed in an oxic environment: dissolved oxygen concentrations of 177  $\mu\text{mol/L}$  and 118  $\mu\text{mol/L}$ , respectively (Fig. 7). The diagenetic part of the Mn-nodule is enveloped in a dissolved oxygen halo (~0.5 cm thick) within which  $[\text{O}_2]$  sharply decreases from 118 to 52  $\mu\text{mol/L}$  (Fig. 7). It seems likely that the dissolved elements in the sediment pore waters are essentially oxidized in this oxygen halo and accreted to the Mn-nodules.

Chemistry of the individual layer growth structures (see 4.4 and Table 5) confirms the genetic conclusions based on the bulk chemistry of the Mn-micronodules. Previous studies (Wegorzewski and Kuhn, 2014) inferred that the layer type 2 growth structures within Mn-nodules were suboxic-diagenetic precipitates. Our data (sub-section 4.4, Table 5, Fig. 10A) clearly confirms that the layer type 2 (both sub-types 2a and 2b) growth structures are diagenetic precipitates, which are a result of suboxic diagenesis. Although, the layer type 1 shows Mn/Fe ratio up to 6 (Table 5) it might be considered as hydrogenetic growth structure according to the previous work (Wegorzewski and Kuhn, 2014). The heterogeneity and porosity (on a fine scale) of the material that composes these layers seem to be responsible for the slightly higher Mn/Fe ratios and overall lower totals than those typical for the hydrogenetic precipitates (Wegorzewski and Kuhn, 2014). Chemistry of the layer type 1 (sub-section 4.4, Table 5, Fig. 10A) growth structures suggests that they are mixed diagenetic-hydrogenetic and pure hydrogenetic precipitates. However, these growth structures are rare.

### 5.2.2. REE constraints

A recent study on the seafloor Fe-Mn-deposits proposed two diagrams for discrimination among the genetic deposit types (Bau et al., 2014). The diagrams are based on the geochemical relationships controlling the REE and Y. According to this discrimination approach the

hydrogenetic Fe-Mn-deposits are characterized by positive Ce anomaly ( $Ce/Ce^* > 1$ ) and high Nd concentrations ( $> 100$  mg/kg). Thus, the USGS standard for Atlantic Mn-nodule (Nod-A-1) appears to be a hydrogenetic deposit (Bau et al., 2014). Our REE data (Table 4; Fig. 6H) as well as the ternary diagram approach (see sub-section 5.2.1) confirm that the Mn-nodule standard Nod-A-1 is hydrogenetic. The USGS standard for Pacific Mn-nodule (Nod-P-1) seems to be diagenetic-hydrogenetic (weak positive Ce anomaly, Nd  $\sim 100$  mg/kg; Bau et al., 2014) and our data are in good agreement with that (Table 4; Fig. 6G). Following the REE criteria of Bau et al. (2014) our Mn-nodules are diagenetic-hydrogenetic deposits (weak positive or no Ce anomaly, Nd  $> 100$  mg/kg; Table 4, Figs 4A, C, E), which is supported by the ternary diagram approach (see 5.2.1).

Following our geochemical interpretations, the Mn micronodules are diagenetic precipitates, which are a result of suboxic diagenesis (see 5.2.1). According to the classification of Bau et al. (2014) the diagenetic Mn-nodules should have Nd concentrations between 10 and 100 mg/kg, and negative (or no) Ce anomaly. The studied Mn-micronodules do have Nd = 10 – 100 mg/kg (Table 4), but they show positive Ce anomaly (Table 4; Fig. 6B, D, F), which is in contradiction with the criteria of Bau et al. (2014). The positive Ce anomaly in the REE distribution pattern of the Mn-micronodules can be explained following the interpretation of the negative Ce anomaly in the diagenetic Mn-nodules by Bau et al. (2014). Mn-oxide particles scattered in the sediment are primary precipitates in open seawater characterized by positive Ce anomaly (Bau and Koschinsky, 2009). Bau et al. (2014) suppose that the suboxic diagenesis has reduced and quantitatively re-mobilized  $Mn^{2+}$  and  $REE^{3+}$ , but not entire  $Ce^{4+}$  from the sediment solid phases into pore waters. This has resulted in Mn-rich pore waters with deficiency of Ce. This Ce deficit could not have been compensated by later preferential scavenging of Ce from the pore waters during the diagenetic Mn-nodule growth and therefore, these nodules have negative Ce anomaly (Bau et al., 2014). If we assume that during the suboxic diagenesis  $Ce^{4+}$  (seawater-derived) in the sediment is reduced, quantitatively re-mobilized and then scavenged by the Mn-micronodules from pore waters the diagenetically forming Mn-micronodules will acquire positive Ce anomaly. We may speculate that because a major part of  $Ce^{3+}$  dissolved in pore waters has been effectively sequestered by the Mn-micronodules dispersed within the sediment the remaining pore fluid would have had Ce deficit, which will then be recorded in the big slowly growing diagenetic Mn-nodules. The negative Ce anomaly detected in the pore waters (Table 6;

calculated relative to La and Nd instead of La and Pr because of lack of Pr concentration data) may be interpreted from this point of view.

In other words, the model of Bau et al. (2014) is correct with the little detail we added here about the intermediate role of the Mn-micronodules: suboxic quantitative re-mobilization of seawater-derived Ce in the sediment and its sequestration by Mn-micronodules that leaves behind pore water with Ce deficit, which feeds the diagenetic Mn-nodules.

### 5.3. Source of elements to the Mn-micronodules

The three patterns of vertical distribution of the elemental concentrations in the sediment pore waters, (1) stable with no substantial fluctuations (Mn, Fe and probably P and Zn), (2) upward decrease (Si, S, Mg, Ca, and Cr) and (3) upward increase (Na, K, Rb, Li, Mo, Cd, B, Ni, V, Cu, Ba, Co, U, and Sr) (Fig. 7), are likely a result of differences in the redox remobilization (dissolution) and immobilization (reprecipitation, scavenging) of the elements. The remobilization and immobilization of elements in the pore waters depend on a number of environmental controls: e.g., Eh, pH, T, ion activities, etc. These controls, excluding dissolved O<sub>2</sub> concentration (a measure for the Eh), were not investigated in the course of this study because our focus was not on the pore waters but on the Mn-micronodules. Therefore, the interpretation of the pore water chemistry (the reasons for different behaviour of the elements in it) is beyond the scope of this work. We can in general, infer that the mild oxic conditions in the pore waters ([O<sub>2</sub>] < 60 µmol/L below 1 cm depth; Fig. 7) may be responsible for the remobilization of some elements (Na, K, Rb, Li, Mo, Cd, B, Ni, V, Cu, Ba, Co, U, and Sr) from the sediment and their upward flux towards the seawater/sediment boundary.

We will comment on the pore waters in the studied sediment as possible source of elements to both the bottom seawater and Mn-micronodules.

We have not studied the chemistry of the bottom seawater at the area of investigation and therefore, we will use the chemical composition of the North Pacific deep seawater (see the references in the figure caption to Figure 7) in our approach. Comparing the chemistry of the North Pacific deep seawater with that of the studied pore waters (Fig. 7) we can suppose that there is a diffusion flux of Mn, Fe, Si, Ca, Na, K, Rb, Li, Mo, Cd, Ni, V, Cu, Ba, Co, P, Zn, Cr, and Sr dissolved in the pore waters towards the bottom seawater. I.e., the pore waters of the

studied sediments are a source of these elements to seawater. Concentrations of S and Mg in the pore waters are close to those in the deep seawater (Fig. 7) which suggests that most probably there is no flux of these elements either from the sediment to the seawater or from the seawater to the sediment. Concentrations of U and B in the bottom seawater are higher than those in the pore waters which means that the bottom seawater may be a source of these elements to the pore waters.

Concentrations of Mn, Si, S, Mg, Na, Li, Mo, Cd, B, Ni, Cu, Ba, U, P, Zn, and Cr in the Mn-micronodules co-vary with those in the pore waters (Fig. 7). This suggests that the pore waters are likely source of these elements in the Mn-micronodules. It is challenging to explain the reverse correlation of the concentrations of Fe, V, Co, Ca, Sr, K, and Rb in the Mn-micronodules with those in the pore waters. It seems reasonable to assume that the concentrations of Fe, V, Co, Sr, K, and Rb in the Mn-micronodules is a function of the micronodule age: the older Mn-micronodules (deeper in the sediment) have had more time to scavenge higher amount of elements than the younger Mn-micronodules (at the sediment surface) notwithstanding the increased concentrations of these elements in the source pore waters towards the sediment surface.

#### 5.4. Fe-Cu-Zn-isotope composition of Mn-micronodules

Studied Mn-micronodules are suboxic diagenetic precipitations formed within the sediment whereas their paired Mn-nodules are hydrogenetic-diagenetic formations formed at the sediment-seawater boundary (see 5.2). A detailed study of the Mn-nodules from the same Clarion-Clipperton zone showed they were composed of alternating diagenetic and hydrogenetic layers (Wegorzewski and Kuhn, 2014). Hence, our bulk Mn-nodule samples likely average the diagenetic and hydrogenetic influence on the nodule Fe-isotope composition.

Although the Fe-isotope composition of seawater ranges from -1.35 to +0.80‰ (Lacan et al., 2008; Conway and John, 2014a; Chever et al., 2015; Fitzsimmons et al., 2016; Abadie et al., 2017) the bottom seawater, which is directly responsible for the hydrogenetic precipitation of Fe has  $\delta^{56}\text{Fe} \sim 0.5\text{‰}$  (Horner et al., 2015; Fitzsimmons et al., 2016; Abadie et al., 2017). Can hydrogenetic precipitation of Fe-oxyhydroxides from deep seawater ( $\delta^{56}\text{Fe} \sim 0.5\text{‰}$ ) account for the observed negative  $\delta^{56}\text{Fe}$  of the Mn-micronodules and nodules (Fig. 8A; Table 7) if we



consider the identified Fe isotope fractionation during hydrogenetic precipitation of Fe? The estimated Fe isotopic fractionation factor between pure hydrogenetic Fe-oxyhydroxide precipitates (Fe-Mn crusts) and seawater is  $\Delta^{56/54}\text{Fe}_{\text{FeMn-SW}} = \delta^{56/54}\text{Fe}_{\text{FeMn}} - \delta^{56/54}\text{Fe}_{\text{SW}} = -0.77\text{‰}$  (Horner et al., 2015). If we consider that the deep seawater responsible for hydrogenetic precipitation of Fe-oxyhydroxides on the seafloor has mean  $\delta^{56}\text{Fe}_{\text{SW}} = 0.5\text{‰}$  (Horner et al., 2015; Fitzsimmons et al., 2016; Abadie et al., 2017) then, the hydrogenetic Fe-oxyhydroxide precipitates on the seafloor will have  $\delta^{56}\text{Fe} = -0.27\text{‰}$ . This  $\delta^{56}\text{Fe}$  is close to the Fe-isotope composition of the studied Mn-micronodules and nodules (Table 7) and implies that the hydrogenetic processes may have played a substantial role in their formation.

However, our mineralogical and geochemical studies suggest that the studied Mn-micronodules have suboxic diagenetic genesis whereas the Mn-nodules are hydrogenetic-diagenetic formations. Can the diagenetic processes in the sediment be major control on the Fe-isotope composition of both the micronodules and nodules? It was found that the oxic clastic sediments have  $\delta^{56}\text{Fe} = 0.09\text{‰}$  (Beard and Johnson 2004). The reduction of the sedimentary Fe (presumably with  $\delta^{56}\text{Fe} = 0.09\text{‰}$ ) fractionates Fe-isotopes and produces an isotopically light dissolved Fe flux ( $\delta^{56}\text{Fe} = -3.91\text{‰}$  to  $+0.00\text{‰}$ ) that may further be transferred to the seawater column (Johnson et al., 2002; Severmann et al., 2002; Welch et al., 2003; Severmann et al., 2010; John et al., 2012; Klar et al., 2017). The precipitation of the Mn-micronodules and nodules from the dissolved negative Fe isotope pool ( $\delta^{56}\text{Fe} = -3.91\text{‰}$  to  $+0.00\text{‰}$ ) in the sediment during diagenetic processes or during hydrogenetic precipitation will result in negative  $\delta^{56}\text{Fe}$  values of both the Mn-micronodules and nodules (Fig. 8A; Table 7). This suggests that the diagenetic processes may have important control on the Fe-isotope composition of the studied Mn-micronodules and nodules. The slightly lighter Fe-isotope composition of the Mn-nodules (lying on the sediment) than that of the paired Mn-micronodules (within the sediment) (Fig. 8A; Table 7) may also be explained with diagenetic processes: the pore waters near the sediment-seawater boundary have Fe-isotope composition lighter than that of the deeper pore waters (Severmann et al., 2010; Klar et al., 2017). The decrease of  $\delta^{56}\text{Fe}$  of the Mn-micronodules from facies 0 upward the sediment cores (towards the seawater-sediment interface) (Fig. 8A; Table 7) supports this interpretation.

Overall, the Fe-isotope composition of the Mn- micronodules and nodules does not give an unambiguous answer about their origin. It can equally be a result of either hydrogenetic or diagenetic nature.

$\delta^{65}\text{Cu}$  of the studied Mn- micronodules and nodules, as well as that of the Mn-nodules and Fe-Mn-crusts studied so far (Fig. 9B) is lower than that of the dissolved Cu in the deep (below 800 m) ocean [ $+0.66 \pm 0.07\%$ ; Vance et al. (2008), Takano et al. (2014), Thompson and Ellwood (2014), Moynier et al. (2017), Little et al. (2018)]. Lighter Cu-isotope composition of hydrogenetic Fe-Mn-crusts [ $\delta^{65}\text{Cu} = +0.12 - +0.58\%$ ; Little et al. (2014b)] and hydrogenetic-diagenetic Mn-nodules [ $\delta^{65}\text{Cu} = +0.05 - +0.60\%$ ; Albarède (2004)] than that of seawater is consistent with preferential scavenging of  $^{63}\text{Cu}$  and gradual accumulation of  $^{65}\text{Cu}$  in seawater (Albarède, 2004; Little et al., 2014a; Takano et al., 2014; Michi et al., 2018). Preferential scavenging of  $^{63}\text{Cu}$  from seawater [ $\delta^{65}\text{Cu} = +0.66\%$ ; Vance et al. (2008)] on the Mn- and Fe-oxyhydroxides explains the Cu-isotope composition of the studied hydrogenetic-diagenetic Mn-nodules ( $\delta^{65}\text{Cu} = +0.21 - +0.35\%$ ; Table 7). However, which are the processes leading to the identical Cu-isotope composition of the truly diagenetic Mn-micronodules ( $\delta^{65}\text{Cu} = +0.20 - +0.35\%$ ; Table 7)? Obviously, the Mn-micronodules and the diagenetic layers in the Mn-nodules have received their Cu from the dissolved Cu pool in the pore waters. Unfortunately, we are not aware of any data for the Cu-isotope composition of the pore waters in marine sediments. Therefore, our interpretations will be preliminary and speculative. The chemical composition of the pore waters is mostly controlled by the interaction between the sediment particles and water: dissolution/precipitation, adsorption/desorption, etc. Thus, the Cu-isotope composition of the pore waters will broadly depend on the isotope composition of the sediment particles. Sediment particles of the sediment are of two major types: detrital (lithogenic) and biogenic (organic matter-related). Average lithogenic Cu isotope composition is  $+0.08\%$  (Moynier et al., 2017), whereas the organic matter-related (bioauthigenic) Cu in the sediments has  $\delta^{65}\text{Cu} = +0.28\%$  (Little et al., 2017). If we assume that no Cu-isotope fractionation occurs upon dissolution or desorption of any of these two sediment components, no binary mixing of dissolved both lithogenic Cu ( $+0.08\%$ ) and bioauthigenic Cu ( $+0.28\%$ ) (in any proportions) can explain the Cu-isotope composition of the micronodules ( $+0.20 - +0.35\%$ ) keeping in mind that scavenging of  $\text{Cu}_{\text{aq}}$  on the Mn-Fe-oxyhydroxides will drive the source  $\delta^{65}\text{Cu}$  to lower values (preferentially retaining lighter  $^{63}\text{Cu}$ ). Thus, the  $\text{Cu}_{\text{aq}}$  released from the sediment particles to the pore waters

needs to be heavier than Cu in the source particles. In fact, it was found that abiotic oxidation of Cu<sup>+</sup>-containing minerals releases isotopically heavier Cu<sub>aq</sub><sup>2+</sup> than the source mineral (e.g., Mathur et al., 2005). This will provide the heavy Cu ( $\delta^{65}\text{Cu} > +0.28\text{‰}$ ) necessary for the Cu-isotope composition (+0.20 – +0.35‰) of the diagenetic Mn-micronodules. The slight decrease of  $\delta^{65}\text{Cu}$  of the Mn-micronodules upward the sediment cores (Table 7) seems to be a result of the progressive depletion of the heavy diagenetic upward flux in <sup>63</sup>Cu. This would mean that the benthic Cu flux from the sediment to bottom seawater must be heavy. Indeed, Takano et al. (2014) reported values of the Cu-isotope composition of the benthic input ( $\delta^{65}\text{Cu} = +0.58\text{‰}$ ) close to that of the deep seawater ( $\delta^{65}\text{Cu} = +0.66\text{‰}$ ).

It is known that the speciation of Cu dissolved in seawater is organically controlled (Coale and Bruland, 1988; Moffett and Dupont, 2007). The major part of Cu dissolved in the pore waters of coastal marine sediments is as organic complexes and a very small fraction of it is as inorganic species (Skrabal et al., 2000). The organic complexation of Cu was found to be associated with Cu isotope fractionation: Cu-binding ligands preferentially complex the heavy Cu isotope (Pokrovsky et al., 2008; Bigalke et al., 2010b; Navarrete et al., 2011; Ryan et al., 2014; Sherman, 2013; Sherman et al., 2015; Sherman and Little, 2020). We are not aware of any investigation of Cu isotope fractionation in the pore waters of abyssal plain sediments, but in view of the previous studies we may suppose that Cu organic complexation plays an essential role in the Cu isotope fractionation in the pore waters and eventually, in the Cu isotope composition of the Mn-micronodules.

It was found (Little et al., 2014b) that the Zn-isotope composition of the Fe-Mn-crusts [hydrogenetic deposits,  $\delta^{66}\text{Zn}_{\text{JMC}} = +0.80 - +1.23\text{‰}$  (Little et al., 2014b)] and Mn-nodules [hydrogenetic and hydrogenetic-diagenetic deposits;  $\delta^{66}\text{Zn}_{\text{JMC}} = +0.53 - +1.16\text{‰}$  (Maréchal et al., 2000)] is heavier than that of the seawater [ $\delta^{66}\text{Zn}_{\text{JMC}} = +0.46 - +0.51\text{‰}$ ; Little et al. (2014b), Lemaitre et al. (2020)]. Zn-isotope composition of the studied Mn-micronodules ( $\delta^{66}\text{Zn}_{\text{JMC}} = +0.61 - +0.90\text{‰}$ ; Table 7) and Mn-nodules ( $\delta^{66}\text{Zn}_{\text{JMC}} = +0.75 - +0.87\text{‰}$ ; Table 7) is also heavier than that of the seawater. Little et al. (2014b) explain the heavier Zn-isotope composition of the hydrogenetic Fe-Mn-deposits relative to that of seawater with equilibrium isotope partitioning between dissolved and adsorbed Zn when Zn<sub>aq</sub> is either free or inorganically-speciated. In such a case the heavy <sup>66</sup>Zn adsorbs more readily than the light <sup>64</sup>Zn due to preferential sorption of heavy

Zn isotopes on Fe-Mn-oxyhydroxides surfaces (e.g., Bryan et al., 2015). This mechanism explains the Zn-isotope composition of the studied hydrogenetic-diagenetic Mn-nodules.

Diagenetic Mn-micronodules receive their Zn content from the pore waters. Therefore, the Zn-isotope composition of the Mn-micronodules seems to be controlled by the processes of Zn isotope fractionation in the pore water (in the sediment). Conway and John (2014b) found that the continental margin sediments are a source of isotopically light Zn ( $\delta^{66}\text{Zn}_{\text{JMC}} = -0.5 - -0.8\%$ ) to the ocean. The light Zn isotope flux is supposed to be released from degrading phytoplankton material [with light Zn-isotope composition; e.g., Kobberich et al. (2019)] within the sediments. Although the studied Mn- micronodules and nodules are within and on top, respectively, of abyssal plain sediments we can suppose that in a similar way (e.g., Conway and John, 2014b) the decay of the buried organic matter in the sediment releases light Zn and creates a light Zn isotope pool ( $\delta^{66}\text{Zn}_{\text{JMC}} < 0\%$ ) in the pore waters. Substantial Zn isotope fractionation is necessary in the pore water (with presumably  $\delta^{66}\text{Zn}_{\text{JMC}} < 0\%$ ) in order to reach the Zn-isotope composition of the Mn-micronodules ( $\delta^{66}\text{Zn}_{\text{JMC}} = +0.61 - +0.90\%$ ). We may speculate again that if the dissolved  $\text{Zn}_{\text{aq}}$  in the pore waters is either free or inorganically-speciated then, the heavy  $^{66}\text{Zn}$  will be adsorbed preferentially on the Mn-Fe-oxyhydroxides than the light  $^{64}\text{Zn}$  (e.g., Bryan et al., 2015). This will result in heavy Zn-isotope composition of the Mn-micronodules and diagenetic layers of the Mn-nodules.

Major part of the Zn dissolved in seawater (up to 98%) is also (like Cu) complexed to organic ligands (Wells et al., 1992; Bruland, 1999; John et al., 2007). The organic complexation of Zn also results in Zn isotope fractionation: heavy Zn isotope enrichment of the organic complexes (Jouvin et al., 2009; Markovic et al., 2017). We do not know of any study on the Zn isotope fractionation in marine sediment pore waters, but are challenged to speculate that the organic complexation of Zn might play an important role in the Zn isotope fractionation in sediment pore waters and Zn isotope composition of the Mn-micronodules.

Fe-Cu-Zn-isotope composition of the Mn-nodule standard Nod-P-1 (Pacific Mn-nodule) (Table 7) agrees well with that measured previously [ $\delta^{56}\text{Fe} = -0.51 \pm 0.09\%$  (Marcus et al., 2015);  $\delta^{65}\text{Cu} = 0.35 - 0.46 (\pm 0.05 - 0.08)\%$  (Jochum et al., 2005; Chapman et al., 2006; Pontér et al., 2021);  $\delta^{66}\text{Zn} = 0.63 - 0.87 (\pm 0.02 - 0.09)\%$  (Chapman et al., 2006; Bigalke et al., 2010a; Gagnevin et al., 2012; Chen et al., 2016; Druce et al., 2020)] and falls within the range of the isotope composition of the studied Mn-nodules (Fig. 9A, B, C) confirming the same

hydrogenetic-diagenetic nature of the studied and standard nodules. However, its Fe- and Zn-isotope compositions are lighter than that of the Mn-nodule standard Nod-A-1 (Atlantic Mn-nodule) [ $\delta^{56}\text{Fe} = -0.42 - -0.37 (\pm 0.06 - 0.08)\%$  (Dideriksen et al., 2006; Ellwood et al., 2015; Marcus et al., 2015);  $\delta^{66}\text{Zn} = 0.96 - 1.01 (\pm 0.01 - 0.03)\%$  (Chen et al., 2016; Druce et al., 2020)] whereas its Cu-isotope composition does not differ (within the uncertainty) from that of the Nod-A-1 standard [ $\delta^{65}\text{Cu} = 0.42 \pm 0.07\%$  (Pont er et al., 2021)]. These differences and similarity in the Fe-Cu-Zn-isotope composition of the hydrogenetic-diagenetic (Nod-P-1) and hydrogenetic (Nod-A-1) Mn-nodules are challenging to be investigated, but not straightforward to be explained and fall beyond the scope of this work.

### 5.5. Can Mn-micronodules be potential resource for valuable elements?

Mn-micronodules are ubiquitous in marine sediments from almost all seafloor settings: from mid-ocean ridges to abyssal deeps excluding the continental margins. Combining their wide global occurrence with narrow stratigraphic distribution [they are mostly concentrated in the uppermost ~1 m of the sediment cover (Sval'nov et al., 1991a; Pattan, 1993; Chauhan and Rao, 1999; Dubinin and Sval'nov, 2000b)] and easy extraction (magnetic or electro-magnetic) from the loose sediment makes them possible active resource for valuable chemical elements.

In order to estimate the potential of Mn-micronodules as a resource for valuable elements we made a compilation of all chemistry data we are aware of (Table 8). We have not included in this data set some of the old data with unclear analytical approach (we could not estimate the quality of the data) as well as the data received with both electron microprobe and laser ablation ICP-MS (these two approaches give the chemical composition at single points and are not representative for the Mn-micronodules as a whole). The compilation (Table 8) shows that the chemical data for Mn-micronodules are scarce. Most of the works report the concentrations of Mn, Fe, some transition metals (Cu, Ni, Co) and REE only. Very few works give the concentrations of wide spectrum of elements. With such a poor data base it is not possible to give a meaningful estimation of the resource potential of the Mn-micronodules in global aspect [locally, Yasukawa et al. (2020) estimated it for the area of the Minamitorishima Island, Pacific Ocean]. In order to get a rough idea about the economic potential of the Mn-micronodules we

have compared their chemistry with that of their big and fairly well studied counterparts, Mn-nodules (Table 8).

Although the concentrations of different elements are variable in the Mn-micronodules from different settings we can see that they, in general, are poorer in most elements than the Mn-nodules (e.g., twice poorer in REE) (Table 8). Manganese, Ni, Cu, Zn, and Mo appear to be the main elements of potential economic interest that are in the Mn-micronodules in concentrations higher than those in the Mn-nodules. In a future more precise estimation of the economic potential of the Mn-micronodules (more studies are necessary) these elements have to receive particular attention.

## 6. Summary

Mn-micronodules in the sediments of the Clarion-Clipperton zone in the Pacific Ocean are composed of 10 Å and 7 Å phyllosulfates, and vernadite ( $\delta$ -MnO<sub>2</sub>). Their internal structure shows fine concentric growth layers, which have varying chemistry and reflectivity. According to that three different layer growth structures were distinguished: (1) layer type 1 with low Mn/Fe ratio (2.6 – 6), low Ni+Cu content (1.11 – 1.88 wt.%), high Co content (0.14 - 0.5 wt.%), and low reflectivity; (2) layer type 2a with high Mn/Fe ratio (34 - 699), high Ni+Cu content (1.44 - 5.45 wt.%), low Co content (<0.07 wt.%), and high reflectivity; (3) layer type 2b with medium Mn/Fe ratio (8 - 95), medium to high Ni+Cu content (1.93 - 4.17 wt.%), high Co content (up to 0.5 wt.%), and low reflectivity.

Interpreting the chemistry of the studied Mn-micronodules and Mn-nodules (Fe, Mn, Ni, Cu, HFSE and REE concentrations) we inferred that: (1) the Mn-micronodules are diagenetic precipitates, which are a result of suboxic diagenesis; and (2) the Mn-nodules are diagenetic-hydrogenetic formations. Fine scale investigations revealed that the most common growth structures (layer type 2) within the Mn-micronodules are suboxic-diagenetic, whereas the rare growth structures (layer type 1) are mixed diagenetic-hydrogenetic and hydrogenetic precipitates. However, the current redox state of the pore waters in the sediments where the Mn-micronodules have formed is oxic (although approaching suboxic values). Thus, the suboxic diagenetic origin of the Mn-micronodules may be explained with temporal fluctuation of the oxic-suboxic front in the sediment. We assume that during the LGP the oxic-suboxic front in the sediments had been

close to the seawater/sediment boundary. This might have resulted in suboxic reduction of solid-phase  $\text{Mn}^{4+}$  and other elements in the sediment and the upward diffusion of the reduced species. Recent deepening of the oxic-suboxic front might have led to re-oxidation of  $\text{Mn}^{2+}$  in the pore waters of the upper sediment layer and Mn-micronodule precipitation.

The positive Ce anomaly and Nd content (10 - 100 mg/kg) of the Mn-micronodules contradict the REE criteria for diagenetic Mn-oxide deposition according to the previous research. We explain these features with suboxic quantitative re-mobilization of seawater-derived Ce in the sediment and its sequestration by Mn-micronodules that results in Ce-deficient pore water. This Ce deficiency is recorded in the diagenetic Mn-nodules.

The pore waters of the studied sediments are the most probable source of Mn, Si, S, Mg, Na, Li, Mo, Cd, B, Ni, Cu, Ba, U, P, Zn, and Cr in the Mn-micronodules. They are also a source of Mn, Fe, Si, Ca, Na, K, Rb, Li, Mo, Cd, Ni, V, Cu, Ba, Co, P, Zn, Cr, and Sr to the bottom seawater. The bottom seawater in turn is a source of U and B to the pore waters.

Investigation of the Fe-Cu-Zn isotope composition of the Mn-micronodules and Mn-nodules provided additional information on the geochemical processes occurring in the sediment and leading to micronodule and nodule precipitation. The measured Fe-isotope composition of the Mn-micronodules and nodules can be explained by either hydrogenetic or diagenetic precipitation of the Fe-oxyhydroxide component. However, relying on the inferred suboxic diagenetic origin of the Mn-micronodules (based on our mineralogical and geochemical studies) we would suggest rather a major diagenetic than hydrogenetic control on their Fe-isotope composition following: (1) reduction of the sedimentary Fe ( $\delta^{56}\text{Fe} = 0.09\text{‰}$ ), (2) fractionation of Fe-isotopes leading to an isotopically light ( $\delta^{56}\text{Fe} = -3.91\text{‰}$  to  $+0.00\text{‰}$ ) dissolved Fe pool in the sediment (and flux to the seawater column), followed by (3) Fe-oxyhydroxide precipitation with preferential uptake of  $^{56}\text{Fe}$  leading to (still) light Fe isotope composition of both the Mn-micronodules and diagenetic layers of the Mn-nodules ( $\delta^{56}\text{Fe} = -0.63$  to  $-0.27\text{‰}$ ). Lighter Fe isotopes of the Mn-nodules ( $-0.63\text{‰}$  -  $-0.39\text{‰}$ ) than that of the Mn-micronodules ( $-0.43\text{‰}$  -  $-0.27\text{‰}$ ) supports the influence of the diagenetic processes on the fractionation of Fe isotopes.

Preferential scavenging of the light  $^{63}\text{Cu}$  from seawater ( $\delta^{65}\text{Cu} = +0.66\text{‰}$ ) on the Mn- and Fe-oxyhydroxides accounts for the Cu-isotope composition of the studied hydrogenetic-diagenetic Mn-nodules ( $\delta^{65}\text{Cu} = +0.21$  -  $+0.35\text{‰}$ ) lighter than that of seawater ( $\delta^{65}\text{Cu} = 0.7$  -  $0.9\text{‰}$ ). The diagenetic Mn-micronodules have Cu-isotope composition ( $\delta^{65}\text{Cu} = +0.20$  -

+0.35‰) identical to that of the hydrogenetic-diagenetic Mn-nodules. The oxidative dissolution of the sedimentary components ( $\delta^{65}\text{Cu} = +0.08 - +0.28\text{‰}$ ) releases isotopically heavy  $\text{Cu}_{\text{aq}}^{2+}$  ( $\delta^{65}\text{Cu} > +0.28\text{‰}$ ) in the pore waters. This diagenetic Cu-isotope pool is subsequently recorded in the diagenetic Mn-micronodules (considering preferential scavenging of the light  $^{63}\text{Cu}$ ) and appears to be similar to that of the hydrogenetic Cu-isotope pool (bottom seawater).

The heavier Zn-isotope composition of the studied hydrogenetic-diagenetic Mn-nodules ( $\delta^{66}\text{Zn}_{\text{JMC}} = +0.75 - +0.87\text{‰}$ ) relative to that of the seawater ( $\delta^{66}\text{Zn}_{\text{JMC}} = +0.46 - +0.51\text{‰}$ ) is interpreted to be a result of equilibrium isotope partitioning between dissolved and adsorbed Zn when  $\text{Zn}_{\text{aq}}$  is either free or inorganically-specified. In such a case, the heavy  $^{66}\text{Zn}$  adsorbs more readily than the light  $^{64}\text{Zn}$  due to preferential sorption of heavy Zn isotopes on Fe-Mn-oxyhydroxides surfaces. Preferential adsorption of  $^{66}\text{Zn}$  from the light Zn isotope pool ( $\delta^{66}\text{Zn}_{\text{JMC}} < 0\text{‰}$ ) of the pore waters ( $\text{Zn}_{\text{aq}}$  is either free or inorganically-specified) on the Mn-Fe-oxyhydroxides has resulted in heavy Zn-isotope composition of the Mn-micronodules ( $\delta^{66}\text{Zn}_{\text{JMC}} = +0.61 - +0.90\text{‰}$ ) and diagenetic layers of the Mn-nodules.

In general, the chemical data for Mn-micronodules are scarce and it is not possible to give a meaningful estimation of their resource potential with such a limited database. The Mn-micronodules are poorer in most elements than the Mn-nodules and only Mn, Ni, Cu, Zn, and Mo are in concentrations higher than those in the Mn-nodules.

## Acknowledgements

The captain and crew of the R/V *L'Atalante* are thanked for their efforts to support the sampling and onboard sample treatment. Sincere thanks go to: M. Ranneberg for supporting the XRD analyses, M. Hein for the IR determinations, and D. Henry (all from BGR) for preparation of the polished block section. This research was supported by a LabexMER Axis 3 (Geobiological interactions in extreme environments; Institut Universitaire Européen de la Mer, Université de Bretagne Occidentale) grant (project NODESIS) to V. M. Dekov.

## References

Abadie, C., Lacan, F., Radic, A., Pradoux, C., Poitrasson, F., 2017. Iron isotopes reveal distinct dissolved iron sources and pathways in the intermediate versus deep Southern Ocean. PNAS 114, 858-863.



- Addy, S.K., 1978. Distribution of Fe, Mn, Cu, Ni and Co in coexisting manganese nodules and micronodules. *Mar. Geol.* 28, M9-M17.
- Addy, S.K., 1979. Rare earth element patterns in manganese nodules and micronodules from northwest Atlantic. *Geochim. Cosmochim. Acta* 43, 1105-1115.
- Albarède, F., 2004. The stable isotope geochemistry of copper and zinc. *Rev. Mineral. Geochem.* 55, 409-427.
- Alibo, D.S., Nozaki, Y., 1999. Rare earth elements in seawater: particle association, shale-normalization, and Ce oxidation. *Geochim. Cosmochim. Acta* 63, 363-372.
- Archer, C., Andersen, M.B., Cloquet, C., Conway, T.M., Dong, S., Ellwood, M., Moore, R., Nelson, J., Rehkämper, M., Rouxel, O., Samanta, M., Shin, K.-C., Sohrin, Y., Takano, S., Wasylenki, L., 2017. Inter-calibration of a proposed new primary reference standard AA-ETH Zn for zinc isotopic analysis. *J. Anal. At. Spectrom.* 32, 415-419.
- Atkins, A.L., Shaw, S., Peacock, C.L., 2014. Nucleation and growth of todorokite from birnessite: Implications for trace-metal cycling in marine sediments. *Geochim. Cosmochim. Acta* 114, 109-125.
- Axelsson, M.D., Rodushkin, I., Ingri, J., Öhlander, B., 2002. Multielemental analysis of Mn-Fe nodules by ICP-MS: optimisation of analytical method. *Analyst* 127, 76-82.
- Banerjee, R., Iyer, S.D., 1991. Biogenic influence on the growth of ferromanganese micronodules in the Central Indian Basin. *Marine Geology* 97, 413-421.
- Bau, M., Koschinsky, A., 2009. Oxidative scavenging of cerium on hydrous Fe oxide: evidence from the distribution of rare earth elements and yttrium between Fe oxides and Mn oxides in hydrogenetic ferromanganese crusts. *Geochem. J.* 43, 37-47.
- Bau, M., Schmidt, K., Koschinsky, A., Hein, J., Kunz, T., Usui, A., 2014. Discriminating between different genetic types of marine ferro-manganese crusts and nodules based on rare earth elements and yttrium. *Chemical Geology* 381, 1-9.
- Beard, B.L., Johnson, C.M., 1999. High precision iron isotope measurements of terrestrial and lunar materials. *Geochimica et Cosmochimica Acta* 63, 1653-1660.
- Beard, B.L., Johnson, C.M., 2004. Fe isotope variations in the modern and ancient Earth and other planetary bodies. *Rev. Mineral. Geochem.* 55, 319-357.
- Beard, B.L., Johnson, C.M., Von Damm, K.L., Poulson, R.L., 2003. Iron isotope constraints on Fe cycling and mass balance in the oxygenated Earth oceans. *Geology* 31, 629-632.
- Bigalke, M., Weyer, S., Kobza, J., Wilcke, W., 2010a. Stable Cu and Zn isotope ratios as tracers of sources and transport of Cu and Zn in contaminated soil. *Geochimica et Cosmochimica Acta* 74, 6801-6813.
- Bigalke, M., Weyer, S., Wilcke, W., 2010b. Copper isotope fractionation during complexation with insolubilized humic acid. *Environ. Sci. Technol.* 44, 5496-5502.
- Bodeř, S., Manceau, A., Geoffroy, N., Baronnet, A., Buatier, M., 2007. Formation of todorokite from vernadite in Ni-rich hemipelagic sediments. *Geochimica et Cosmochimica Acta* 71, 5698-5716.
- Bonatti, E., Kraemer, T., Rydell, H., 1972. Classification and genesis of submarine iron manganese deposits. In: Horn, D.R. (Ed.), *Ferromanganese Deposits on the Ocean Floor*. Lamont-Doherty Geological Observatory of Columbia University, Palisades, N.Y., pp. 147-166.

- Bruland, K.W., 1980. Oceanographic distributions of cadmium, zinc, nickel and copper in the North Pacific. *Earth Planet. Sci. Lett.* 47, 176-198.
- Bruland, K.W., 1999. Complexation of zinc by natural organic ligands in the central North Pacific. *Limnol. Oceanogr.* 34, 269-285.
- Bryan, A.L., Dong, S., Wilkes, E.B., Wasylenki, L.E., 2015. Zinc isotope fractionation during adsorption onto Mn oxyhydroxide at low and high ionic strength. *Geochimica et Cosmochimica Acta* 157, 182-197.
- Chan, L.H., Edmond, J.M., Stallard, R.F., Broecker, W.S., Chung, Y.C., Weiss, R.F., Ku, T.L., 1976. Radium and barium at GEOSECS stations in the Atlantic and Pacific. *Earth Planet. Sci. Lett.* 32, 258-267.
- Chapman, J.B., Mason, T.F.D., Weiss, D.J., Coles, B.J., Wilkinson, J.J., 2006. Chemical separation and isotopic variations of Cu and Zn from five geological reference materials. *Geostandards and Geoanalytical Research* 30, 5-16.
- Chauhan, O.S., Rao, Ch.M., 1999. Influence of sedimentation on enrichment of manganese and growth of ferromanganese micronodules, Bengal Fan, India. *Marine Geology* 161, 39-47.
- Chen, H., Savage, P.S., Teng, F.-Z., Helz, R.T., Moynier, F., 2013. Zinc isotope fractionation during magmatic differentiation and the isotopic composition of the bulk Earth. *Earth Planet. Sci. Lett.* 369-370, 34-42.
- Chen, J.H., Edwards, R.L., Wasserburg, G.J., 1986.  $^{238}\text{U}$ ,  $^{234}\text{U}$  and  $^{232}\text{Th}$  in seawater. *Earth Planet. Sci. Lett.* 80, 241-251.
- Chen, S., Liu, Y., Hu, J., Zhang, Z., Hou, Z., Huang, F., Yu, H., 2016. Zinc isotopic compositions of NIST SRM 683 and whole-rock reference materials. *Geostandards and Geoanalytical Research* 40, 417-432.
- Chester, R., Hughes, M.J., 1967. A chemical technique for the separation of ferro-manganese minerals, carbonate minerals and adsorbed trace elements from pelagic sediments. *Chemical Geology* 2, 249-262.
- Chever, F., Rouxel, O.J., Croot, P.L., Ponzevara, E., Wuttig, K., Auro, M., 2015. Total dissolvable and dissolved iron isotopes in the water column of the Peru upwelling regime. *Geochim. Cosmochim. Acta* 162, 66-82.
- Chu, N.-C., Johnson, C.M., Beard, B.L., German, C.R., Nesbitt, R.W., Usui, A., 2003. Secular Fe isotope variations in the central Pacific Ocean. *Geochim. Cosmochim. Acta* 67, A66.
- Coale, K.H., Bruland, K.W., 1988. Copper complexation in the northeast Pacific. *Limnol. Oceanogr.* 33, 1084-1101.
- Collier, R.W., 1984. Particulate and dissolved vanadium in the North Pacific Ocean. *Nature* 309, 441-444.
- Conway, T.M., John, S.G., 2014a. Quantification of dissolved iron sources to the North Atlantic Ocean. *Nature* 511, 212-215.
- Conway, T.M., John, S.G., 2014b. The biogeochemical cycling of zinc and zinc isotopes in the North Atlantic Ocean. *Global Biogeochem. Cycles* 28, 1111-1128.
- Dauphas, N., John, S.G., Rouxel, O., 2017. Iron isotope systematic. *Reviews in Mineralogy and Geochemistry* 82, 276-371.
- Dekov, V.M., Marchig, V., Rajta, I., Uzonyi, I., 2003. Fe-Mn micronodules born in the metalliferous sediments of two spreading centers: East Pacific Rise and Mid-Atlantic Ridge. *Marine Geology* 199, 101-121.
- de Villiers, S., 1998. Excess dissolved Ca in the deep ocean: a hydrothermal hypothesis. *Earth Planet. Sci. Lett.* 164, 627-641.

- de Villiers, S., 1999. Seawater strontium and Sr/Ca variability in the Atlantic and Pacific Oceans. *Earth Planet. Sci. Lett.* 171, 623-634.
- Dideriksen, K., Baker, J.A., Stipp, S.L.S., 2006. Iron isotopes in natural carbonate minerals determined by MC-ICP-MS with a Fe-58-Fe-54 double spike. *Geochimica et Cosmochimica Acta* 70, 118-132.
- Druce, M., Stirling, C.H., Rolison, J.M., 2020. High-precision zinc isotopic measurement of certified reference materials relevant to the environmental, earth, planetary and biomedical sciences. *Geostandards and Geoanalytical Research* 44, 711-732.
- Dubinina, A.V., Sval'nov, V.N., 1995. Micronodules from Guatemala Basin: Geochemistry of rare earth elements. *Lithology and Mineral Resources* 5, 473-479. (in Russian).
- Dubinina, A.V., Sval'nov, V.N., 1996. Differentiated mobility of iron oxyhydroxides during the processes of formation of micro- and macronodules (Guatemala Basin, Pacific Ocean). *Doklady Academy of Sciences* 348, 100-103. (in Russian).
- Dubinina, A.V., Sval'nov, V.N., 2000a. Geochemistry of rare earth elements in micro- and macronodules from the Pacific bioproductive zone. *Lithology and Mineral Resources* 35, 1, 19-31.
- Dubinina, A.V., Sval'nov, V.N., 2000b. Geochemistry of rare earth elements in ferromanganese micro- and macronodules from the Pacific nonproductive zone. *Lithology and Mineral Resources* 35, 6, 520-537.
- Dubinina, A.V., Sval'nov, V.N., 2003. Geochemistry of the manganese ore process in the ocean: Evidence from rare earth elements. *Lithology and Mineral Resources* 38, 2, 91-100.
- Dubinina, A.V., Sval'nov, V.N., Uspenskaya, T.Y., 2008. Geochemistry of the authigenic ferromanganese ore formation in sediments of the Northeast Pacific Basin. *Lithology and Mineral Resources* 43, 2, 99-110.
- Dubinina, A.V., Sval'nov, V.N., Berezhrayev, L.D., Rimskaya-Korsakova, M.N., Demidova, T.P., 2013. Geochemistry of trace and minor elements in sediments and manganese micronodules from the Angola Basin. *Lithology and Mineral Resources* 48, 3, 175-197.
- Dubinina, A.V., Rimskaya-Korsakova, M.N., Demidova, T.P., 2020. Anomalies of rare elements in manganese micronodules from Ethmodon oozes in the Brazil Basin of the Atlantic Ocean. *Bulletin of Kamchatka regional association "Educational - scientific center", Earth sciences* 48, 64-84. (in Russian).
- Ellwood, M.J., Hutchins, D.A., Lohan, M.C., Milne, A., Nasemann, P., Nodder, S.D., Sander, S.G., Strzepek, R., Wilhelm, S.W., Boyd, P.W., 2015. Iron stable isotopes track pelagic iron cycling during a subtropical phytoplankton bloom. *PNAS* 112, E15-E20.
- Fitzsimmons, J.N., Conway, T.M., Lee, J.-M., Kayser, R., Thyng, K.M., John, S.G., Boyle, E.A., 2016. Dissolved iron and iron isotopes in the southeastern Pacific Ocean. *Global Biogeochem. Cycles* 30, 1372-1395.
- Flanagan, F.J., Gottfried, D., 1980. USGS Rock Standards, III: Manganese-Nodule Reference Samples USGS-Nod-A-1 and USGS-Nod-P-1. *Geological Survey Professional Paper* 1155, 46 p.
- Gagnevin, D., Boyce, A.J., Barrie, C.D., Menuge, J.F., Blakeman, R.J., 2012. Zn, Fe and S isotope fractionation in a large hydrothermal system. *Geochimica et Cosmochimica Acta* 88, 183-198.
- Golden, D.C., Dixon, J.B., Chen, C.C., 1986. Ion exchange, thermal transformations, and oxidizing properties of birnessite Clays. *Clay Miner.* 34, 511-520.

- Halbach, P., Friedrich, G., Von Stackelberg, U. (Eds), 1988. The Manganese Nodule Belt of the Pacific Ocean. Geological Environment, Nodule Formation, and Mining Aspects. Ferdinand Enke Verlag, Stuttgart, 254 pp.
- Heath, G.R., 1981. Ferromanganese nodules of the deep sea. *Econ. Geol.* 75th Anniv. Vol., 736-765.
- Hein, J.R., Koschinsky, A., 2014. Deep-ocean ferromanganese crusts and nodules. In: Holland, H.D., Turekian, K.K. (Eds), *Treatise on Geochemistry*, 2<sup>nd</sup> edition, Elsevier, Amsterdam, 13, 273-291.
- Hishida, H., Uchio, T., 1981. Sedimentological and geochemical studies of manganese micronodules and the associated sediments in some piston cores in the North Pacific Ocean. *Jour. Fac. Eng., Univ. Tokyo, ser. B*, 36, 463-522.
- Horner, T.J., Williams, H.M., Hein, J.R., Saito, M.A., Burton, K.W., Halliday, A.N., Nielsen, S.G., 2015. Persistence of deeply sourced iron in the Pacific Ocean. *PNAS* 112, 1297-1297.
- Ijichi, Y., Ohno, T., Sakata, S., 2018. Copper isotopic fractionation during adsorption on manganese oxide: Effects of pH and desorption. *Geochemical Journal* 52, e1-e6.
- Immel, R.L., 1974. Origin of micromanganese nodules determined from uranium-234/uranium-238 ratios. *Antarctic journal of the United States* 9, 259-260.
- Immel, R., Osmond, J.K., 1976. Micromanganese nodules in deep-sea sediments: Uranium-isotopic evidence for post-depositional origin. *Chemical Geology* 18, 263-272.
- Ito, T., Komuro, K., Hatsuya, K., Nishi, H., 2005. Chemical compositions of ferromanganese micronodules in sediments at Site 1216, ODP Leg 199, Paleogene equatorial transect. In: Wilson, P.A., Lyle, M. and Firth, J.V. (Eds.), *Proc. ODP, Sci. Results*, 199, 1-20.
- Jeandel, C., Minster, J.F., 1987. Chromium behavior in the ocean: global versus regional processes. *Global Biogeochem. Cycles* 1, 131-154.
- Jochum, K.P., Nohl, U., Herwig, K., Lammer, P., Stoll, B., Hofmann, A.W., 2005. GeoReM: A new geochemical database for reference materials and isotopic standards. *Geostand. Geoanalyt. Res.* 29, 333-338.
- John, S.G., Geis, R., Saito, M., Boyle, E.A., 2007. Zn isotope fractionation during high-affinity zinc transport by the marine diatom *Thalassiosira oceanica*. *Limnol. Oceanogr.* 52, 2710-2714.
- John, S.G., Mendez, J., Moffett, J., Adkins, J., 2012. The flux of iron and iron isotopes from San Pedro Basin sediments. *Geochim. Cosmochim. Acta* 93, 14-29.
- Johnson, C.M., Skulan, J.L., Beard, B.L., Sun, H., Nealon, K.H., Braterman, P.S., 2002. Isotopic fractionation between Fe(III) and Fe(II) in aqueous solutions. *Earth Planet. Sci. Lett.* 195, 141-153.
- Josso, P., Pelleter, E., Pourret, O., Fouquet, Y., Etoubleau, J., Cheron, S., Bollinger, C., 2017. A new discrimination scheme for oceanic ferromanganese deposits using high field strength and rare earth elements. *Ore Geology Reviews* 87, 3-15.
- Jouvin, D., Louvat, P., Juillot, F., Maréchal, C.N., Benedetti, M.F., 2009. Zinc isotopic fractionation: why organic matters. *Environ. Sci. Technol.* 43, 5747-5754.
- Julien, C.M., Massot, M., Poinsignon, C., 2004. Lattice vibrations of manganese oxides: Part I. Periodic structures. *Spectrochim. Acta A: Mol. Biomol. Spectrosc.* 60, 689-700.
- Kang, L., Zhang, M., Liu, Z.H., Ooi, K., 2007. IR spectra of manganese oxides with either layered or tunnel structures. *Spectrochim. Acta A: Mol. Biomol. Spectrosc.* 67, 864-869.

- Kato, Y., Fujinaga, K., Nakamura, K., Takaya, Y., Kitamura, K., Ohta, J., Toda, R., Nakashima, T., Iwamori, H., 2011. Deep-sea mud in the Pacific Ocean as a potential resource for rare-earth elements. *Nat. Geosci.* 4, 535-539.
- Kidd, R.B., Ármannson, H., 1979. Manganese and iron micronodules from a volcanic seamount in the Tyrrhenian Sea. *Jl geol. Soc. Lond.* 136, 71-76.
- Klar, J.K., Homoky, W.B., Statham, P.J., Birchill, A.J., Harris, E.L., Woodward, E.M.S., Silburn, B., Cooper, M.J., James, R.H., Connelly, D.P., Chever, F., Lichtschlag, A., Graves, C., 2017. Stability of dissolved and soluble Fe(II) in shelf sediment pore waters and release to an oxic water column. *Biogeochemistry* 135, 49-67.
- Köbberich, M., Vance, D., 2019. Zn isotope fractionation during uptake into marine phytoplankton: Implications for oceanic zinc isotopes. *Chem. Geol.* 523, 154-161.
- Kuhn, T., Versteegh, G.J.M., Villinger, H., Dohrmann, I., Heller, C., Koschinsky, A., Kaul, N., Ritter, S., Wegorzewski, A.V., Kasten, S., 2017a. Widespread seawater circulation in 18-22 Ma oceanic crust: Impact on heat flow and sediment geochemistry. *Geology* 45, 799-802.
- Kuhn, T., Wegorzewski, A., Rühlemann, C., Vink, A., 2017b. Composition, formation, and occurrence of polymetallic nodules. In: Sharma, R. (Ed.), *Deep-Sea Mining: Resource Potential, Technical and Environmental Considerations*, Springer International Publishing AG, 23-63.
- Kunzendorf, H., Gwozdz, R., Glasby, G.P., Stoffers, P., Renner, R.M., 1989. The distribution of rare earth elements in manganese micronodules and sediments from the equatorial and southwest Pacific. *Applied Geochemistry* 4, 183-193.
- Kunzendorf, H., Glasby, G.P., Stoffers, P., Plüger, W.L., 1993. The distribution of rare earth and minor elements in manganese nodules, micronodules and sediments along an east-west transect in the southern Pacific. *Lithos* 30, 45-56.
- Lacan, F., Radic, A., Jeandel, C., Poitasson, F., Sarthou, G., Pradoux, C., Freydier, R., 2008. Measurement of the isotopic composition of dissolved iron in the open ocean. *Geophys. Res. Lett.* 35, L24610.
- Lallier-Verges, E., Clinard, C., 1983. Ultra-thin section study of the mineralogy and geochemistry of Mn micronodules from the South Pacific. *Marine Geology* 52, 267-280.
- Landing, W.M., Bruland, K.W., 1980. Manganese in the North Pacific. *Earth Planet. Sci. Lett.* 49, 45-56.
- Lemaitre, N., de Souza, G.F., Archer, C., Wang, R-M., Planquette, H., Sarthou, G., Vance, D., 2020. Pervasive sources of isotopically light zinc in the North Atlantic Ocean. *Earth and Planetary Science Letters* 539, 116216.
- Le Suavé, R., 1989. Campagne NIXO 47: Etude détaillée de deux sites de ramassage de nodules polymétalliques. Colloque Tour du Monde du Jean Charcot. Paris, 2-3 Mars 1989, pp. 249-256.
- Levasseur, S., Frank, M., Hein, J.R., Halliday, A.N., 2004. The global variation in the iron isotope composition of marine hydrogenetic ferromanganese deposits: implications for seawater chemistry? *Earth and Planetary Science Letters* 224, 91-105.
- Li, D., Fu, Y., Liu, Q., Reinfelder, J.R., Hollings, P., Sun, X., Tan, C., Dong, Y., Ma, W., 2020. High-resolution LA-ICP-MS mapping of deep-sea polymetallic micronodules and its implications on element mobility. *Gondwana Research* 81, 461-474.

- Liao, J., Sun, X., Wu, Z., Sa, R., Guan, Y., Lu, Y., Li, D., Liu, Y., Deng, Y., Pan, Y., 2019. Fe-Mn (oxyhydr)oxides as an indicator of REY enrichment in deep-sea sediments from the central North Pacific. *Ore Geology Reviews* 112, 103044.
- Little, S.H., Sherman, D.M., Vance, D., Hein, J.R., 2014a. Molecular controls on Cu and Zn isotopic fractionation in Fe-Mn crusts. *Earth and Planetary Science Letters* 396, 213-222.
- Little, S.H., Vance, D., Walker-Brown, C., Landing, W.M., 2014b. The oceanic mass balance of copper and zinc isotopes, investigated by analysis of their inputs, and outputs to ferromanganese oxide sediments. *Geochim. Cosmochim. Acta* 125, 673-693.
- Little, S.H., Vance, D., McManus, J., Severmann, S., Lyons, T.W., 2017. Copper isotope signatures in modern marine sediments. *Geochim. Cosmochim. Acta* 212, 253-273.
- Little, S.H., Archer, C., Milne, A., Schlosser, C., Achterberg, E.P., Lohan, M.C., Vance, D., 2018. Paired dissolved and particulate phase Cu isotope distributions in the South Atlantic. *Chem. Geol.* 502, 29-43.
- Marcus, M.A., Edwards, K.J., Gueguen, B., Fakra, S.C., Horn, G., Jelin ki, M.A., Rouxel, O., Sorensen, J., Toner, B.M., 2015. Iron mineral structure, reactivity, and isotopic composition in a South Pacific Gyre ferromanganese nodule over 4 Ma. *Geochimica et Cosmochimica Acta* 171, 61-79.
- Marechal, C.N., Telouk, P., Albarede, F., 1999. Precise analysis of copper and zinc isotopic compositions by plasma-source mass spectrometry. *Chemical Geology* 156, 251-273.
- Maréchal, C., Nicolas, E., Douchet, C., Albarède, F., 2000. Abundance of zinc isotopes as a marine biogeochemical tracer. *Geochem. Geophys. Geosyst.* 1, 1015-15.
- Markovic, T., Manzoor, S., Humphreys-Williams, E., Kirk, G., Vilar, R., Weiss, D., 2017. Experimental determination of zinc isotope fractionation in complexes with the phytosiderophore 2'-deoxymugeneic acid (DMA) and its structural analogues, and implications for plant uptake mechanisms. *Environmental Science and Technology* 51, 98-107.
- Martin, J.H., Gordon, R.M., Fitzwater, S., Broenkow, W.W., 1989. VERTEX: phytoplankton/iron studies in the Gulf of Alaska. *Deep-Sea Res.* 35, 649-680.
- Mathur, R., Ruiz, J., Tittle, S., Liermann, L., Buss, H., Brantley, S., 2005. Cu isotopic fractionation in the supergene environment with and without bacteria. *Geochim. Cosmochim. Acta* 69, 5233-5246.
- McLennan, S.M., 1989. Rare earth elements in sedimentary rocks: Influence of provenance and sedimentary processes. In: B.R. Lipin and G.A. McKay (Eds), *Geochemistry and Mineralogy of Rare Earth Elements*, *Rev. Miner.* 21, 169-200.
- Menendez, A., James, R.H., Roberts, S., Peel, K., Connelly, D., 2017. Controls on the distribution of rare earth elements in deep-sea sediments in the North Atlantic Ocean. *Ore Geol. Rev.* 87, 100-113.
- Mewes, K., Mogollón, J.M., Picard, A., Rühlemann, C., Kuhn, T., Nöthen, K., Kasten, S., 2014. Impact of depositional and biogeochemical processes on small scale variations in nodule abundance in the Clarion-Clipperton Fracture Zone. *Deep-Sea Research I* 91, 125-141.
- Mewes, K., Mogollón, J.M., Picard, A., Rühlemann, C., Eisenhauer, A., Kuhn, T., Ziebis, W., Kasten, S., 2016. Diffusive transfer of oxygen from seamount basaltic crust into overlying sediments: An example from the Clarion-Clipperton Fracture Zone. *Earth and Planetary Science Letters* 433, 215-225.

- Millero, F., 1974. Seawater as a multicomponent electrolyte solution. In: Goldberg, E. (Ed.), *The Sea*, 5, Wiley, pp. 3-80.
- Moffett, J.W., Dupont, C., 2007. Cu complexation by organic ligands in the sub-Arctic NW Pacific and Bering Sea. *Deep-Sea Res., Part 1* 54, 586-595.
- Morel, Y., Le Suavé, R., 1986. Variabilité de l'environnement morphologique et sédimentaire dans un secteur intraplaque du Pacifique Nord (zone Clarion-Clipperton). *Bull. Soc. Géol. France II*, 361-372.
- Moynier, F., Vance, D., Fujii, T., Savage, P., 2017. The isotope geochemistry of zinc and copper. *Rev. Mineral. Geochem.* 82, 543-600.
- Mukhopadhyay, S., Dasgupta, S., Roy, S., 1988. Distribution and character of micronodules in pelagic sediments from Central Indian Basin, Indian ocean and their implications. *Marine Mining* 7, 351- 358.
- Navarrete, J.U., Borrok, D.M., Viveros, M., Ellzey, J.T., 2011. Copper isotope fractionation during surface adsorption and intracellular incorporation by bacteria. *Geochim. Cosmochim. Acta* 75, 784-799.
- Ohashi, M., 1985. Depositional environments and chemical compositions of manganese micronodules. *J. Geol. Soc. Japan* 91, 787-803.
- Pattan, J.N., 1993. Manganese micronodules: A possible indicator of sedimentary environments. *Marine Geology* 113, 331-344.
- Pattan, J.N., Colley, S., Higgs, N.C., 1994. Behavior of rare earth elements in coexisting manganese macronodules, micronodules, and sediments from the Central Indian Basin. *Marine Georesources and Geotechnology* 12, 283-295.
- Pokrovsky, O.S., Viers, J., Emnova, E.E., Kompantseva, E.I., Freydier, R., 2008. Copper isotope fractionation during its interaction with soil and aquatic microorganisms and metal oxy(hydr)oxides: possible structural control. *Geochim. Cosmochim. Acta* 72, 1742-1757.
- Pontér, S., Sutliff-Johansson, S., Engström, E., Widerlund, A., Mäki, A., Rodushkina, K., Paulukat, C., Rodushkin, I., 2021. Evaluation of a multi-isotope approach as a complement to concentration data within environmental forensics. *Minerals* 11, 37.
- Poppe, L.J., Commeau, R.L., Commeau, J.A., Manheim, F.T., Aruscavage, P.J., 1984. Ferromanganese micronodules from the surficial sediments of Georges Bank. *Journal of Marine Research* 42, 463-472.
- Potter, R.M., Rossman, G.R., 1979. The tetravalent manganese oxides: identification, hydration, and structural relationships by infrared spectroscopy. *Am. Mineral.* 64, I199-I1218.
- Rouxel, O.J., Bekker, A., Edwards, K.J., 2005. Iron Isotope Constraints on the Archean and Paleoproterozoic Ocean Redox State. *Science* 307, 1088-1091.
- Ryan, B.M., Kirby, J.K., Degryse, F., Scheiderich, K., McLaughlin, M.J., 2014. Copper isotope fractionation during equilibration with natural and synthetic ligands. *Environ. Sci. Technol.* 48, 8620-8626.
- Seeberg-Elverfeldt, J., Schlüter, M., Feseker, T., Kölling, M., 2005. Rhizon sampling of porewaters near the sediment-water interface of aquatic systems. *Limnology and Oceanography: Methods* 3, 361-371.
- Severmann, S., Larsen, O., Palmer, M.R., Nüster, J., 2002. The isotopic signature of Fe-mineralization during early diagenesis. *Geochim. Cosmochim. Acta* 66, A698.

- Severmann, S., Johnson, C.M., Beard, B.L., German, C.R., Edmonds, H.N., Chiba, H., Green, D.R.H., 2004. The effect of plume processes on the Fe isotope composition of hydrothermally derived Fe in the deep ocean as inferred from the Rainbow vent site, Mid-Atlantic Ridge, 36°14'N. *Earth Planet. Sci. Lett.* 225, 63-76.
- Severmann, S., McManus, J., Berelson, W.M., Hammond, D.E., 2010. The continental shelf benthic iron flux and its isotope composition. *Geochim. Cosmochim. Acta* 74, 3984-4004.
- Sherman, D.M., 2013. Equilibrium isotopic fractionation of copper during oxidation/reduction, aqueous complexation and ore-forming processes: predictions from hybrid density functional theory. *Geochim. Cosmochim. Acta* 118, 85-97.
- Sherman, D.M., Little, S.H., 2020. Isotopic disequilibrium of Cu in marine ferromanganese crusts: Evidence from ab initio predictions of Cu isotope fractionation on sorption to birnessite. *Earth and Planetary Science Letters* 549, 116540.
- Skrabal, S.A., Donat, J.R., Burdige, D.J., 2000. Pore water distributions of dissolved copper and copper-complexing ligands in estuarine and coastal marine sediments. *Geochim. Cosmochim. Acta* 64, 1843-1857.
- Sohrin, Y., Isshiki, K., Kuwamoto, T., 1987. Tungsten in North Pacific waters. *Mar. Chem.* 22, 95-103.
- Spencer, D.W., Robertson, D.E., Turekian, K.K., Folsom, T.R., 1970. Trace element calibrations and profiles at the Geosecs test station in the Northeast Pacific Ocean. *J. Geophys. Res.* 75, 7688.
- Stoffers, P., Glasby, G.P., Thijssen, T., Srivastava, P., Meggen, M., 1981. The geochemistry of coexisting manganese nodules, micronodules, sediments and pore waters from five areas in the equatorial and southwest Pacific. *Chem. Erde* 40, 273-297.
- Stoffers, P., Glasby, G.P., Frenzel, G., 1984. Comparison of the characteristics of manganese micronodules from the equatorial and south-west Pacific. *Tschernak Mineralogische und Petrographische Mitteilungen* 33, 1-23.
- Stoffyn-Egli, P., MacKenzie, F.T., 1984. Mass balance of dissolved lithium in the oceans. *Geochim. Cosmochim. Acta* 48, 859-872.
- Sugisaki, R., Ohashi, M., Sugitani, K., Suzuki, K., 1987. Compositional variations in manganese micronodules: A possible indicator of sedimentary environments. *The Journal of Geology* 95, 433-454.
- Sugitani, K., 1987. A geochemical study of hydrothermal manganese micronodules from marine sediments and sedimentary rocks on land. *J. Geol. Soc. Japan* 93, 555-574.
- Sval'nov, V.N., Lyapin, A.B., Novikova, Z.T., 1991a. Manganese micronodules. Report 1. General characteristics and distribution in pelagic sediments. *Lithology and Mineral Resources* 3, 3-20. (in Russian).
- Sval'nov, V.N., Lyapin, A.B., Novikova, Z.T., 1991b. Manganese micronodules. Report 2. Composition and origin. *Lithology and Mineral Resources* 4, 32-50. (in Russian).
- Takano, S., Tanimizu, M., Hirata, T., Sohrin, Y., 2014. Isotopic constraints on biogeochemical cycling of copper in the ocean. *Nat. Commun.* 5, 5663.
- Thompson, C.M., Ellwood, M.J., 2014. Dissolved copper isotope biogeochemistry in the Tasman Sea, SW Pacific Ocean. *Mar. Chem.* 165, 1-9.
- Tostevin, R., Poulton, S., 2019. Suboxic sediments. In: Gargaud, M., Irvine, W.M., Amils, R., Cleaves, H.J., Pinti, D., Cernicharo Quintanilla, J., Viso, M., (Eds), *Encyclopedia of Astrobiology*. Springer, Berlin, Heidelberg, 4 p.



- Uppstrom, L.R., 1974. The boron/chlorinity ratio of deep-sea water from the Pacific Ocean. *Deep-Sea Res.* 21, 161-162.
- Vance, D., Archer, C., Bermin, J., Perkins, J., Statham, P.J., Lohan, M.C., Ellwood, M.J., Mills, R.A., 2008. The copper isotope geochemistry of rivers and the oceans. *Earth and Planetary Science Letters* 274, 204-213.
- Veillette, J., Juniper, S.K., Gooday, A.J., Sarrazin, J., 2007. Influence of surface texture and microhabitat heterogeneity in structuring nodule faunal communities. *Deep-Sea Research I* 54, 1936-1943.
- Volz, J.B., Mogollón, J.M., Geibert, W., Arbizu, P.M., Koschinsky, A., Kasten, S., 2018. Natural spatial variability of depositional conditions, biogeochemical processes and element fluxes in sediments of the eastern Clarion-Clipperton Zone, Pacific Ocean. *Deep-Sea Research Part I* 140, 159-172.
- Volz, J.B., Liu, B., Köster, M., Henkel, S., Koschinsky, A., Kasten, S., 2020. Post-depositional manganese mobilization during the last glacial period in sediments of the eastern Clarion-Clipperton Zone, Pacific Ocean. *Earth and Planetary Science Letters* 532, 116012.
- Wegorzewski, A.V., Kuhn, T., 2014. The influence of suboxic diagenesis on the formation of manganese nodules in the Clarion Clipperton nodule belt of the Pacific Ocean. *Marine Geology* 357, 123-138.
- Wegorzewski, A.V., Kuhn, T., Dohrmann, R., Wirth, R., Grangeon, S., 2015. Mineralogical characterization of individual growth structures of Mn-nodules with different Ni/Cu content from the central Pacific Ocean. *American Mineralogist* 100, 2497-2508.
- Wegorzewski, A.V., Grangeon, S., Webb, S.M., Keller, C., Kuhn, T., 2020. Mineralogical transformations in polymetallic nodules and the change of Ni/Cu and Co crystal-chemistry upon burial in sediments. *Geochimica et Cosmochimica Acta* 282, 19-37.
- Welch, S.A., Beard, B.L., Johnson, C.M., Bratton, P.S., 2003. Kinetic and equilibrium Fe isotope fractionation between aqueous Fe(II) and Fe(III). *Geochim. Cosmochim. Acta* 67, 4231-4250.
- Wells, M.L., Kozelka, P.B., Bruland, K.W., 1998. The complexation of “dissolved” Cu, Zn, Cd and Pb by soluble and colloidal organic matter in Narragansett Bay, RI. *Mar. Chem.* 62, 203-217.
- Williams, H.M., Bizimis, M., 2014. Iron isotope tracing of mantle heterogeneity within the source regions of oceanic basalts. *Earth and Planetary Science Letters* 404, 396-407.
- Winter, B.L., Johnson, C.M., Clark, D.L., 1997. Geochemical constraints on the formation of Late Cenozoic ferromanganese micronodules from the central Arctic Ocean. *Marine Geology* 138, 149-169.
- Xu, H., Peng, X., Ta, K., Song, T., Du, M., Li, J., Chen, S., Qu, Z., 2020. Structure and composition of micro-manganese nodules in deep-sea carbonate from the Zhaoshu Plateau, north of the South China Sea. *Minerals* 10, 1016.
- Yasukawa, K., Ohta, J., Miyazaki, T., Vaglarov, B.S., Chang, Q., Ueki, K., Toyama, C., Kimura, J.-I., Tanaka, E., Nakamura, K., Fujinaga, K., Iijima, K., Iwamori, H., Kato, Y., 2019. Statistic and isotopic characterization of deep-sea sediments in the Western North Pacific Ocean: Implications for genesis of the sediment extremely enriched in rare earth elements. *Geochemistry, Geophysics, Geosystems* 20, 10.1029/2019GC008214.
- Yasukawa, K., Kino, S., Azami, K., Tanaka, E., Mimura, K., Ohta, J., Fujinaga, K., Nakamura, K., Kato, Y., 2020. Geochemical features of Fe-Mn micronodules in deep-sea sediments of the western North Pacific Ocean: Potential for co-product metal extraction from REY-rich mud. *Ore Geology Reviews* 127, 103805.

- Yasukawa, K., Kino, S., Ohta, J., Azami, K., Tanaka, E., Mimura, K., Fujinaga, K., Nakamura, K., Kato, Y., 2021. Stratigraphic variations of Fe-Mn micronodules and implications for the formation of extremely REY-rich mud in the western North Pacific Ocean. *Minerals* 11, 270.
- Zhu, X.K., O’Nions, R.K., Guo, Y., Reynolds, B.C., 2000. Secular variation of iron isotopes in north Atlantic Deep Water. *Science* 287, 2000-2002.

Journal Pre-proof

## Figure captions

**Fig. 1.** Bathymetric map of the studied area with distribution of the Mn-nodule facies and location of the studied sediment cores. Inset map shows the location of the studied area (red rectangle) in the Pacific Ocean.

**Fig. 2.** Photographs of the Mn-nodule facies at the seafloor (taken by *DSV Nautila*) and corresponding Mn-nodules (insets). (A) facies 0 and a Mn-nodule from facies 0 (spherical; sample NODKGS51 0-5cm); (B) facies A and a Mn-nodule from facies A (spherical; sample EBS07); (C) facies B and a Mn-nodule from facies B (flat, upper surface; sample NODKGS53 0-7 cm); (D) facies C and a Mn-nodule from facies C (flat, ellipsoidal, upper surface; sample NODKGS63 0-5cm).

**Fig. 3.** SEM photomicrographs of: (A) elongated botryoidal Mn-micronodules (SEI; sample NODKGS58 0-5cm); (B) isometric Mn-micronodule (SEI; sample NODKGS58 0-5cm); (C, D, E, F) cross sections of Mn-micronodules showing their internal structure and layer types (BEI; sample NODKGS63 0-5 cm).

**Fig. 4.** XRD patterns of two selected Mn-micronodule samples after drying at 30°C (black patterns) and after heating at 105°C for 24h (red patterns). [a.u.] = arbitrary units; Fsp = feldspar; Qz = quartz.

**Fig. 5.** IR spectra of five selected Mn-micronodule samples compared with the IR spectra of a phyllosilicate-rich Mn-nodule and a todorokite-rich Mn-nodule from Wegorzewski et al. (2020). The black arrows mark the IR bands that are characteristic for Mn-oxides: phyllosilicate (400 – 515  $\text{cm}^{-1}$ ) and todorokite ( $\sim 760\text{cm}^{-1}$ ). Quartz (Qz) and other minor impurities (1200 – 900  $\text{cm}^{-1}$ ) were detected.

**Fig. 6.** NASC-normalized (McLennan, 1989) REE distribution patterns of Mn-nodules and Mn-micronodules from facies 0 (A and B, respectively), 1 (C and D, respectively) and 2 (E and F, respectively), and of Pacific (Nod-P-1) and Atlantic (Nod-A-1) Mn-nodule standards (G and H, respectively) and North Pacific Deep Water [x15000000; Alibo and Nozaki (1999)] (G).

**Fig. 7.** Vertical distributions of the elemental concentrations in the pore waters along the sediment cores NODKGS63 ( $\text{O}_2$ ; black closed circles = profile close to a Mn-nodule, red closed squares = profile beneath the Mn-nodule) and NODKGS65 (the other elements; black closed circles). Blue stars, elemental concentrations in the North Pacific deep seawater:  $\text{O}_2$ , our data; Mn from Landing and Bruland (1980); Fe, and Co from Martin et al. (1989); S, Mg, Na, and K from Millero (1974); Ca from de Villiers (1998); Rb from Spencer et al. (1970); Li from Stoffyn-Egli and MacKenzie (1984); Mo from Sohrin et al. (1987); Cd, Ni, Cu, and Zn from Bruland (1980); B from Uppstrom (1974); V from Collier (1984); Ba from Chan et al. (1976); U from Chen et al. (1986); Cr from Jeandel and Minster (1987); Sr from de Villiers (1999). Concentrations of the same elements in the Mn-micronodules collected from the

same core (NODKGS65) are shown on the same plots with red vertical bars covering the sediment layers from which the Mn-micronodules were extracted (0-5 cm and 5-10 cm). Concentration scales are given in red on top of each plot.

**Fig. 8.** Fe-Cu-Zn isotope composition of Mn-micronodules and Mn-nodules from this study. (A) Fe-isotope composition; (B) Cu-isotope composition; (C) Zn-isotope composition. Colored dots represent the isotope composition of the Mn-nodules laying at the sediment surface, and colored vertical bars show the isotope composition of the Mn-micronodules for the depth range where they were collected (i.e., 0-5 cm depth and 5-10 cm depth, except for NODKGS53, 0-7 cm depth).

**Fig. 9.** Fe-Cu-Zn-isotope composition (range) of seafloor Fe-Mn-oxyhydroxide deposits. (A) Fe-isotope composition of Fe-Mn-crusts (Zhu et al., 2000; Chu et al., 2003; Levasseur et al., 2004; Hoyer et al., 2015) and Mn-nodules (Beard and Johnson, 1999; Levasseur et al., 2004; Marcus et al., 2015); (B) Cu-isotope composition of Fe-Mn-crusts (Little et al., 2014b) and Mn-nodules (Albarède, 2004); (C) Zn-isotope composition of Fe-Mn-crusts (Little et al., 2014b) and Mn-nodules (Maréchal et al., 2000). Isotope composition of terrestrial igneous rocks:  $\delta^{56}\text{Fe}$  (Beard and Johnson, 2004),  $\delta^{65}\text{Cu}$  (Albarède, 2004), and  $\delta^{66}\text{Zn}$  (Albarède, 2004). For data of this study see Table 7. Red crosses = isotope composition of Mn-nodule standard Nod-P-1.

**Fig. 10.** Ternary discriminative diagrams for genetic classification of the seafloor Fe-Mn-oxyhydroxide deposits and positions of the studied Mn-micronodules and Mn-nodules: (A) Fe-Mn-(Ni+Cu)\*10 diagram according to Wegorzewski and Kuhn (2014) (based on Halbach et al., 1988) showing the geochemical relationships between the diagenetic (A), diagenetic-hydrogenetic (AB) and hydrogenetic (B) nodule types; (B) diagram of Josso et al. (2017) with some refinement.

## Appendixes

**Appendixes 1 – 2:** XRD patterns of Mn-micronodule samples after drying at 30°C (black patterns) and after heating at 105°C for 24h (grey patterns). [a.u.] = arbitrary units; Fsp = feldspar; Qz = quartz.

**Appendix 3:** XRD patterns of Mn-micronodule samples after drying at 30°C. [a.u.] = arbitrary units; Fsp = feldspar; Qz = quartz.

**Appendix 4:** IR spectra of five Mn-micronodule samples compared with the IR spectra of a phyllomangante-rich Mn-nodule and a todorokite-rich Mn-nodule from Wegorzewski et al. (2020) as well as with the IR spectra of two Mn-nodule standards (Nod-P-1 and Nod-A-1). The black arrows mark the IR bands that are characteristic for Mn-oxides: phyllomanganate (400 – 515  $\text{cm}^{-1}$ ) and todorokite (~760 $\text{cm}^{-1}$ ). Quartz (Qz) and other minor impurities (1200 – 900  $\text{cm}^{-1}$ ) were detected.

**Table 1.** Investigated box cores.

Box core #	Latitude (N)	Longitude (W)	Depth (m)	Mn-nodule facies	Nodule density coverage (kg/m <sup>2</sup> )	Remarks
NODKGS44	14°03.99′	130°05.64′	5033	0	0	deepest
NODKGS48	14°03.11′	130°05.16′	5017	0	0	deepest
NODKGS49	14°04.00′	130°05.24′	5032	0	0	deepest
NODKGS50	14°03.36′	130°04.80′	5035	0	0	deepest
NODKGS51	14°03.41′	130°05.48′	5010	0	0	deepest
NODKGS52	14°02.99′	130°05.24′	5027	0	0	deepest
NODKGS53	14°02.34′	130°08.29′	4957	B	22.4	shallowest
NODKGS54	14°02.82′	130°08.10′	4905	B	18.4	shallowest
NODKGS55	14°03.05′	130°08.00′	4910	B	16.3	shallowest
NODKGS56	14°03.18′	130°08.64′	4838	B	18.6	shallowest
NODKGS57	14°03.24′	130°07.80′	4938	B	16.7	shallowest
NODKGS58	14°03.24′	130°08.16′	4900	B	12.3	shallowest
NODKGS60	14°03.67′	130°06.25′	5000	C	9.8	middle depth
NODKGS63	14°04.28′	130°07.06′	4978	C	18.4	middle depth
NODKGS65	14°03.71′	130°06.80′	4969	C	18.3	middle depth

**Table 2.** Mineralogy (XRD, IR) of the studied Mn-micronodules and Mn-nodules.

Sample ID	Description	Mn-nodule facies	Mineralogy
NODKGS44 0-5cm <sup>a</sup>	Mn-micronodules	0	10 Å and 7 Å phyllomanganates, vernadite, quartz, feldspar
NODKGS44 5-10cm <sup>a</sup>	Mn-micronodules	0	10 Å and 7 Å phyllomanganates, vernadite, quartz, feldspar
NODKGS48 0-5cm <sup>a</sup>	Mn-micronodules	0	10 Å and 7 Å phyllomanganates, vernadite, quartz, feldspar
NODKGS48 5-10cm <sup>a</sup>	Mn-micronodules	0	10 Å and 7 Å phyllomanganates, vernadite, quartz, feldspar
NODKGS49 0-5cm	Mn-micronodules	0	10 Å and 7 Å phyllomanganates, vernadite, quartz
NODKGS49 5-10cm	Mn-micronodules	0	10 Å and 7 Å phyllomanganates, vernadite, quartz
NODKGS51 0-5cm	Mn-micronodules	0	10 Å and 7 Å phyllomanganates, vernadite, quartz
NODKGS51 5-10cm	Mn-micronodules	0	10 Å and 7 Å phyllomanganates, vernadite, quartz
NODKGS52 0-5cm <sup>a</sup>	Mn-micronodules	0	10 Å and 7 Å phyllomanganates, vernadite, quartz, feldspar
NODKGS52 5-10cm <sup>a</sup>	Mn-micronodules	0	10 Å and 7 Å phyllomanganates, vernadite, quartz, feldspar

NODKGS53	Mn-nodule	B	10 Å and 7 Å phyllomanganates, vernadite, quartz, feldspar
NODKGS53 0-7 cm	Mn-micronodules	B	10 Å and 7 Å phyllomanganates, vernadite, quartz
NODKGS54 0-5cm <sup>a</sup>	Mn-micronodules	B	10 Å and 7 Å phyllomanganates, vernadite, quartz
NODKGS54 5-10cm	Mn-micronodules	B	10 Å and 7 Å phyllomanganates, vernadite, quartz
NODKGS55 0-5cm	Mn-micronodules	B	10 Å and 7 Å phyllomanganates, vernadite, quartz
NODKGS55 5-10cm	Mn-micronodules	B	10 Å and 7 Å phyllomanganates, vernadite, quartz
NODKGS56 0-5cm	Mn-micronodules	B	10 Å and 7 Å phyllomanganates, vernadite, quartz
NODKGS56 5-10cm <sup>a</sup>	Mn-micronodules	B	10 Å and 7 Å phyllomanganates, vernadite, quartz
NODKGS57 0-5cm <sup>a</sup>	Mn-micronodules	B	10 Å and 7 Å phyllomanganates, vernadite, quartz, feldspar
NODKGS57 5-10cm	Mn-micronodules	B	10 Å and 7 Å phyllomanganates, vernadite, quartz
NODKGS58 0-5cm	Mn-micronodules	B	10 Å and 7 Å phyllomanganates, vernadite, quartz, feldspar
NODKGS58 5-10cm	Mn-micronodules	B	10 Å and 7 Å phyllomanganates, vernadite, quartz, feldspar
NODKGS60 0-5cm <sup>a</sup>	Mn-micronodules	C	10 Å and 7 Å phyllomanganates, vernadite, quartz
NODKGS60 5-10cm	Mn-micronodules	C	10 Å and 7 Å phyllomanganates, vernadite, quartz
NODKGS63	Mn-nodule	C	10 Å and 7 Å phyllomanganates, vernadite, quartz, feldspar
NODKGS63 0-5cm <sup>a</sup>	Mn-micronodules	C	10 Å and 7 Å phyllomanganates, vernadite, quartz
NODKGS65 0-5cm	Mn-micronodules	C	10 Å and 7 Å phyllomanganates, vernadite, quartz
NODKGS65 5-10cm	Mn-micronodules	C	10 Å and 7 Å phyllomanganates, vernadite, quartz

<sup>a</sup> samples analysed by both XRD and IR

**Table 3.** Chemical composition (ICP-MS) of the studied Mn-micronodules and Mn-nodules.

Sample ID	Description	Mn-nodule facies	Mn (wt. %)	Fe	Mn/Fe	Si	Al	Ca	Mg	Na	K	Ti	P	S	Li (mg/kg)	Be	B
NODKGS4Mn-8 0-5cm	Mn-micronodules	0	41.0	2.2 9	17.9	19. 6	1.9 0	1.6 8	2.3 0	1.1 6	1.1 5	0.2 0	0.0 7	0.0 7	104	0.9 7	103
NODKGS4Mn-8 5-10cm	Mn-micronodules	0	37.8	2.1 5	17.6	15. 1	1.7 3	1.4 8	2.1 0	1.1 9	1.0 3	0.1 8	0.0 7	0.0 5	46.4	0.8 8	66.7
NODKGS4Mn-nodule 4	Mn-nodule	0	27.4	4.6 4	5.90	-	0.8 7	1.3 0	0.7 0	2.1 3	0.8 6	0.1 8	0.1 2	0.1 1	181	1.6 0	93.9
NODKGS4Mn-9 0-5cm	Mn-micronodules	0	44.5	2.4 7	18.0	9.8 5	1.9 5	1.8 6	2.3 7	1.0 8	1.1 1	0.2 2	0.0 7	0.0 4	95.3	1.0 8	65.0

NODKGS4Mn- 9 5-10cm micronodules	0	36.8	2.0 8	17.7	49.1	1.6 9	1.6 2	1.9 2	0.9 3	0.9 7	0.1 9	0.0 6	0.0 5	43.4	0.8 3	55.3
NODKGS5Mn- 0 0-5cm micronodules	0	31.4	1.7 7	17.7	11.6	1.4 9	1.2 7	1.7 3	0.8 0	0.8 5	0.1 6	0.0 6	0.0 4	80.1	0.9 9	71.2
NODKGS5Mn- 0 5-10cm micronodules	0	44.6	2.3 6	18.9	4.2 6	1.9 2	1.8 3	2.4 0	1.2 4	1.1 6	0.2 3	0.0 8	0.0 6	87.0	0.8 3	76.8
NODKGS5Mn-nodule 1	0	25.9	4.7 8	5.41	-	2.5 8	1.5 4	1.6 7	2.3 2	0.8 4	0.1 9	0.1 2	0.1 3	155	1.7 9	90.3
NODKGS5Mn- 1 0-5cm micronodules	0	43.1	2.3 8	18.1	6.6 9	2.0 1	1.7 1	2.3 0	1.2 0	1.1 4	0.2 3	0.0 7	0.0 7	70.1	1.0 3	106
NODKGS5Mn- 1 5-10cm micronodules	0	41.5	2.5 5	16.3	23.2	2.0 0	1.6 0	2.1 3	1.1 4	1.1 5	0.2 2	0.0 8	0.0 5	80.1	1.0 8	85.9
NODKGS5Mn- 2 0-5cm micronodules	0	39.4	2.1 7	18.2	29.2	1.7 8	1.5 7	2.0 0	1.1 5	1.1 0	0.2 0	0.0 7	0.0 4	67.9	0.8 5	63.5
NODKGS5Mn- 2 5-10cm micronodules	0	35.3	2.1 1	16.7	13.1	1.6 7	1.3 8	2.0 0	1.0 0	1.1 5	0.1 9	0.0 6	0.0 4	70.7	0.9 4	71.9
NODKGS5Mn-nodule 3	B	29.3	5.7 7	5.07	-	2.4 9	1.5 8	1.9 6	2.2 3	0.9 9	0.3 2	0.1 4	0.1 1	133	2.3 1	94.6
NODKGS5Mn- 3 0-7 cm micronodules	B	33.2	2.8 9	11.5	13.5	2.0 8	1.4 6	1.7 9	2.3 2	1.1 3	0.2 7	0.0 7	0.0 8	112	1.1 3	86.1
NODKGS5Mn-nodule 4	B	29.3	5.9 9	4.89	-	2.5 9	1.5 6	2.0 0	2.7 0	0.9 6	0.3 5	0.1 5	0.1 2	183	2.2 8	101
NODKGS5Mn- 4 0-5cm micronodules	B	37.0	3.2 7	11.3	9.8 6	2.0 5	1.5 5	1.9 5	1.3 6	0.9 7	0.3 0	0.0 7	0.0 7	54.6	1.1 9	107
NODKGS5Mn- 4 5-10cm micronodules	B	31.8	2.7 9	11.4	63.0	1.9 6	1.2 5	1.8 6	0.9 0	0.9 5	0.2 3	0.0 6	0.0 5	87.0	1.2 2	89.8
NODKGS5Mn-nodule 5	B	28.4	6.7 4	4.21	-	2.7 1	1.6 8	2.0 2	2.3 8	0.9 8	0.3 9	0.2 1	0.1 3	121	2.5 8	107
NODKGS5Mn- 5 0-5cm micronodules	B	37.0	3.2 1	11.3	6.6 0	2.0 8	1.5 1	2.0 6	1.2 3	1.1 2	0.2 9	0.0 7	0.1 0	76.8	1.2 6	102
NODKGS5Mn- 5 5-10cm micronodules	B	35.4	2.3 0	10.7	3.0 3	2.1 7	1.4 5	2.0 6	1.0 8	1.0 3	0.2 8	0.0 7	0.0 6	89.5	1.2 6	104
NODKGS5Mn-nodule 6	B	30.9	5.8 7	5.26	-	2.4 2	1.6 2	2.0 8	2.6 8	0.9 8	0.3 5	0.1 5	0.1 2	132	2.3 5	106
NODKGS5Mn- 6 0-5cm micronodules	B	35.6	3.6 8	9.95	7.3 3	2.4 5	1.5 8	2.0 8	1.2 3	1.0 6	0.3 3	0.0 8	0.0 6	77.9	1.2 9	89.7
NODKGS5Mn- 6 5-10cm micronodules	B	36.3	3.6 9	9.82	1.1 7	2.3 0	1.4 8	2.2 3	0.9 7	1.0 5	0.3 6	0.0 8	0.0 5	72.7	1.3 1	65.0
NODKGS5Mn-nodule 7	B	27.6	6.2 0	4.44	-	2.3 6	3.0 6	1.8 6	2.4 0	0.8 4	0.3 6	0.7 7	0.1 4	109	2.5 2	104
NODKGS5Mn- 7 0-5cm micronodules	B	35.2	2.8 5	12.3	14.2	2.0 2	1.4 9	1.8 9	1.1 2	0.9 6	0.2 6	0.0 7	0.0 6	62.7	1.0 4	61.2
NODKGS5Mn- 7 5-10cm micronodules	B	42.5	3.4 2	12.4	3.4 4	2.5 2	1.7 4	2.3 7	1.3 8	1.2 4	0.3 1	0.0 8	0.0 7	127	1.1 8	109
NODKGS5Mn-nodule 8	B	26.6	5.4 8	4.85	-	2.1 1	1.4 5	1.7 7	2.2 3	0.8 5	0.3 1	0.1 4	0.1 1	119	2.0 6	98.9
NODKGS5Mn- 8 0-5cm micronodules	B	38.2	3.5 9	10.6	9.3 7	2.2 9	1.6 3	2.1 5	1.2 7	1.1 4	0.3 1	0.0 8	0.0 7	74.4	1.3 7	101
NODKGS5Mn- 8 5-10cm micronodules	B	39.7	3.7 2	10.7	16.8	2.5 0	1.6 5	2.3 2	1.1 0	1.0 9	0.3 2	0.0 8	0.0 6	74.9	1.4 0	81.2

NODKGS6Mn-nodule 0	C	26.7	4.5	5.94	-	2.1	1.4	1.5	2.6	0.9	0.1	0.1	0.1	165	1.5	84.7
NODKGS6Mn-0 0-5cm micronodules	C	38.8	1.9	19.7	3.1	1.8	1.4	2.0	1.2	1.1	0.1	0.0	0.0	208	0.9	58.7
NODKGS6Mn-0 5-10cm micronodules	C	40.8	2.0	20.0	22.6	2.0	1.5	2.0	1.3	1.3	0.1	0.0	0.0	252	0.8	54.7
NODKGS6Mn-nodule 3	C	31.4	5.3	5.88	-	2.1	1.5	1.9	2.6	1.0	0.3	0.1	0.1	240	2.1	99.7
NODKGS6Mn-3 0-5cm micronodules	C	37.2	2.4	15.1	6.9	2.1	1.4	2.0	1.5	1.0	0.2	0.0	0.0	163	1.0	64.4
NODKGS6Mn-5 0-5cm micronodules	C	39.3	2.2	17.4	6.8	2.0	1.5	1.9	1.3	1.1	0.2	0.0	0.0	175	0.8	74.4
NODKGS6Mn-5 5-10cm micronodules	C	37.9	2.3	16.1	11.6	2.3	1.4	2.1	1.2	1.1	0.2	0.0	0.0	167	0.9	67.3
<i>Average Mn-nodule</i>	0	26.6	4.7	5.65	-	1.7	1.4	1.1	2.2	0.8	0.1	0.1	0.1	168	1.6	92.1
<i>Mn-micronodules</i>	0	39.5	2.2	17.7	18.2	1.8	1.6	2.1	1.1	1.1	0.2	0.0	0.0	74	0.9	76.5
<i>Mn-nodule Mn-micronodules</i>	B	28.7	6.0	4.77	-	2.4	1.8	1.9	1.4	0.9	0.3	0.2	0.1	133	2.3	101.9
<i>Mn-nodule Mn-micronodules</i>	B	36.6	3.3	11.1	13.5	2.2	1.5	2.0	1.1	1.0	0.3	0.0	0.0	83	1.2	90.6
<i>Mn-nodule Mn-micronodules</i>	C	29.1	4.9	5.91	-	2.1	1.5	1.7	2.6	0.9	0.2	0.1	0.1	203	1.8	92.2
<i>Mn-nodule Mn-micronodules</i>	C	38.8	2.2	17.5	10.2	2.2	1.4	2.0	1.3	1.1	0.2	0.0	0.0	193	0.9	63.9
<i>Mn-nodule Mn-micronodules</i>	C average	28.2	5.3	5.28	-	2.2	1.6	1.7	2.5	0.9	0.2	0.1	0.1	159	2.0	95.8
<i>Mn-nodule Mn-micronodules</i>	C average	38.2	2.6	14.7	11.7	2.0	1.5	2.0	1.1	1.0	0.2	0.0	0.0	101	1.0	80.0
Nod-P-1, Mn-nodule, split #4-25 standard (average)		34.1	5.9	5.75	2.2	2.4	2.2	2.0	1.7	1.0	0.2	0.1	0.0	149	2.4	104
Nod-P-1, Mn-nodule, split 9-3 standard (average)		33.7	7.6	5.98	10.0	2.2	2.1	1.8	1.6	0.9	0.2	0.1	0.0	144	2.2	103
Nod-P-1 Mn-nodule, (reference) <sup>a</sup> standard		39.6	5.8	5.03	5.8	2.4	2.2	2.0	1.7	1.0	0.2	0.2	0.1	140	2.3	95.0
Nod-A-1, Mn-nodule, split #16-7 standard (average)		10.4	9.9	1.65	1.1	1.9	10.8	2.7	0.7	0.4	0.2	0.3	0.2	73.1	5.8	117
Nod-A-1, Mn-nodule, split 62-16 standard (average)		19.3	9.9	1.95	5.4	1.8	10.2	2.5	0.7	0.4	0.2	0.3	0.2	71.8	5.1	103
Nod-A-1 Mn-nodule, (reference) <sup>a</sup> standard		18.3	11.2	1.63	1.7	2.0	11.4	2.8	0.8	0.4	0.3	0.5	0.3	76.1	5.6	120

<sup>a</sup> data from Axelsson et al. (2002)

**Table 3 (continued)**

Sample ID	Description	Mn-nodule facies	Sc (mg/kg)	V	Cr	Co	Ni	Cu	Zn	Se	As	Rb	Sr	Y	Zr	Nb	Mo
NODKGS4Mn-8 0-5cm	micronodules	0	<7	46	12.8	148	1537	2142	313	-	53.7	25.9	523	29.4	70.6	10.5	942
NODKGS4Mn-8 5-10cm	micronodules	0	<7	39	12.4	139	1342	1944	293	-	49.6	24.4	562	29.3	73.6	11.0	826



NODKGS4Mn-nodule 4	0	<7	45	11.	219	1067	1378	186	1.9	63.	19.	471	29.3	176	12.	755
NODKGS4Mn-9 0-5cm micronodules	0	8.54	47	14.	170	1522	2196	313	-	53.	28.	652	34.7	82.1	11.	101
NODKGS4Mn-9 5-10cm micronodules	0	<7	38	11.	145	1335	1841	353	-	49.	23.	589	28.7	70.1	9.7	822
NODKGS5Mn-0 0-5cm micronodules	0	<7	34	11.	121	1105	1639	285	-	43.	21.	418	23.7	61.0	8.0	702
NODKGS5Mn-0 5-10cm micronodules	0	<7	50	16.	167	1506	2462	335	-	53.	28.	624	31.7	77.7	11.	101
NODKGS5Mn-nodule 1	0	<7	43	13.	207	1100	1455	170	2.4	63.	24.	501	58.8	206	14.	690
NODKGS5Mn-1 0-5cm micronodules	0	<7	45	14.	163	1517	2158	330	-	55.	27.	545	31.8	87.2	12.	934
NODKGS5Mn-1 5-10cm micronodules	0	<7	42	15.	156	1466	2104	341	-	51.	27.	552	29.8	80.8	12.	939
NODKGS5Mn-2 0-5cm micronodules	0	<7	41	16.	147	1357	1878	271	-	49.	25.	585	30.0	75.1	10.	895
NODKGS5Mn-2 5-10cm micronodules	0	<7	38	12.	138	1310	1893	274	-	48.	26.	535	28.9	74.9	10.	882
NODKGS5Mn-nodule 3	B	10.4	53	9.7	254	1476	1636	195	4.3	83.	21.	625	91.2	317	23.	819
NODKGS5Mn-3 0-7 cm micronodules	B	7.37	40	14.	199	1290	1454	227	-	57.	28.	452	33.0	100	13.	705
NODKGS5Mn-nodule 4	B	11.6	51	17.	219	1456	1487	212	4.9	82.	22.	624	94.3	326	23.	799
NODKGS5Mn-4 0-5cm micronodules	B	<7	42	15.	222	1518	1604	257	-	65.	28.	507	35.6	111	13.	709
NODKGS5Mn-4 5-10cm micronodules	B	<7	36	14.	82	1252	1312	215	-	55.	29.	449	29.9	89.2	12.	679
NODKGS5Mn-nodule 5	B	11.3	53	10.	270	1363	1117	183	5.1	94.	23.	673	102	387	28.	709
NODKGS5Mn-5 0-5cm micronodules	B	<7	42	14.	216	1497	2166	250	-	69.	30.	553	35.7	112	14.	741
NODKGS5Mn-5 5-10cm micronodules	B	<7	41	19.	204	1469	1499	246	-	62.	31.	528	35.3	108	14.	764
NODKGS5Mn-nodule 6	B	11.0	54	9.2	244	1393	1510	197	4.8	81.	21.	645	98.0	328	24.	720
NODKGS5Mn-6 0-5cm micronodules	B	7.14	44	15.	239	1455	1509	260	-	68.	31.	573	39.4	132	16.	670
NODKGS5Mn-6 5-10cm micronodules	B	7.02	45	16.	228	1360	1555	226	-	68.	31.	579	37.1	119	15.	730
NODKGS5Mn-nodule 7	B	13.3	51	10.	263	1403	1142	184	6.4	82.	21.	694	197	355	26.	706
NODKGS5Mn-7 0-5cm micronodules	B	7.45	39	13.	196	1413	1539	224	-	59.	26.	476	32.3	95.4	13.	681
NODKGS5Mn-7 5-10cm micronodules	B	7.75	49	18.	234	1663	1776	266	-	65.	35.	565	36.3	111	15.	893
NODKGS5Mn-nodule 8	B	8.25	48	9.9	245	1260	1131	172	4.0	78.	20.	573	83.0	299	22.	698
NODKGS5Mn-8 0-5cm micronodules	B	7.22	43	16.	234	1501	1642	250	-	72.	32.	582	42.0	128	17.	727

NODKGS5Mn- 8 5-10cm micronodul es	B	7.69	46 3	17. 2	249 7	1548 1	1665 8	262 4	-	68. 9	33. 1	629	38.0	118	16. 8	774
NODKGS6Mn-nodule 0	C	<7	44 6	10. 8	201 4	1100 2	1549 2	174 5	2.8 3	61. 9	22. 3	465	57.9	188	13. 8	717
NODKGS6Mn- 0 0-5cm micronodul es	C	<7	34 9	15. 2	116 1	1293 0	1876 4	251 0	-	45. 5	27. 9	460	28.5	72.7	11. 5	892
NODKGS6Mn- 0 5-10cm micronodul es	C	<7	35 8	15. 0	106 1	1251 3	1813 7	261 7	-	39. 2	30. 5	468	26.1	63.2	9.3 2	904
NODKGS6Mn-nodule 3	C	10.2	50 9	9.8 8	222 6	1306 6	1136 6	206 0	4.8 1	80. 5	21. 0	576	91.1	308	20. 9	746
NODKGS6Mn- 3 0-5cm micronodul es	C	<7	38 8	16. 4	150 5	1375 8	1752 0	261 7	-	52. 8	31. 0	477	30.0	81.2	10. 7	757
NODKGS6Mn- 5 0-5cm micronodul es	C	<7	37 8	15. 4	128 2	1504 0	1856 2	288 7	-	48. 2	30. 9	454	29.3	74.8	10. 2	817
NODKGS6Mn- 5 5-10cm micronodul es	C	10.0	38 5	17. 2	133 3	1388 3	1840 0	256 7	-	44. 5	32. 3	485	29.0	75.4	10. 4	787
Average Mn-nodule	0	<7	44 2	12. 7	213 4	1084 0	1417 0	178 4	2.2 2	63. 6	21. 9	486	44.0	190. 8	13. 6	723
Mn- micronodul es	0	<7	42 5	13. 7	149 9	1400 1	2026 2	311 3	-	50. 9	25. 9	559	29.8	75.3	10. 8	898
Mn-nodule	B	11.0	51 9	11. 2	249 7	1388 9	1311 6	190 8	5.0 5	83. 8	21. 7	639	110. 9	335. 1	24. 7	742
Mn- micronodul es	B	7.4	42 8	16. 0	219 0	1400 1	1610 7	244 3	-	64. 9	30. 7	536	35.9	111. 2	14. 9	734
Mn-nodule	C	10.2	47 7	10. 4	212 0	1200 4	1342 9	190 3	3.8 3	71. 2	21. 7	520	74.5	248. 1	17. 3	731
Mn- micronodul es	C	10.0	37 2	15. 8	126 5	1362 6	1827 0	264 0	-	46. 0	30. 5	469	28.6	73.4	10. 4	831
Mn-nodule	average	10.9	48 8	11. 4	228 8	1255 3	1368 0	186 4	3.9 2	74. 2	22. 1	566	83.4	268	19. 3	740
Mn- micronodul es	average	7.79	41 5	15. 1	174 7	1414 8	1812 2	273 8	-	55. 9	28. 8	532	32.1	90	12. 5	816
Nod-P-1, Mn-nodule, split #4-25 (average)	C	<7	48 3	13. 2	227 6	1380 1	1204 4	212 6	-	11 9	26. 6	681	96.5	286	22. 3	702
Nod-P-1, Mn-nodule, split 9-3 (average)	C	11.1	48 4	13. 8	220 5	1286 2	1083 5	192 2	-	10 1	25. 5	661	89.4	268	22. 3	705
Nod-P-1 Mn-nodule, (reference) standard		9.70	51 0	13. 3	229 0	1350 0	1120 0	202 0	-	88. 5	23. 7	670	90	280	21. 3	675
Nod-A-1, Mn-nodule, split #16-7 (average)	C	<7	57 8	18. 0	298 8	6122 1	1034 4	812 2	-	36. 3	10. 2	152 5	115	299	42. 2	358
Nod-A-1, Mn-nodule, split 62-16 (average)	C	11.7	58 0	18. 0	289 8	5630 1	950 4	701 2	-	32 9	9.9 1	145 1	113	298	45. 7	391
Nod-A-1 Mn-nodule, (reference) standard		12.4	66 0	20. 9	318 0	6450 1	1130 4	800 2	-	31 0	10. 6	163 0	120	310	43. 1	390

Table 3 (continued)

Sample ID	Description Mn-nodule facies	Cd (mg/kg)	Sn	Sb	Te	Ba	Hf	Ta	W	Tl	Pb	Bi	Th	U	Au	Pt
NODKGS4Mn-	0	13.3	0.7	61.	1.2	156	1.1	0.2	77.	67.	41	4.2	7.70	2.6	<0.03	0.05

8 0-5cm	micronodules		4	2	1	7	2	2	8	1	9	3		3	0	2	
NODKGS4 Mn-		0	12.0	0.7	54.	1.1	152	1.0	0.1	57.	53.	37	4.2	7.58	2.3	<0.03	0.04
8 5-10cm	micronodules		4	5	2	1	9	8	7	5	8	2		9	0	6	
NODKGS4 Mn-nodule		0	18.0	0.2	46.	1.9	191	2.3	0.2	34.	121	29	2.6	7.41	3.2	-	0.05
4			4	1	7	2	7	7	5	9	8	8		3	3	-	0.05
NODKGS4 Mn-		0	13.9	0.8	64.	1.4	174	1.2	0.1	78.	77.	47	4.8	9.34	2.9	<0.03	0.05
9 0-5cm	micronodules		2	1	0	6	7	9	6	1	1	1		3	0	5	
NODKGS4 Mn-		0	11.3	0.7	53.	1.1	144	1.0	0.1	57.	54.	38	4.0	7.48	2.3	<0.03	0.03
9 5-10cm	micronodules		2	1	3	9	4	9	3	3	1	3		5	0	8	
NODKGS5 Mn-		0	10.6	0.6	46.	0.7	127	0.9	0.1	55.	45.	32	3.5	6.46	2.1	<0.03	0.03
0 0-5cm	micronodules		9	8	9	1	1	8	0	1	8	2		1	0	8	
NODKGS5 Mn-		0	15.0	0.8	62.	1.2	171	1.2	0.2	87.	69.	42	4.6	8.65	2.8	<0.03	0.04
0 5-10cm	micronodules		2	3	2	9	4	4	9	4	7	1		1	0	9	
NODKGS5 Mn-nodule		0	15.9	0.2	40.	2.4	206	2.8	0.3	38.	112	31	2.7	11.9	3.2	-	0.06
1			8	3	5	4	7	6	1	9	6	6		1	1	-	0.06
NODKGS5 Mn-		0	12.6	0.8	62.	1.4	180	1.2	0.2	67.	67	46	4.8	9.20	2.6	<0.03	0.06
1 0-5cm	micronodules		9	2	6	2	5	6	7	4	3	0		4	0	2	
NODKGS5 Mn-		0	12.5	1.6	62.	1.3	180	1.1	0.2	70.	60.	45	4.8	8.79	2.5	<0.03	0.05
1 5-10cm	micronodules		9	8	8	2	9	5	1	2	5	8		8	0	0	
NODKGS5 Mn-		0	12.3	0.7	54.	1.0	158	1.1	0.2	54.	63.	39	4.0	7.81	2.4	<0.03	0.04
2 0-5cm	micronodules		7	7	4	1	3	2	0	0	4	2		8	0	9	
NODKGS5 Mn-		0	12.0	0.7	53.	1.0	152	1.1	0.2	70.	55.	40	4.4	7.85	2.4	<0.03	0.05
2 5-10cm	micronodules		9	9	8	7	2	0	6	7	5	0		3	0	7	
NODKGS5 Mn-nodule		B	19.5	0.3	48.	3.5	231	4.5	0.3	69.	238	45	6.2	24.2	3.9	-	0.12
3			6	9	8	2	9	0	2	2	3	7		3	3	-	0.12
NODKGS5 Mn-		B	10.9	0.9	43.	1.3	157	1.6	0.2	53.	74.	42	5.6	12.2	2.2	<0.03	0.04
3 0-7 cm	micronodules		8	9	6	9	3	8	9	4	3	2		3	0	7	
NODKGS5 Mn-nodule		B	18.5	0.4	48.	3.7	222	4.7	0.3	61.	260	48	7.5	28.9	4.2	-	0.12
4			0	7	8	0	6	3	0	0	1	6		0	0	-	0.12
NODKGS5 Mn-		B	11.1	1.0	46.	1.5	163	1.7	0.2	54.	84.	46	6.6	13.9	2.5	<0.03	0.07
4 0-5cm	micronodules		1	2	9	9	1	4	4	1	9	0		3	0	9	
NODKGS5 Mn-		B	9.91	0.5	43.	1.3	165	1.4	0.2	57.	67.	42	5.8	12.2	2.1	<0.03	0.06
4 5-10cm	micronodules		6	7	3	2	8	6	5	7	3	2		9	0	4	
NODKGS5 Mn-nodule		B	15.1	0.4	39.	4.3	251	5.6	0.3	75.	199	55	8.0	28.6	4.3	-	0.14
5			3	5	1	7	0	6	4	4	9	7		9	9	-	0.14
NODKGS5 Mn-		B	11.9	1.1	51.	1.6	163	1.8	0.3	54.	90.	48	6.7	14.9	2.6	<0.03	0.06
5 0-5cm	micronodules		2	6	6	9	4	0	2	2	4	8		6	0	3	
NODKGS5 Mn-		B	11.6	1.1	47.	1.6	177	1.7	0.2	60.	81.	48	7.0	14.8	2.5	<0.03	0.07
5 5-10cm	micronodules		0	0	4	9	9	9	7	4	9	3		1	0	3	
NODKGS5 Mn-nodule		B	18.7	0.3	43.	3.6	238	4.8	0.3	66.	281	49	7.1	23.9	4.0	-	0.12
6			7	8	5	2	0	2	9	7	7	9		7	7	-	0.12
NODKGS5 Mn-		B	11.4	1.2	45.	1.7	199	2.1	0.3	66.	91.	53	7.9	16.4	2.8	<0.03	0.09
6 0-5cm	micronodules		4	4	5	9	3	4	3	6	6	9		6	0	5	
NODKGS5 Mn-		B	10.6	1.1	44.	1.9	206	1.9	0.2	80.	69.	51	8.1	15.8	2.7	<0.03	0.09
6 5-10cm	micronodules		0	3	3	3	3	8	4	0	7	6		3	0	5	
NODKGS5 Mn-nodule		B	16.4	0.3	41.	3.9	234	5.2	0.3	69.	217	51	7.5	24.9	4.7	-	0.13
7			8	9	0	6	1	5	5	5	5	9		3	3	-	0.13
NODKGS5 Mn-		B	10.2	0.9	43.	1.4	140	1.5	0.2	50.	78.	40	5.4	12.0	2.2	<0.03	0.05
7 0-5cm	micronodules		1	8	1	3	0	6	2	6	2	4		4	0	0	
NODKGS5 Mn-		B	12.7	1.1	56.	1.6	197	1.8	0.3	63.	86.	51	6.8	14.6	2.7	<0.03	0.07
7 5-10cm	micronodules		8	5	3	4	5	4	5	8	5	7		1	0	1	

NODKGS5 Mn-nodule 8	B	16.7	0.3	40.	3.3	201	4.2	0.2	63.	190	47	6.4	21.5	3.8	-	0.11
		4	3	5	5	8	9	9	6	6	0	9	7	7		0
NODKGS5 Mn- 8 0-5cm micronodul es	B	12.1	1.1	45.	1.5	185	2.0	0.3	57.	89.	51	7.4	15.8	2.8	<0.03	0.07
		7	7	7	2	2	2	2	2	6	9	6	3	0	0	3
NODKGS5 Mn- 8 5-10cm micronodul es	B	11.4	1.1	47.	1.8	199	1.9	0.3	60.	73.	52	7.5	15.8	2.6	<0.03	0.07
		6	2	1	6	3	1	8	4	5	2	6	6	0	0	0
NODKGS6 Mn-nodule 0	C	17.0	0.2	45.	2.2	166	2.6	0.2	43.	152	34	3.2	12.5	3.3	-	0.07
		5	8	5	5	5	5	5	6	0	1	5	5	5		0
NODKGS6 Mn- 0 0-5cm micronodul es	C	11.0	0.8	59.	1.0	148	1.1	0.2	69.	68.	35	3.9	7.50	2.0	<0.03	0.04
		6	8	4	6	9	5	9	0	4	1	6	6	0	0	1
NODKGS6 Mn- 0 5-10cm micronodul es	C	10.7	0.7	56.	0.9	142	1.0	0.2	80.	62.	31	3.3	6.64	1.9	<0.03	0.04
		8	6	6	8	8	2	9	3	9	5	5	0	0	0	3
NODKGS6 Mn-nodule 3	C	19.8	0.3	47.	3.1	173	4.4	0.3	68.	220	41	6.7	27.8	4.0	-	0.10
		7	7	5	2	6	1	3	3	2	3	3	1	1		5
NODKGS6 Mn- 3 0-5cm micronodul es	C	11.0	0.9	51.	1.0	165	1.3	0.2	54.	61.	37	4.3	8.62	2.2	<0.03	0.05
		2	1	4	6	1	4	7	3	7	0	9	9	0	0	6
NODKGS6 Mn- 5 0-5cm micronodul es	C	11.3	0.9	58.	1.0	148	1.2	0.2	55.	71.	34	3.9	7.77	2.1	<0.03	0.05
		0	0	2	5	0	3	6	6	9	7	7	1	1	0	5
NODKGS6 Mn- 5 5-10cm micronodul es	C	10.9	0.8	55.	1.0	165	1.2	0.2	61.	64.	34	3.7	7.69	2.1	<0.03	0.04
		8	1	2	6	4	2	7	3	4	7	7	0	0	0	9
<i>Average</i> Mn-nodule	0	16.9	0.2	43.	2.2	198	2.6	0.3	36.	116	32	2.7	9.64	3.2	-	0.06
		6	2	1	8	2	2	3	3	4	2	2	2	2		
Mn- micronodul es	0	12.6	0.8	57.	1.1	179	1.1	0.2	68.	61.	41	4.3	8.09	2.5	<0.03	0.05
		7	6	8	4	4	1	7	2	2	5	5	3	0	0	
Mn-nodule Mn- micronodul es	B	17.6	0.3	43.	3.7	255	4.8	0.3	67.	231	49	7.1	25.3	4.2	-	0.13
		8	8	0	0	8	2	6	6	6	9	3	0	0		
Mn-nodule Mn- micronodul es	B	11.3	1.0	46.	1.6	178	1.8	0.2	59.	80.	48	6.8	14.4	2.5	<0.03	0.07
		9	8	0	0	0	9	9	9	6	2	4	0	6	0	
Mn-nodule Mn- micronodul es	C	18.4	0.3	46.	2.7	169	3.5	0.2	56.	186	37	4.9	20.1	3.6	-	0.09
		1	7	0	8	5	8	0	0	9	7	8	8	8		
Mn-nodule Mn- micronodul es	C	11.0	0.8	55.	1.0	154	1.2	0.2	64.	70.	34	3.8	7.65	2.0	<0.03	0.05
		7	1	2	2	0	3	6	1	9	6	6	9	0	0	
Mn-nodule Mn- micronodul es	average	17.9	0.3	45.	2.9	207	3.8	0.3	56	188	41	5.2	19.4	3.8	-	0.10
		2	0	4	6	3	0	0	6	4	4	4	3	3		
Mn-nodule Mn- micronodul es	average	11.7	0.9	52.	1.3	166	1.4	0.2	64.	71.	42	5.3	10.6	2.4	<0.03	0.06
		6	7	3	4	3	5	2	2	1	9	1	7	6	0	
Nod-P-1, Mn-nodule, split #4-25 (average)		23.1	2.2	54.	5.1	258	4.2	0.4	59.	238	50	6.1	17.0	4.2	<0.03	0.11
		8	6	8	7	5	0	7	7	7	4	4	4	0	0	5
Nod-P-1, Mn-nodule, split 9-3 (average)		20.4	2.3	48.	4.4	326	3.9	0.3	62.	225	46	5.1	15.6	4.0	<0.03	0.10
		1	6	2	4	6	8	0	0	5	4	4	4	0	0	7
Nod-P-1 Mn-nodule, (reference) standard		22.6	1.9	49.	4.8	269	4.2	0.3	57.	210	47	5.8	16.7	4.0	<0.00	0.12
		0	4	0	0	0	0	3	8	5	0	0	0	0	9	0
Nod-A-1, Mn-nodule, split #16-7 (average)		8.07	2.9	34.	33.	141	6.0	0.7	80.	109	88	11.	23.1	7.1	0.030	0.50
		3	1	6	1	0	0	3	7	8	5	5	4	4	5	5
Nod-A-1, Mn-nodule, split 62-16 (average)		7.58	2.9	30.	27.	151	5.9	0.8	88.	119	81	9.7	22.6	6.7	0.036	0.49
		4	7	7	0	6	0	5	5	1	3	3	6	6	5	5
Nod-A-1 Mn-nodule, (reference) standard		7.5	3	33.	30.	153	5.8	0.7	87	120	86	10.	25.1	7	<0.00	0.52
		8	9	0	0	0	6	6	0	0	2	2	9	9	0	0

**Table 4.** REE concentrations (ICP-MS) of the studied Mn-micronodules and Mn-nodules.

Sample	Descripti	Mn- La	C	Pr	N	S	E	G	T	D	Ho	Er	T	Y	L	ΣR	(Ce/C	(Eu/E	L <sub>NASC</sub> /L
--------	-----------	-----------	---	----	---	---	---	---	---	---	----	----	---	---	---	----	-------	-------	----------------------

ID	Location	nodule (mg/facies kg)	e	d	m	u	d	b	y	m	b	u	EE	e*) <sup>a</sup>	u*) <sup>b</sup>	u <sub>NASC</sub>					
NODKGMn-S48 0-	micronodules	0	1	6	13	58	15	3.	13	2.	11	1.	4.	0.	5.	0.					
		40.4	3	.6	.3	.1	90	.3	12	.3	96	94	71	06	69	334	1.50	1.21	0.88		
NODKGMn-S48 5-	micronodules	0	1	5	12	54	14	3.	12	1.	10	1.	4.	0.	4.	0.					
		36.2	3	.9	.0	.4	54	.5	95	.5	76	69	66	79	65	312	1.52	1.16	0.84		
NODKGMn-S44	nodule	0	1	4	18	76	18	4.	16	2.	14	2.	6.	0.	5.	0.					
		58.4	6	.7	.3	.5	51	.7	63	.0	44	12	79	17	68	371	0.96	1.13	1.29		
NODKGMn-S49 0-	micronodules	0	1	9	15	64	16	4.	14	2.	12	2.	5.	0.	6.	0.					
		43.5	5	.1	.0	.8	04	.6	32	.2	18	80	80	26	75	383	1.64	1.13	0.87		
NODKGMn-S49 5-	micronodules	0	1	5	12	52	14	3.	12	1.	10	1.	4.	0.	5.	0.					
		35.8	4	.4	.8	.0	48	.2	94	.0	79	79	65	65	63	311	1.57	1.17	0.85		
NODKGMn-S50 0-	micronodules	0	1	3	11	47	12	3.	10	1.	8.	1.	3.	0.	4.	0.					
		30.9	2	.0	.6	.4	02	.8	70	82	56	89	57	94	55	270	1.53	1.14	0.85		
NODKGMn-S50 5-	micronodules	0	1	8	14	64	16	3.	14	2.	11	2.	5.	0.	7.	0.					
		41.4	5	.8	.0	.5	98	.2	21	.8	06	32	7.	71	71	367	1.60	1.14	0.87		
NODKGMn-S51	nodule	0	1	5	20	84	20	5.	19	3.	18	3.	8.	1.	8.	1.					
		65.0	3	.6	.8	.9	18	.5	21	.0	30	7.	23	76	24	414	0.90	1.12	0.79		
NODKGMn-S51 0-	micronodules	0	1	8	14	62	16	3.	13	2.	11	2.	5.	0.	4.	0.					
		41.9	4	.4	.0	.2	92	.9	22	.6	08	19	76	86	72	364	1.61	1.14	0.87		
NODKGMn-S51 5-	micronodules	0	1	7	13	57	15	3.	13	2.	11	1.	5.	0.	4.	0.					
		39.5	6	.4	.5	.2	72	.0	63	.0	96	00	71	61	68	344	1.64	1.16	0.87		
NODKGMn-S52 0-	micronodules	0	1	6	13	56	14	3.	12	2.	10	1.	4.	0.	4.	0.					
		37.3	1	.0	.0	.7	64	.8	01	.4	86	93	68	75	65	323	1.56	1.16	0.86		
NODKGMn-S52 5-	micronodules	0	1	5	12	54	14	3.	12	1.	10	1.	4.	0.	5.	0.					
		35.7	9	.6	.0	.1	49	.2	91	.1	77	56	65	23	63	316	1.61	1.17	0.86		
NODKGMn-S53	nodule	B	3	2	34	14	35	8.	33	5.	31	5.	14	2.	14	2.					
		113	0	.9	.2	.4	62	.9	50	.1	55	.8	07	.7	06	764	1.10	1.09	0.82		
NODKGMn-S53 0-7	micronodules	B	2	1	14	62	16	3.	14	2.	11	2.	5.	0.	5.	0.					
		41.0	3	.5	.3	.3	88	.6	32	.8	08	24	73	47	70	394	1.87	1.10	0.88		
NODKGMn-S54	nodule	B	3	6	38	15	39	9.	37	6.	34	6.	16	2.	16	2.					
		121	8	.6	.8	.7	44	.7	16	.5	00	.1	26	.0	25	854	1.16	1.07	0.80		
NODKGMn-S54 0-	micronodules	B	2	3	15	67	17	4.	15	2.	12	2.	5.	0.	5.	0.					
		45.6	7	.7	.1	.7	19	.2	39	.1	22	71	80	06	74	431	1.90	1.12	0.92		
NODKGMn-S54 5-	micronodules	B	2	1	13	58	15	3.	13	2.	11	1.	4.	0.	4.	0.					
		40.2	8	.8	.7	.5	70	.5	08	.0	94	86	69	60	66	389	1.99	1.13	0.92		
NODKGMn-S55	nodule	B	3	8	42	16	41	10	40	6.	36	6.	16	2.	16	2.					
		133	6	.0	.9	.9	.1	.5	61	.4	33	.8	40	.7	37	910	1.12	1.08	0.84		
NODKGMn-S55 0-	micronodules	B	2	4	16	69	18	4.	16	2.	13	2.	6.	0.	5.	0.					
		47.4	7	.6	.9	.5	31	.1	50	.1	39	09	84	22	82	451	1.89	1.10	0.86		
NODKGMn-S55 5-	micronodules	B	2	5	15	67	17	4.	15	2.	12	2.	5.	0.	4.	0.					
		46.5	6	.8	.9	.5	27	.6	43	.8	24	72	81	49	77	453	2.03	1.13	0.90		
NODKGMn-S56	nodule	B	3	2	37	15	37	9.	36	5.	32	5.	15	2.	15	2.					
		122	8	.5	.0	.5	12	.8	95	.4	83	.7	22	.8	24	802	1.05	1.08	0.82		
NODKGMn-S56 0-	micronodules	B	2	6	17	73	18	4.	16	2.	13	2.	6.	0.	3.	0.					
		50.5	7	.3	.4	.9	57	.9	66	.9	50	35	92	87	86	479	1.94	1.12	0.88		
NODKGMn-		B	2	47.3	2	15	63	16	4.	15	2.	12	2.	5.	0.	6.	0.	472	2.23	1.13	0.91



25 standard		8																		
Nod-P-1,Mn-split 9-3 nodule, standard	109	0	32	13	31	7	30	4	26	5	13	1	12	1						
Nod-P-1 Mn-(referenc e) <sup>c</sup> standard	105	0	31	13	31	7	30	4	27	5	13	1	12	1						
Nod-A-1, split #16-7 standard	111	1	24	98	21	5	26	3	23	4	14	2	13	2	107					
Nod-A-1, split 62-16 standard	107	2	23	94	20	5	24	3	22	4	13	1	13	1	103					
Nod-A-1 Mn-(referenc e) <sup>c</sup> standard	115	2	25	98	21	5	25		23	5	14	2	13	2	107					
		0	.0	.0	.9	20	.4	4	.8	00	.4	00	.9	10	6	2.92	0.96			0.82

<sup>a</sup> Ce/Ce\* = 2Ce<sub>SN</sub> / (La<sub>SN</sub> + Pr<sub>SN</sub>)<sup>b</sup> Eu/Eu\* = 2Eu<sub>SN</sub> / (Sm<sub>SN</sub> + Gd<sub>SN</sub>)<sup>c</sup> data from Axelsson et al. (2002)**Table 5.** Electron microprobe data for Mn-micronodules from sample NODKGS63 0-5 cm.

Layer type	Layer description	Mn (wt. %)	Fe	Mn/Fe	Co	Ni	Cu	Ni+Cu	Si	Al	Ca	Mg	Ti	Na	K	P	S	V (mg/kg)	Mg	Ba
1 (hydrogenetic)	low average (n <sup>a</sup> = 13)	22.2	5.78	4.15	0.22	0.71	0.68	1.44	4.08	1.50	1.50	1.62	0.68	0.46	0.15	0.15	0.2	490	65	104
	reflectivity, high	3.61	1.35	0.99	0.05	0.15	0.22	0.22	0.97	0.48	0.30	0.18	0.2	0.23	0.1	0.03	0.1	164	23	473
	porosity, min	22.9	5.52	4.19	0.22	0.72	0.60	1.30	3.65	1.58	1.5	1.63	0.73	0.44	0.5	0.15	0.2	414	58	888
	porosity, max	14.6	2.80	2.56	0.14	0.37	0.19	1.11	2.86	1.01	0.8	1.4	0.3	0.14	0.2	0.08	0.0	269	41	521
	porosity, max	27.0	8.31	5.96	0.30	0.91	0.26	1.88	6.33	2.78	2.1	1.98	1.0	1.04	0.9	0.19	0.5	823	11	207
	dense	39.9	0.56	104	0.02	0.24	0.18	3.42	2.47	1.01	1.3	2.09	0.5	0.21	1.4	0.08	0.0	282	11	400
2a (suboxic-diagenetic)	growth	2.05	0.27	127	0.02	0.70	0.57	1.06	1.90	0.66	0.1	0.44	0.0	0.40	0.1	0.03	0.0	158	19	137
	structures	39.9	0.62	62	0.02	0.98	0.38	3.39	2.18	0.88	1.3	3.19	0.0	1.5	0.5	0.08	0.0	322	10	377
	with high reflectivity	34.6	0.00	327	0.00	0.41	0.03	1.44	0.04	0.10	1.0	0.38	0.0	1.0	0.3	0.02	0.0	<DL <sup>b</sup>	90	<D
	porous	44.1	1.18	37	0.07	0.88	0.00	5.45	10.4	3.74	1.6	2.59	0.1	2.17	0.7	0.14	0.5	498	17	731
	porous	24.2	0.34	30.9	0.11	0.33	0.25	3.11	3.87	1.51	0.9	1.74	0.2	0.71	0.8	0.07	0.1	359	88	620
	growth	7.03	0.71	24.8	0.10	0.48	0.41	0.61	2.23	0.74	0.2	0.38	0.1	0.27	0.3	0.02	0.1	126	29	284
2b (suboxic-diagenetic)	structures	23.6	1.25	19.8	0.09	0.19	0.31	3.05	3.80	1.49	0.9	1.82	0.2	0.67	0.8	0.06	0.0	357	84	579
	with low reflectivity	12.0	0.08	8.25	0.00	0.52	0.46	1.93	0.14	0.10	0.5	0.92	0.0	0.17	0.5	0.02	0.0	<DL	32	<D
	porous	39.5	3.15	95.5	0.50	0.40	0.20	4.17	10.4	3.74	2.3	2.50	0.5	2.17	1.7	0.05	0.5	749	18	165
	porous	15	0.50	30	0.11	0.33	0.25	3.11	3.87	1.51	0.9	1.74	0.2	0.71	0.8	0.07	0.1	359	88	620
	porous	15	0.50	30	0.11	0.33	0.25	3.11	3.87	1.51	0.9	1.74	0.2	0.71	0.8	0.07	0.1	359	88	620

<sup>a</sup> n = number of analyses<sup>b</sup> <DL = below detection limits**Table 6.** Chemical composition (ICP-MS) of the pore waters from the sediment core NODKGS65.

Sample ID <sup>a</sup>	Na (g/kg)	K	Ca	Mg	S	Si (mg/kg)	B	Sr	Fe (µg/kg)	Mn	Al	P	Li	Rb	Ba	Mo	V	Zn	Cu	Ni	Co
Detection limits <sup>c</sup>	0.00	0.00	0.000	0.000	0.00	0.007	0.01	0.00	0.22	0.06	1.19	0.62	0.46	0.37	0.06	0.09	0.01	1.74	0.09	0.27	0.01

NODK GS65 (0-1)	11.8	0.46	0.42	1.34	0.93	5.93	53	4.	8.08	4.76	1.	7.	20	15	32	12	7.	12	6.	1.4	0.	
NODK GS65 (1-2)	12.2	0.46	0.43	1.35	0.93	6.64	61	4.	7.91	1.54	0.	2.	11	20	15	32	11	3.	5.	1.	0.7	0.
NODK GS65 (2-3)	11.3	0.45	0.44	1.37	0.95	7.17	61	4.	7.93	3.51	0.	4.	11	20	14	33	11	3.	7.	2.	0.6	0.
NODK GS65 (3-4)	11.8	0.45	0.44	1.38	0.95	7.27	55	4.	7.95	3.24	0.	4.	11	20	14	33	10	3.	7.	1.	0.5	0.
NODK GS65 (5-6)	11.6	0.45	0.44	1.38	0.93	7.76	48	4.	7.92	3.31	0.	1.	11	20	14	33	10	2.	7.	1.	0.4	0.
NODK GS65 (6-7)	11.5	0.44	0.45	1.39	0.96	8.05	51	4.	7.84	1.66	0.	3.	10	20	13	33	9.	2.	8.	1.	0.5	0.
NODK GS65 (7-8)	11.5	0.44	0.45	1.39	0.95	8.36	53	4.	7.96	0.54	0.	4.	11	20	13	33	9.	2.	10	1.	0.4	0.
NODK GS65 (8-9)	11.6	0.43	0.45	1.43	0.96	8.25	56	4.	7.95	3.06	0.	-	11	20	13	33	9.	2.	13	1.	0.5	0.
NODK GS65 (9-10)	11.8	0.44	0.45	1.40	0.95	8.41	35	4.	7.84	0.37	0.	1.	10	20	13	32	9.	2.	6.	1.	<D	0.
NODK GS65 (10-11)	12.1	0.44	0.45	1.42	0.97	8.40	47	4.	7.80	3.16	0.	-	10	20	13	32	9.	2.	6.	1.	0.4	0.
NODK GS65 (11-12)	11.6	0.44	0.44	1.42	0.96	8.72	36	4.	7.84	2.70	0.	-	11	20	13	32	9.	2.	8.	1.	<D	0.
NODK GS65 (12-13)	11.9	0.43	0.45	1.42	0.97	8.60	41	4.	7.82	2.79	0.	-	11	19	13	31	9.	2.	12	1.	0.4	0.
NODK GS65 (13-14)	11.8	0.43	0.45	1.41	0.96	8.67	40	4.	7.87	1.65	0.	2.	11	19	13	32	9.	2.	19	2.	0.4	0.
NODK GS65 (14-15)	11.7	0.44	0.45	1.43	0.96	8.95	39	4.	7.89	2.90	0.	12	11	19	13	32	9.	2.	11	1.	0.2	0.
NODK GS65 (15-16)	11.9	0.43	0.44	1.41	0.95	8.73	43	4.	8.04	2.36	0.	2.	11	20	13	33	9.	2.	16	1.	0.7	0.
NODK GS65 (16-17)	10.9	0.44	0.45	1.40	0.94	9.21	40	4.	7.81	7.28	0.	4.	14	19	13	31	8.	2.	6.	0.	0.4	0.
NODK GS65 (17-18)	11.4	0.45	0.44	1.42	0.96	8.87	39	4.	7.71	10.9	0.	3.	13	19	13	31	8.	2.	8.	1.	0.3	0.
NODK GS65 (18-19)	12.1	0.44	0.45	1.43	0.95	9.68	25	4.	7.91	2.55	0.	D	10	19	13	32	8.	2.	6.	1.	0.4	0.
NODK GS65 (19-20)	12.0	0.43	0.45	1.43	0.96	9.59	35	4.	7.99	25.6	0.	1.	11	19	13	31	8.	2.	15	1.	0.3	0.
NODK GS65 (20-22)	12.3	0.44	0.45	1.42	0.96	9.84	30	4.	7.88	5.54	0.	-	10	19	13	31	8.	2.	10	0.	0.3	0.
NODK GS65 (22-24)	12.1	0.44	0.45	1.42	0.95	10.6	25	4.	7.93	5.41	1.	2.	12	19	13	31	8.	1.	17	1.	0.7	0.
NODK GS65 (24-26)	11.9	0.43	0.44	1.41	0.96	10.5	43	4.	8.03	3.26	0.	-	12	20	13	31	8.	2.	31	1.	<D	0.
NODK GS65 (26-28)	12.6	0.43	0.45	1.43	0.96	10.0	40	4.	7.98	3.22	0.	-	10	19	13	30	8.	2.	10	1.	0.3	0.
NODK	12.2	0.44	0.44	1.38	0.94	9.99	4.	4.	8.01	4.71	0.	-	12	19	13	29	8.	2.	11	1.	<D	0.



GS65 (28-30) NODK							40			46		5	9	3	.7	02	54	.4	25	L	03	
GS65 (30-32) NODK	12.4	0.45	0.43	1.43	0.93	12.2	39	8.10	1.08	0.	8.	14	19	13	30	8.	2.	8.	0.	0.3	0.	
GS65 (32-34) NODK	12.6	0.44	0.45	1.42	0.97	10.1	42	7.84	1.93	0.	-	11	19	13	29	7.	2.	14	1.	<D	0.	
GS65 (34-36) NODK	12.3	0.45	0.45	1.41	0.95	11.0	42	7.84	5.16	0.	-	10	19	13	29	7.	2.	9.	1.	<D	0.	
GS65 (36-38) NODK	12.0	0.44	0.45	1.38	0.95	11.0	42	7.88	4.21	0.	-	12	19	13	31	7.	2.	13	1.	<D	0.	
GS65 (38-40)	12.4	0.46	0.44	1.37	0.93	12.4	42	7.75	1.48	0.	-	10	20	14	30	7.	3.	8.	1.	<D	0.	
SW-XR-2 (average)	10.3	0.38	0.40	1.25	0.86	3.8	3	7.46	284	18	77	13	17	11	60	19	97	19	11	151	57	
SW-XR-2 (reference)						3.8	3			18	77	13	17	11	60	19	97	19	11		57	
NASS-5 (average)	9.47	0.35	0.35	1.10	0.76	-	55	6.58	<DL	-	<DL	10	10	5.	9.	1.	D	0.	<D	<D	D	
NASS-5 (reference)	-	-	0.37	1.18	0.81	0.0	7	67	6.95	1.40	2.	1.	17	16	10	4.	9.	1.	0.	0.	0.3	0.
IAPSO (average)	12.4	0.45	0.45	1.42	0.98	1.7	4	75	8.50	1.97	9	8	.1	8	9	.2	.1	55	8	65	7	13
IAPSO (reference)	10.2	0.39	0.41	1.27	0.90	-	-	7.46	-	-	-	-	18	-	-	11	-	-	-	-	-	-

<sup>a</sup> numbers in parentheses = depth in core in cm

<sup>b</sup>  $Ce/Ce^{*}=2Ce_{SN}/(La_{SN}+Nd_{SN})$

<sup>c</sup> long-term averages obtained over multiple sessions of pore waters analyses. For each session the detection limits were obtained after measuring repeated blank solutions intercalated with pore water samples (1 blank for 5 samples).

<sup>d</sup> below detection limits

**Table 6 (continued)**

Sample ID	Cr ( $\mu\text{g/kg}$ )	Cl	U	Ti	Ge	La	Ce	Nd	(Ce/Ce*) <sup>b</sup>
Detection limits	0.01	0.03	0.0006	0.05	0.01	0.01	0.01	0.002	
NODKGS65 (0-1)	0.63	0.26	2.63	0.10	0.04	0.02	0.01	0.01	0.39
NODKGS65 (1-2)	0.65	0.26	2.54	<DL	0.03	0.01	0.01	0.01	0.27
NODKGS65 (2-3)	0.41	0.26	2.56	-	0.03	0.02	0.01	0.01	0.35
NODKGS65 (3-4)	0.43	0.25	2.59	-	0.05	0.02	0.01	0.01	0.36
NODKGS65 (5-6)	0.49	0.22	2.45	-	0.05	0.02	0.01	0.01	0.33
NODKGS65 (6-7)	0.47	0.21	2.48	-	0.04	0.01	0.01	-	-
NODKGS65 (7-8)	0.59	0.24	2.52	0.27	0.05	0.02	0.02	0.01	0.80
NODKGS65 (8-9)	0.80	0.24	2.51	<DL	0.04	0.02	0.01	0.01	0.46
NODKGS65 (9-10)	0.59	0.20	2.51	-	0.05	0.02	0.01	0.01	0.35
NODKGS65 (10-11)	0.71	0.26	2.53	-	0.05	0.02	0.01	0.01	0.26
NODKGS65 (11-12)	0.52	0.20	2.47	-	0.05	0.02	0.01	0.01	0.42
NODKGS65 (12-13)	0.62	0.21	2.50	-	0.04	0.02	0.01	-	-
NODKGS65 (13-14)	0.59	0.20	2.58	-	0.02	0.02	0.03	0.01	1.24
NODKGS65 (14-15)	0.56	0.21	2.57	<DL	0.05	0.02	0.01	0.01	0.33
NODKGS65 (15-16)	0.57	0.20	2.55	-	0.04	0.02	0.01	0.01	0.34
NODKGS65 (16-17)	0.57	0.18	2.58	0.21	0.05	0.01	0.01	-	-
NODKGS65 (17-18)	0.82	0.19	2.56	<DL	0.04	0.01	0.01	0.01	0.25
NODKGS65 (18-19)	0.62	0.21	2.57	<DL	0.04	0.03	0.02	0.01	0.59
NODKGS65 (19-20)	0.64	0.21	2.60	-	0.02	0.02	0.01	0.01	0.31
NODKGS65 (20-22)	0.72	0.19	2.60	0.17	0.04	0.02	0.01	0.01	0.31
NODKGS65 (22-24)	0.73	0.18	2.35	0.07	0.04	0.02	0.01	-	-
NODKGS65 (24-26)	0.71	0.20	2.52	-	0.04	0.02	0.01	-	-
NODKGS65 (26-28)	0.74	0.17	2.63	-	0.05	0.02	0.01	-	-
NODKGS65 (28-30)	0.75	0.19	2.60	-	0.04	0.02	0.01	0.01	0.28
NODKGS65 (30-32)	0.64	0.19	2.64	0.05	0.07	0.01	-	-	-
NODKGS65 (32-34)	0.62	0.16	2.51	-	0.04	0.02	0.01	-	-

NODKGS65 (34-36)	0.75	0.19	2.49	-	0.04	0.02	0.01	-	-
NODKGS65 (36-38)	0.61	0.17	2.49	-	0.05	0.02	0.01	-	-
NODKGS65 (38-40)	0.67	0.18	2.32	<DL	0.04	0.02	0.01	-	-
SW-XR-2 (average)	3.15	2.09	4.89	95.9	1.96	2.92	19.2	19.2	-
SW-XR-2 (reference)	3.16	2.09	4.87	96.2	1.97	2.91	19.1	19.1	-
NASS-5 (average)	0.11	<DL	2.63	<DL	<DL	<DL	<DL	<DL	-
NASS-5 (reference)	0.10	0.02	3.09	0.31	-	0.02	0.00	0.03	-
IAPSO (average)	0.34	0.28	3.34	0.23	0.02	0.03	0.01	0.01	-
IAPSO (reference)	-	-	-	-	-	-	-	-	-

**Table 7.** Fe-Cu-Zn-isotope composition (MC-ICP-MS) of the studied Mn-micronodules and Mn-nodules.

Sample ID	Description	Mn-nodule	$\delta^{56/54}\text{Fe}_{\text{IR}}$ (‰)	2s	$\delta^{57/54}\text{Fe}_1$ (‰)	2s	$\delta^{57/56}\text{Fe}_{\text{IR}}$ (‰)	2s	$\delta^{65/63}\text{Cu}_{\text{S}}$ (‰)	2s	$\delta^{66/64}\text{Zn}$ (‰)	2s	$\delta^{66/64}\text{Zn}_{\text{SR}}$ (‰)	2s	$\delta^{68/66}\text{Zn}_{\text{SR}}$ (‰)	2s
		MM-14			RMM-14		MM-14		RM976		n <sub>JMC</sub>		M3168a		M3168a	
NODKG Mn-S44	Mn-nodule	0	-0.63	0.04	-0.92	0.09	-0.29	0.03	0.21	0.03	0.76	0.06	1.66	0.06	1.65	0.11
NODKG Mn-S49 0-5cm	micronodules	0	-0.40	0.04	-0.60	0.09	-0.19	0.03	0.31	0.03	0.54	0.06	1.74	0.06	1.72	0.11
NODKG Mn-S49 5-10cm	micronodules	0	-0.34	0.04	-0.49	0.09	-0.15	0.03	0.30	0.03	0.11	0.06	1.51	0.06	1.49	0.11
NODKG Mn-S51	Mn-nodule	0	-0.53	0.04	-0.77	0.09	-0.23	0.03	0.26	0.03	0.75	0.06	1.65	0.06	1.59	0.11
NODKG Mn-S51 0-5cm	micronodules	0	-0.39	0.04	-0.54	0.09	-0.15	0.03	0.24	0.03	0.77	0.06	1.67	0.06	1.65	0.11
NODKG Mn-S51 5-10cm	micronodules	0	-0.32	0.04	-0.42	0.09	-0.10	0.03	0.27	0.03	0.73	0.06	1.63	0.06	1.54	0.11
NODKG Mn-S53	Mn-nodule	B	-0.48	0.04	-0.71	0.09	-0.22	0.03	0.35	0.03	0.85	0.06	1.75	0.06	1.70	0.11
NODKG Mn-S53 0-7cm	micronodules	B	-0.43	0.04	-0.65	0.09	-0.22	0.03	0.24	0.03	0.83	0.06	1.73	0.06	1.72	0.11
NODKG Mn-S54	Mn-nodule	B	-0.39	0.04	-0.62	0.09	-0.23	0.03	0.30	0.03	0.86	0.06	1.76	0.06	1.75	0.11
NODKG Mn-S54 0-5cm	micronodules	B	-0.33	0.04	-0.46	0.09	-0.15	0.03	0.30	0.03	0.84	0.06	1.74	0.06	1.67	0.11
NODKG Mn-S54 5-10cm	micronodules	B	-0.34	0.04	-0.49	0.09	-0.16	0.03	0.34	0.03	0.82	0.06	1.72	0.06	1.68	0.11
NODKG Mn-S55	Mn-nodule	B	-0.35	0.04	-0.67	0.09	-0.21	0.03	0.33	0.03	0.87	0.06	1.77	0.06	1.71	0.11
NODKG Mn-S55 0-5cm	micronodules	B	-0.39	0.04	-0.55	0.09	-0.16	0.03	0.29	0.03	0.90	0.06	1.80	0.06	1.72	0.11
NODKG Mn-S55 5-10cm	micronodules	B	-0.40	0.04	-0.59	0.09	-0.19	0.03	0.32	0.03	0.88	0.06	1.78	0.06	1.69	0.11
NODKG Mn-S56	Mn-nodule	B	-0.44	0.04	-0.70	0.09	-0.26	0.03	0.32	0.03	0.86	0.06	1.76	0.06	1.72	0.11
NODKG Mn-S56 0-5cm	micronodules	B	-0.40	0.04	-0.55	0.09	-0.15	0.03	0.31	0.03	0.75	0.06	1.65	0.06	1.65	0.11
NODKG Mn-S56 5-10cm	micronodules	B	-0.37	0.04	-0.53	0.09	-0.17	0.03	0.35	0.03	0.88	0.06	1.78	0.06	1.72	0.11
NODKG Mn-S57	Mn-nodule	B	-0.55	0.04	-0.75	0.09	-0.21	0.03	0.33	0.03	0.84	0.06	1.74	0.06	1.69	0.11
NODKG Mn-S57 0-5cm	micronodules	B	-0.37	0.04	-0.50	0.09	-0.13	0.03	0.27	0.03	0.86	0.06	1.76	0.06	1.72	0.04
NODKG Mn-S57 5-10cm	micronodules	B	-0.36	0.04	-0.52	0.09	-0.16	0.03	0.28	0.03	0.84	0.06	1.74	0.06	1.72	0.04

10cm nodule														
NODKG Mn-S58 nodule	B	-0.48	0.0	-0.67	0.09	-0.19	0.32	0.03	0.86	0.06	1.76	0.06	1.71	0.11
NODKG Mn-S58 0-5cm nodule	B	-0.43	0.0	-0.59	0.09	-0.16	0.20	0.03	0.73	0.06	1.63	0.06	1.99	0.11
NODKG Mn-S58 5-10cm nodule	B	-0.39	0.0	-0.58	0.09	-0.19	0.35	0.03	0.81	0.06	1.71	0.06	1.47	0.11
NODKG Mn-S60 nodule	C	-0.59	0.0	-0.89	0.09	-0.30	0.29	0.03	0.80	0.06	1.70	0.06	1.67	0.11
NODKG Mn-S60 0-5cm nodule	C	-0.31	0.0	-0.43	0.09	-0.13	0.26	0.03	0.84	0.06	1.74	0.06	1.67	0.11
NODKG Mn-S60 5-10cm nodule	C	-0.27	0.0	-0.37	0.09	-0.10	0.23	0.03	0.77	0.06	1.67	0.06	1.66	0.11
NODKG Mn-S63 nodule	C	-0.41	0.0	-0.50	0.09	-0.09	0.33	0.03	0.84	0.06	1.74	0.06	1.68	0.11
NODKG Mn-S63 0-5cm nodule	C	-0.35	0.0	-0.52	0.09	-0.17	0.25	0.03	0.85	0.06	1.75	0.06	1.68	0.11
NODKG Mn-S65 0-5cm nodule	C	-0.33	0.0	-0.42	0.09	-0.09	0.21	0.03	0.79	0.06	1.69	0.06	1.65	0.11
NODKG Mn-S65 5-10cm nodule	C	-0.35	0.0	-0.51	0.09	-0.17	0.26	0.03	0.85	0.06	1.75	0.06	1.68	0.11
Nod-P-1, Mn-split 9-3 nodule, standard		-0.55	0.0	-0.78	0.09	-0.23	0.30	0.03	0.82	0.06	1.72	0.06	1.69	0.04
Nod-P-1, Mn-split 9-3 nodule, standard		-0.59	0.0	-0.83	0.09	-0.24	0.38	0.03	0.81	0.06	1.71	0.06	1.71	0.11
Nod-P-1, Mn-split 9-3 nodule, standard		-0.59	0.0	-0.83	0.09	-0.24	0.37	0.03	0.83	0.06	1.73	0.06	1.67	0.11
Nod-P-1, Mn-split #4-25 nodule, standard		-0.57	0.0	-0.86	0.09	-0.30	0.31	0.03	0.80	0.06	1.70	0.06	1.67	0.11
Nod-P-1, Mn-split #4-25 nodule, standard		-0.61	0.0	-0.88	0.09	-0.28	0.31	0.03	0.83	0.06	1.73	0.06	1.68	0.11

**Table 8.** Average chemical composition of Mn-micronodules and Mn-nodules of the ocean.

Location	Mn-micronodules	Mn-nodules	Mn-nodule standard Nod-A-1	Mn-nodule standard Nod-A-1	Mn-micronodules	Mn-micronodules	Mn-micronodules	Mn-micronodules
	CCZ	CCZ	CCZ	Atlantic Ocean	CCZ	CCZ	Central Pacific Basin	Equatorial North Pacific
Reference	this study	this study	this study	this study	Dubinin and Sval'nov, 2003	Dubinin et al., 2008	Ito et al., 2005	Dubinin and Sval'nov, 2000a
Mn (wt.%)	38.2	28.2	29.6	18.3	24.1	29.9	28.3	33.0
Fe	2.69	5.33	5.89	11.2	3.17	4.35	2.62	0.81
Si	14.7	-	5.85	1.74	-	-	-	-
Al	2.04	2.24	2.46	2.08	1.72	1.56	3.74	0.73
Ca	1.55	1.64	2.24	11.4	-	-	1.65	-
Mg	2.09	1.73	2.03	2.83	-	-	2.90	-
Na	1.17	2.53	1.71	0.87	-	-	0.63	-
K	1.09	0.93	1	0.49	-	-	3.48	-
Ti	0.24	0.27	0.27	0.3	0.47	0.47	0.21	-
P	0.07	0.19	0.21	0.59	0.10	0.09	0.07	0.14
S	0.06	0.11	0.1	0.34	-	-	-	-
Li (mg/kg)	101	159	140	76.1	-	-	48.7	-
Be	1.07	2.02	2.3	5.6	-	-	2.20	-
B	80	95.8	95	120	-	-	-	-
Sc	7.79	10.9	9.7	12.4	-	-	5.31	-
V	416	488	510	660	-	-	104	-
Cr	15.1	11.4	13.3	20.9	-	-	34.7	-
Co	1747	2288	2290	3180	1625	2871	1620	420
Ni	14148	12553	13500	6450	13163	19212	38800	13980
Cu	18122	13680	11200	1130	14963	8191	9250	11020



Te	-	-	-	-	-	-	1.44	-
Ba	4800	1950	-	-	4433	900	846	-
Hf	-	-	-	-	-	-	0.85	-
Ta	-	-	-	-	-	-	0.04	-
W	-	-	-	-	-	-	6.16	45.5
Tl	-	-	-	-	-	-	20.2	-
Pb	-	-	-	-	267	100	99.8	-
Bi	-	-	-	-	-	-	0.46	-
Th	-	-	-	-	-	-	0.78	9.01
U	-	-	-	-	-	-	5.05	-
Au	-	-	-	-	-	-	-	-
Pt	-	-	-	-	-	-	-	-
La	-	-	22.2	28.8	-	-	69.8	115
Ce	-	-	50.8	102	-	-	38.4	478
Pr	-	-	5.38	7.05	-	-	11.0	29.1
Nd	-	-	22.9	33.3	-	-	46.6	124
Sm	-	-	5.00	7.57	-	-	9.28	28.1
Eu	-	-	1.18	1.78	-	-	2.63	6.69
Gd	-	-	5.08	8.13	-	-	11.9	30.2
Tb	-	-	0.82	1.20	-	-	1.78	4.40
Dy	-	-	5.02	7.81	-	-	11.4	27.5
Ho	-	-	1.12	1.60	-	-	2.47	5.82
Er	-	-	3.39	4.35	-	-	7.21	16.5
Tm	-	-	0.49	0.66	-	-	1.05	2.15
Yb	-	-	3.22	4.13	-	-	6.59	14.1
Lu	-	-	0.51	0.64	-	-	1.08	2.12

Table 8 (continued).

	Mn-micronodules Southwest Pacific Basin	Mn-micronodules western North Pacific Ocean	Mn-micronodules Angola Basin	Mn-micronodules Mid-Atlantic Ridge	Mn-micronodules Central Indian Basin	Mn-nodules CCZ	Mn-nodules Peru Basin
Reference	Stoffers et al., 1984	Yasukawa et al., 2020	Dubin et al., 2013	Dekov et al. 2003	Polunin et al., 1994	Hein and Koschinsky, 2014	Hein and Koschinsky, 2014
Mn	17.9	-	18.6	8.82	26.7	28.1	34.2
(wt.%)	-	20.3	-	-	-	-	-
Fe	9.92	4.67	8.15	5.9	4.00	5.92	6.12
Si	-	-	-	0.59	-	-	4.82
Al	-	3.74	2.57	0.84	2.96	2.31	1.5
Ca	-	2.06	-	1.80	1.74	1.72	1.82
Mg	-	1.93	-	1.16	1.95	1.88	1.71
Na	-	1.08	-	0.83	0.91	1.98	2.65
K	-	1.32	-	0.33	0.98	1.01	0.81
Ti	-	0.33	-	0.07	0.38	0.28	0.16
P	-	0.42	0.28	-	0.17	0.22	0.15
S	-	-	-	-	-	-	-
Li	-	-	62.7	12.8	-	129	311
(mg/kg)	-	-	-	-	-	-	-
Be	-	-	2.13	1.30	-	-	1.4
B	-	-	-	57.3	-	-	-
Sc	-	1.7	-	3.20	-	11	7.58
V	-	23.5	288	183	126	429	431
Cr	-	26.1	-	33.3	-	-	16
Co	1667	1677	2327	420	927	2011	475
Ni	6767	1553	7393	549	8525	13159	13008
Cu	3133	884	2376	3963	7275	10631	5988
Zn	1067	1058	1126	1224	1049	1385	1845
Se	-	-	-	-	-	-	0.5
As	-	48.6	85.7	-	-	-	65
Rb	-	36.4	31.3	4.33	-	23.6	12.2
Sr	-	374	514	561	455	633	687
Y	-	168	75.8	29.5	71.0	92	69
Zr	-	109	-	44.8	-	286	325
Nb	-	10.4	-	1.00	-	18.9	13.2
Mo	-	338	223	76.7	249	587	547
Cd	-	-	18.7	2.18	-	-	18.8
Sn	-	-	-	0.45	-	-	0.9
Sb	-	-	-	3.38	-	-	61
Te	-	-	-	-	-	3.5	1.7
Ba	1533	710	974	1507	1637	3752	3158
Hf	-	1.54	-	0.78	-	4.28	4.74
Ta	-	0.29	-	0.03	-	0.31	0.23
W	-	-	34.6	1.98	-	61	75
Tl	-	-	39.1	22.8	-	-	129
Pb	500	176	595	173	469	311	121
Bi	-	-	9.27	0.45	-	-	3.25
Th	-	5.36	36.1	10.9	-	14	6.9
U	-	2.52	4.18	10.2	-	3.96	4.39
Au	-	-	-	-	-	-	-
Pt	-	-	-	-	-	-	0.04
La	-	95.9	77.3	49.3	72.7	108	68

Ce	-	212	826	204	384	255	110
Pr	-	25.5	20.4	13.7	-	32	14.1
Nd	-	116	75.9	53.9	86.8	135	63
Sm	-	26.1	17.7	11.9	27.5	32.7	14
Eu	-	6.40	4.11	3.18	6.93	7.83	3.87
Gd	-	29.0	17.9	11.7	25.2	31	15.6
Tb	-	4.43	2.74	1.78	-	4.78	2.52
Dy	-	27.6	15.9	9.53	18.9	27.5	15.8
Ho	-	5.54	3.14	1.67	3.68	5.12	3.42
Er	-	16.0	8.37	4.44	10.6	14.1	9.8
Tm	-	2.24	1.16	0.62	-	2.02	1.49
Yb	-	14.1	7.17	3.73	10.3	13.1	10.3
Lu	-	2.10	1.20	0.58	3.65	1.95	1.61

Table 8 (continued).

		Mn-nodules	
Location	Reference	Indian Ocean	
		Hein and Koschinsky, 2014	
Mn (wt.%)			24.4
Fe			7.10
Si			9.2
Al			2.8
Ca			1.63
Mg			1.9
Na			1.8
K			1.1
Ti			0.4
P			0.17
S			-
Li (mg/kg)			97
Be			-
B			-
Sc			-
V			-
Cr			-
Co			1100
Ni			11000
Cu			10400
Zn			1200
Se			-
As			-
Rb			-
Sr			679
Y			102
Zr			-
Nb			-
Mo			570
Cd			-
Sn			-
Sb			-
Te			-
Ba			1570
Hf			-
Ta			-
W			-
Tl			-
Pb			712
Bi			-
Th			-
U			-
Au			0.003
Pt			0.075
La			128
Ce			452
Pr			33
Nd			144
Sm			32.1
Eu			7.78
Gd			31
Tb			5
Dy			26.2
Ho			4.87
Er			12.4
Tm			2
Yb			11.6
Lu			1.92

## Declaration of interests

The authors declare that they have no known competing financial interests or personal relationships that could have appeared to influence the work reported in this paper.

The authors declare the following financial interests/personal relationships which may be considered as potential competing interests:

Journal Pre-proof

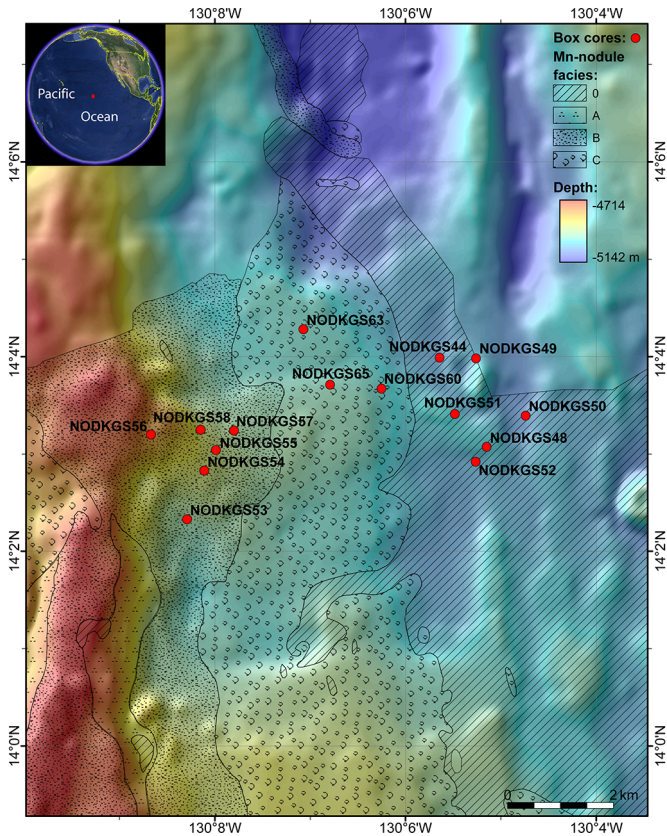


Figure 1



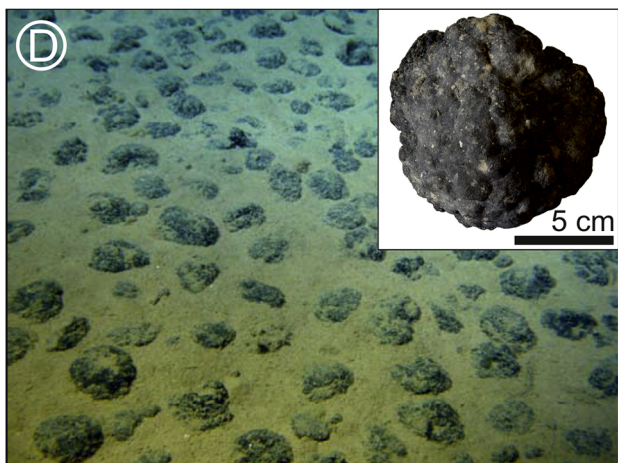
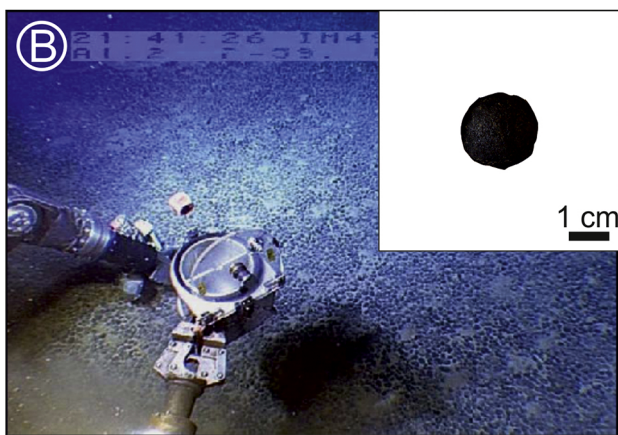
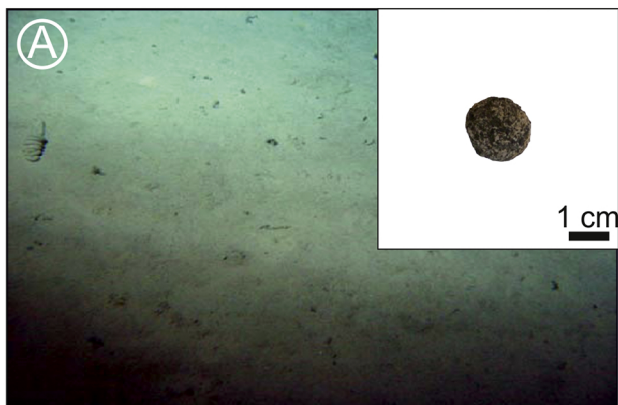


Figure 2

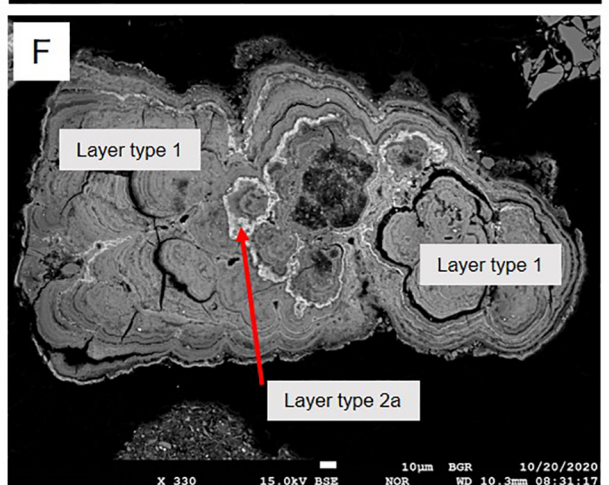
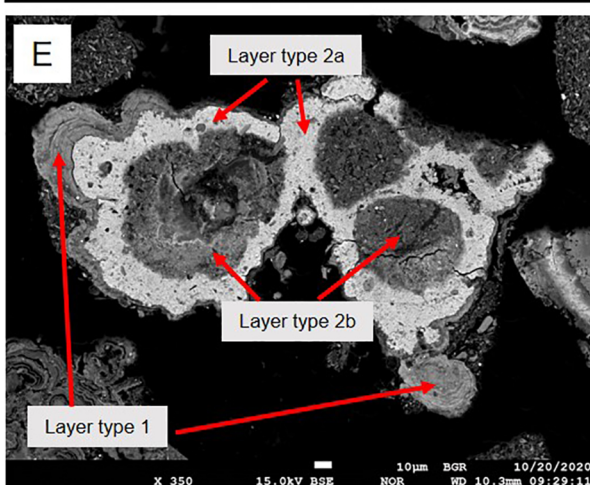
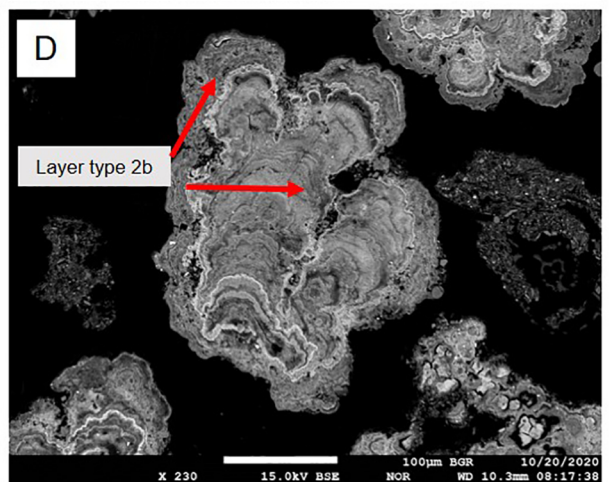
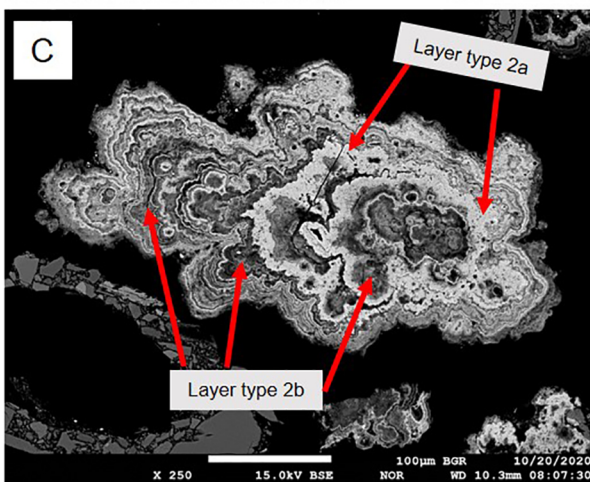
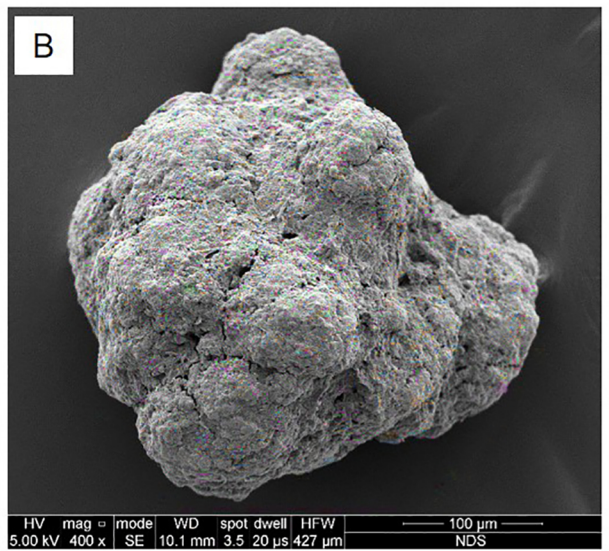
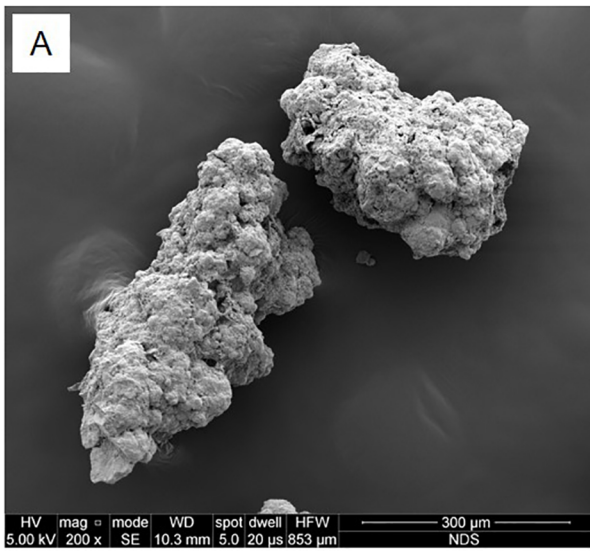


Figure 3

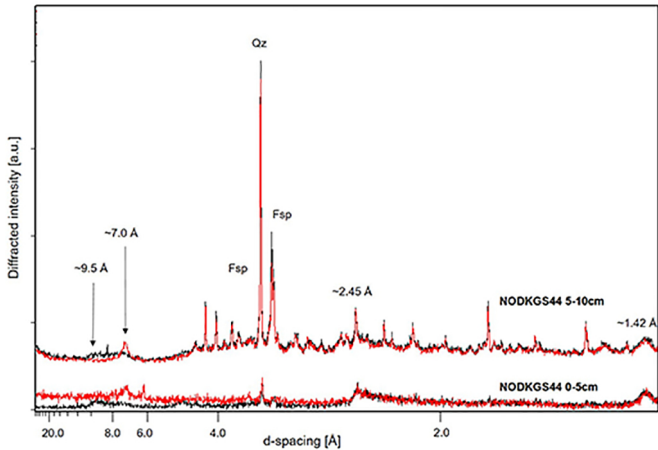


Figure 4

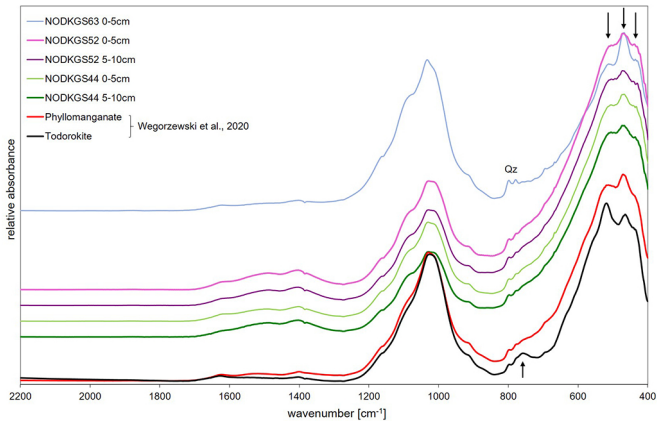


Figure 5

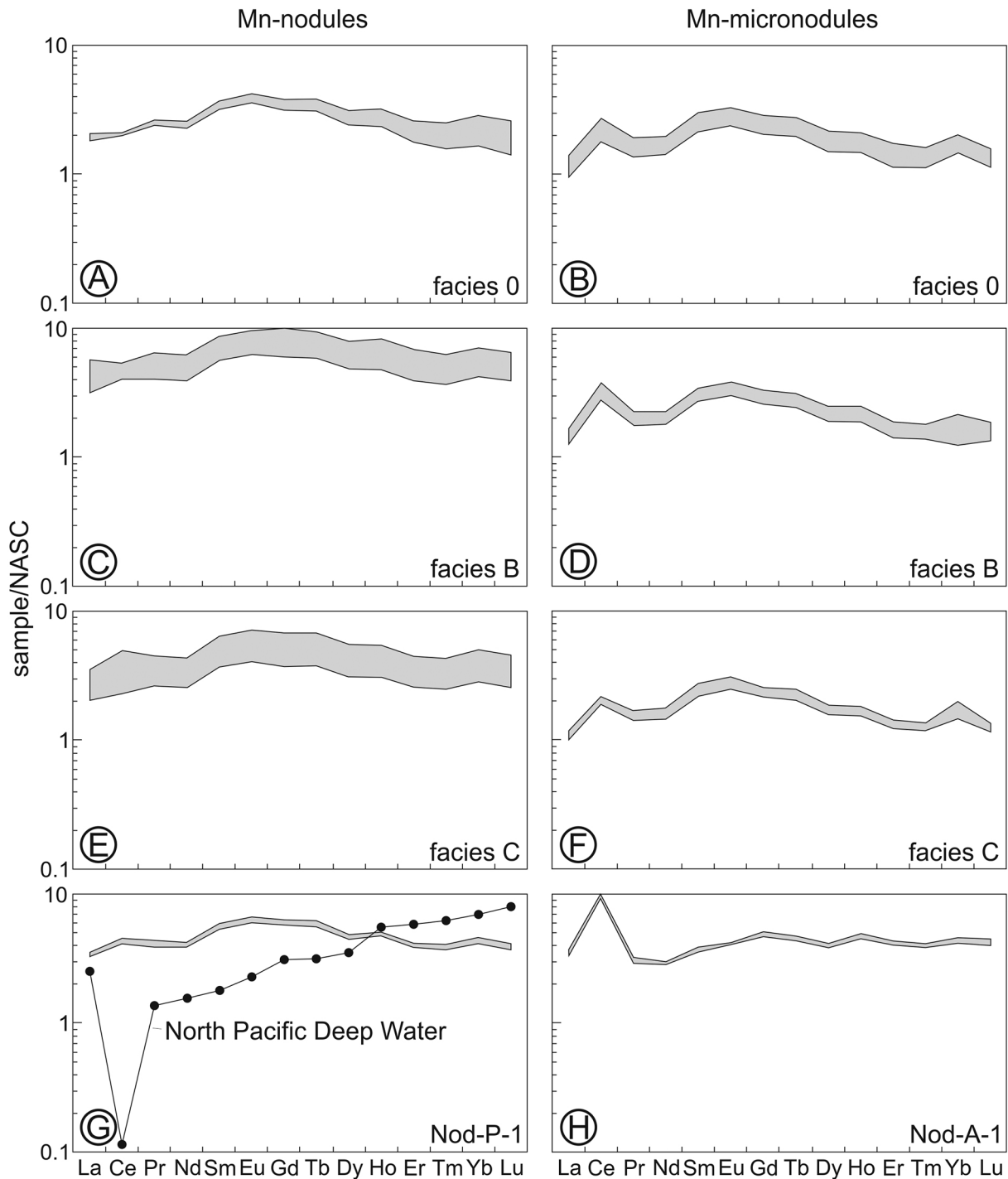


Figure 6

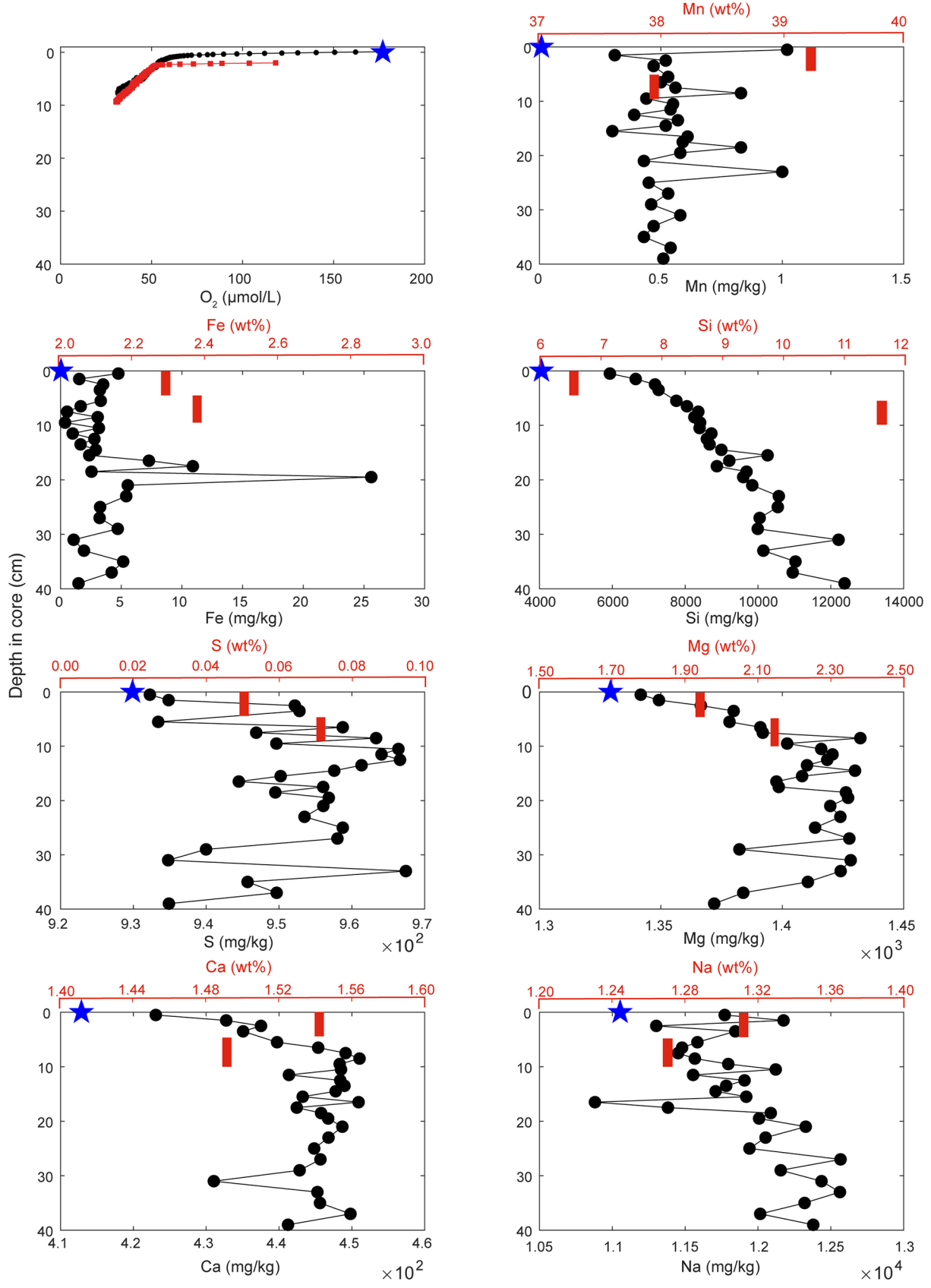


Figure 7A

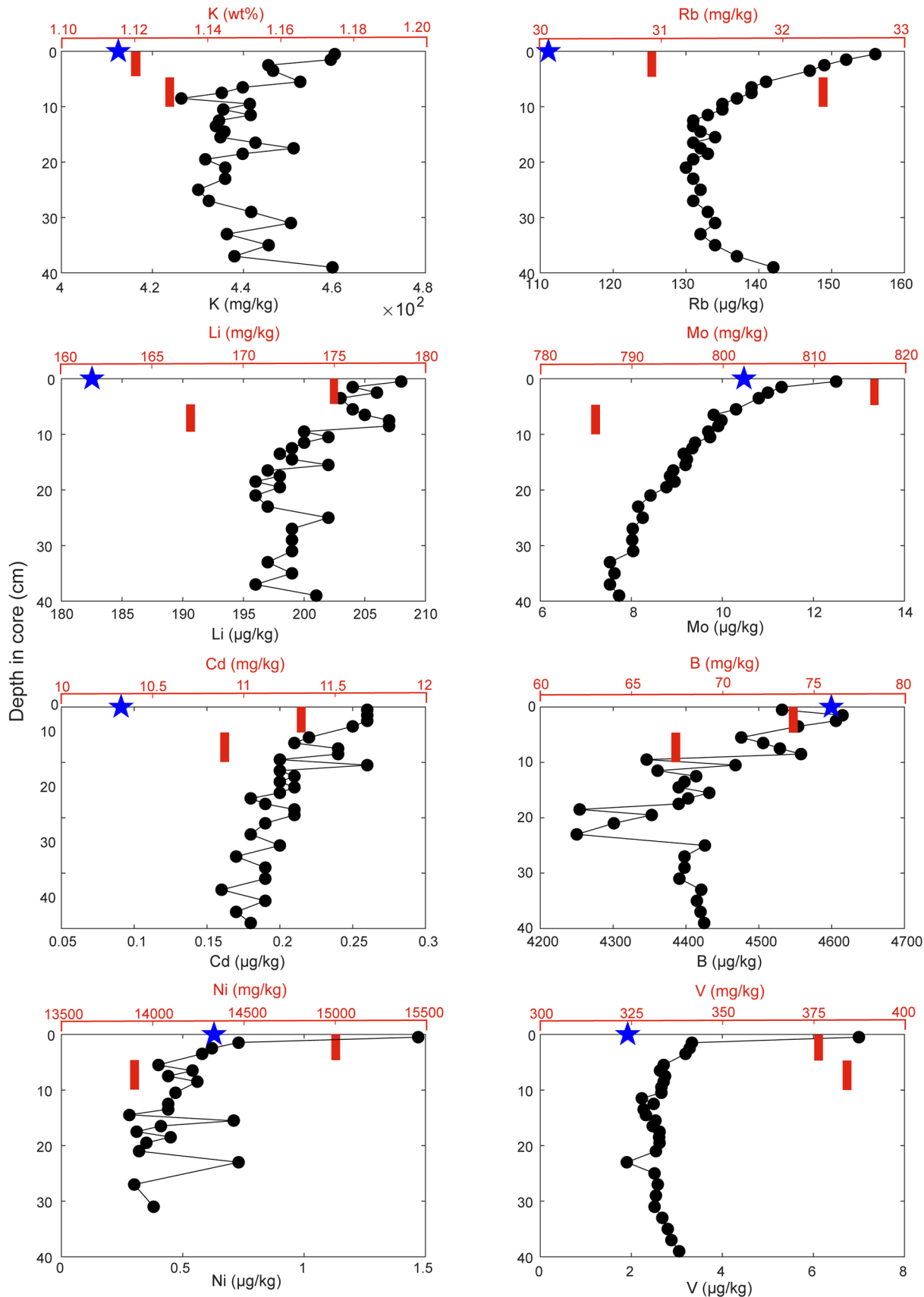


Figure 7B

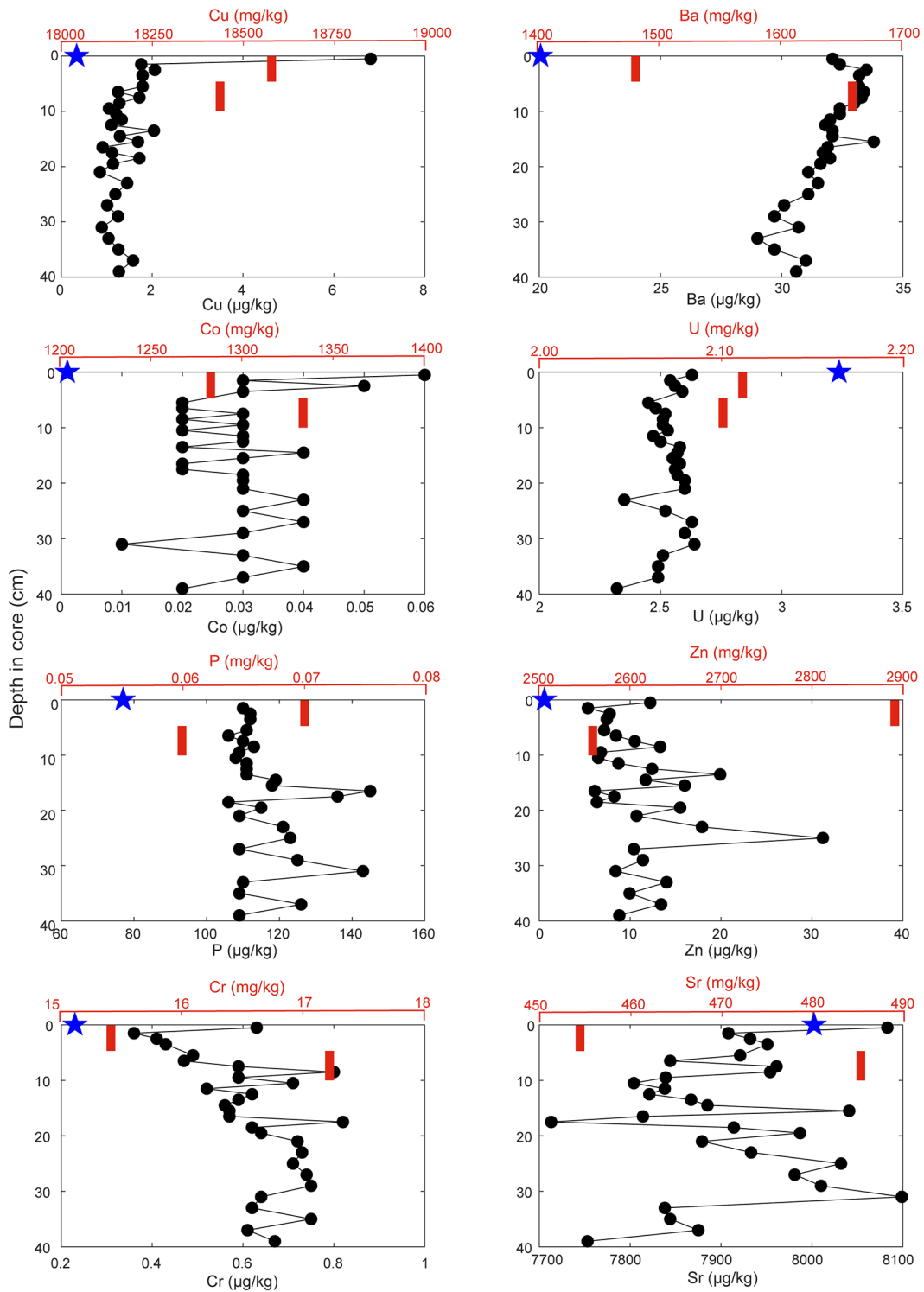


Figure 7C



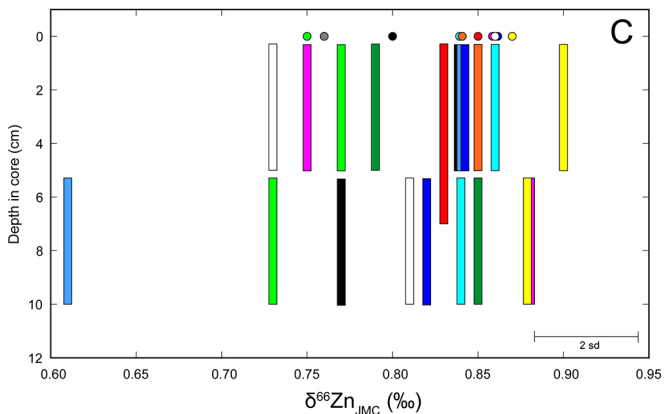
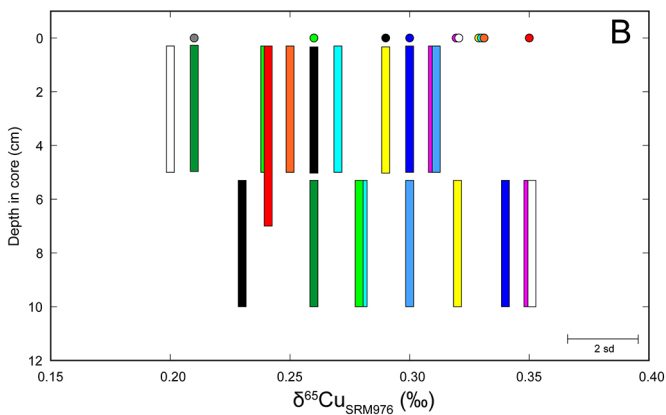
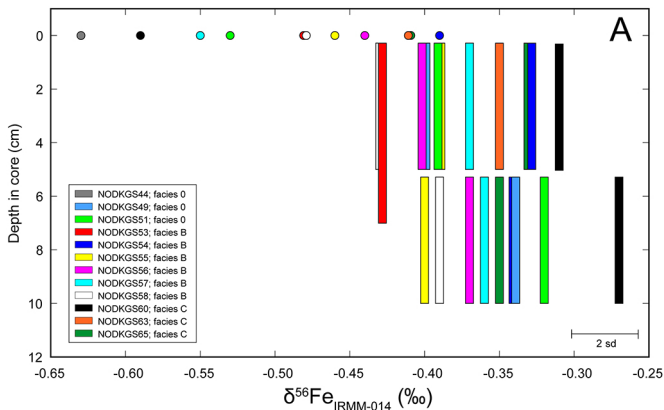


Figure 8

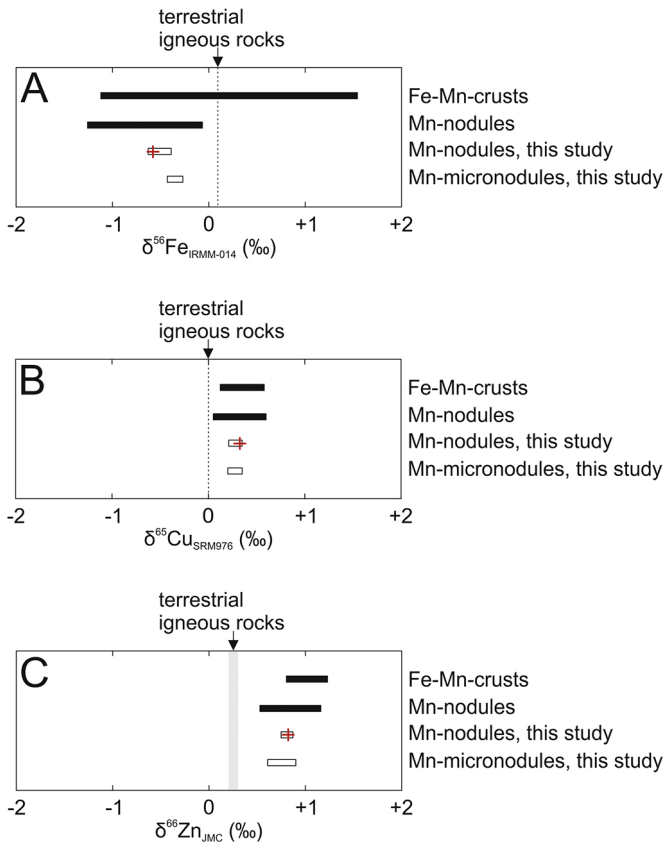


Figure 9

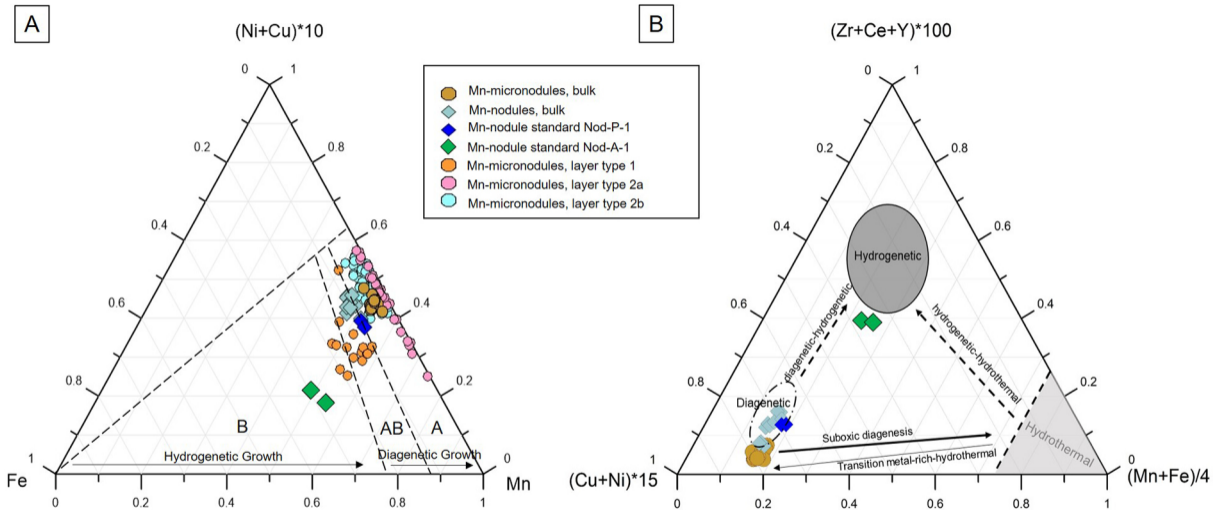


Figure 10